KNOWLEDGE BASED SYNTHESIS SYSTEM FOR INJECTION MOLDING

by

SANG-GOOK KIM

B.S., Seoul National University
(1978)
M.S., Korea Advanced Institute of Science
(1980)

SUBMITTED TO THE DEPARTMENT OF MECHANICAL
ENGINEERING IN PARTIAL FULFILLMENT OF THE
REQUIREMENTS FOR THE DEGREE OF
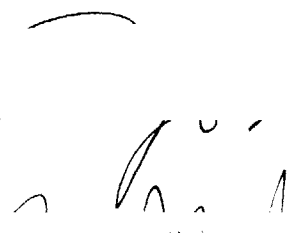
DOCTOR OF PHILOSOPHY

IN MECHANICAL ENGINEERING

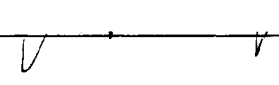at the

MASSACHUSETTS INSTITUTE OF TECHNOLOGY

May 1985

Signature of Author _____

Department of Mechanical Engineering
May 13, 1985

Certified by _____

Prof. Nam P. Suh
Thesis Supervisor

Accepted by _____

Prof. A. A. Sonin
Chairman, Department Graduate Committee

KNOWLEDGE BASED
SYNTHESIS SYSTEM FOR
INJECTION MOLDING

by

SANG-GOOK KIM

Submitted to the Department of Mechanical Engineering on May 13, 1985 in partial fulfillment of the requirements for the degree of DOCTOR OF PHILOSOPHY IN MECHANICAL ENGINEERING.

Abstract

An interactive computer-based design system is developed to eliminate the need for costly iterations of protype tooling in injection molding. A knowledge-based synthesis system is constructed to embody the principle of a rational design strategy for injection molding by combining a rule-based expert system with process analysis programs.

The thermomechanical properties of a molded part are predicted *via* a user-transparent cavity filling simulation program. A unique automatic mesh generation program is developed to complete the cavity filling simulation in real time. A boundary-pressure-reflection scheme is established to solve the moving boundary problem of mold filling. A theoretical model for weldline strength is presented to provide a comprehensive knowledge of the bonding process at the weldline interface. Based on the mathematical models for weldline and molecular orientation, the spatial variation of microstructural anisotropies within a molded part is predicted from the result of cavity filling simulation.

Heuristic knowledge of injection molding is formalized as production rules of the expert consultation system. The expert system interprets the analytical results from the process simulation, evaluates the design and generates recommendations for optimal design alternatives. A prototype knowledge-based system is built to integrate the two domains of knowledge of injection molding, heuristics and analytics, into a rational design strategy.

Thesis Supervisor: Prof. Nam P. Suh
        Title: Professor of Mechanical Engineering

Acknowledgement

I would like to express my sincere gratitude to my mentor, Professor Nam P. Suh, for his support, encouragement and guidance from the beginning of my study at MIT to the end of my thesis. I have learned much from him about the proper way to approach a real world problem. The inspiration he gave me will last for many years to come.

I am also grateful to other members of my thesis committee, Professors Timothy G. Gutowski and Robert C. Armstrong. Their efforts and discussions have been of great benefit to me.

I would like to thank Dr.-ing Chun Sik Lee and Dr. Chong Won Lee of Korea Advanced Institute of Science and Technology for their support and encouragement during my study at MIT.

This research was sponsored by the MIT-Industry Polymer Processing Program. The sponsors of the program are Boeing Commercial Aircrafts Co., C.R. Industries, E.I. DuPont de Nemours and Co., Hysol Division/Dexter Corp., Eastman Kodak Co., KRAFT, Martin Marietta Corp., and Xerox Corp. I would like to thank all of the members of this program.

I would express special thanks to Professor K.K. Wang of Cornell University and Professor S. Weiss of Rutgers University for their generous support in my thesis.

To the staff of the Laboratory for Manufacturing and Productivity, Fred Cote, Bob Cane, Ralph Aves, Steve Holmberg, and Anne Diamond, I am most thankful for their assistance and patience. A special thanks goes to Theresa Harrison for caring

the progress of my thesis with warmth and enthusiasm.

My colleagues around the laboratory deserve thanks for their precious time in discussing many academic and non-academic problems. They include Dr. Hyo-Chul Sin, Dr. Jae Youn, Chong Nam Chu, Dr. Byung H. Kim, Jeff Dohner, Ying Hsu, Steve Liang, Avi Benator, Jon Colton, Al Plioplys, Karl Seeler, Ming Liou, Min Yang, Dae Gil Lee, and Dae Kim. Special thanks goes to my office mates, Kamal Youcef-Toumi, Joe Kwasnoski, Youngje Park, and Hamid Salehizadeh.

Finally, I wish to express my deepest gratitude to my parents for their boundless love, support and sacrifice. I lovingly thank my wife, SoAh, whose endless love, patience and encouragement have made this thesis possible. Special mention goes to my daughter, Catherine, who is worth far more than the Ph.D. degree which I have tried for.

Table of Contents

List of Figures

List of Tables

Chapter 1
Introduction

1.1 Rational Design in Manufacturing

Design is, within the scope of engineering applications, a series of transformation processes from a functional description of a product to a physical entity [1, 2].

The design task is to specify the physical components, the geometry and the processes required to produce a product which performs a function needed by a user. The design processes involve creative, analytical, theoretical and experimental aspects in a complex, iterative and recursive structure. In this respect, the object of rational design, as defined, is to make the specifications such that the designing, production and utilization of the product consume a minimum of societal resources [2, 3].

A rational design strategy differs from an exhaustive generation and test[1] problem-solving technique [4], since it has a criterion for evaluating decisions and an index that directs the generation of design alternatives. Therefore, rational design has been regarded as an essential activity of mankind due to its complexity and the demands of creativity. A number of rational design strategies have been studied to enhance the proficiency of designers and the quality of design. However, most of

---

[1]Like unlocking a multi-digit combination lock.

them mainly focus on the creative aspect of product design and overlook the importance of the manufacturing processes, process design, and manufacturability.

Some of the major manufacturing processes often cause the quality of the product to deteriorate significantly depending upon the interaction between various aspects of design. Injection molding, for example, alters the mechanical performance and the appearance of the product as determined by the choice of processing conditions, material and the topological configuration of the part. Therefore, it requires the designer to have profound knowledge about the nature of the process to design a successful product. A shallow understanding of the process could result in poor product designs. Sometimes, such a product or part design is not even processible.

A process-based product design strategy needs to be established and be linked to the higher level design strategies which mainly deal with the principles of design. Then the ultimate objective of rational design can be accomplished by evaluating the proposed design and generating a set of desirable design alternatives from both the functional and manufacturing point of views. This is the main theme pursued in this study. This thesis deals with injection molded plastic parts as a case study. In particular, the basic understanding of the rheological and thermodynamic history of flow of molten plastics and the resulting orientation of polymer molecules and the weldline strength are used to develop a strategy for thermoplastic part design using an expert system.

1.2 Background and Problems

Three-dimensional complex thermoplastic parts are produced by the injection molding process. The final mechanical properties of these parts are affected by the microstructural anisotropies which result from the complex thermomechanical history experienced by the molded parts. However, it is still difficult to predict the ultimate mechanical properties at the design stage due to the strongly coupled nature of this process.

Manufacture by injection molding includes the creation of the geometry of parts and molds and the choice of processing variables and materials. At the present time, this is done empirically, often involving iterative corrections and modifications of prototype tooling because it is difficult to predict the mechanical properties before the physical entity is made. Therefore, the empirically acquired knowledge has been the primary design guideline for the injection molding process to offset the lack of analyzing tools.

Although many good designs have resulted from experts' intuition and experience, many poor designs have also resulted mainly because the success of a design can be confirmed only by prototype testings (Fig. 1-1). This often results in expensive and laborious iterations of prototype tooling.

Empirical remedies can not be generalized if a scientific tool for design evaluation is not provided. In this respect, many efforts have been made to analyze the nature of the process and the phenomenological behavior of the product [16, 28, 37, 48, 63, 70]. Those analyses mainly deal with limited subsets of the overall problem in injection molding. These studies established the causality of certain mechanical anisotropies, although there are still much to be learned.

NEED → ⊕ → |DESIGN| → |PROCESS| → ⊕ → PRODUCT
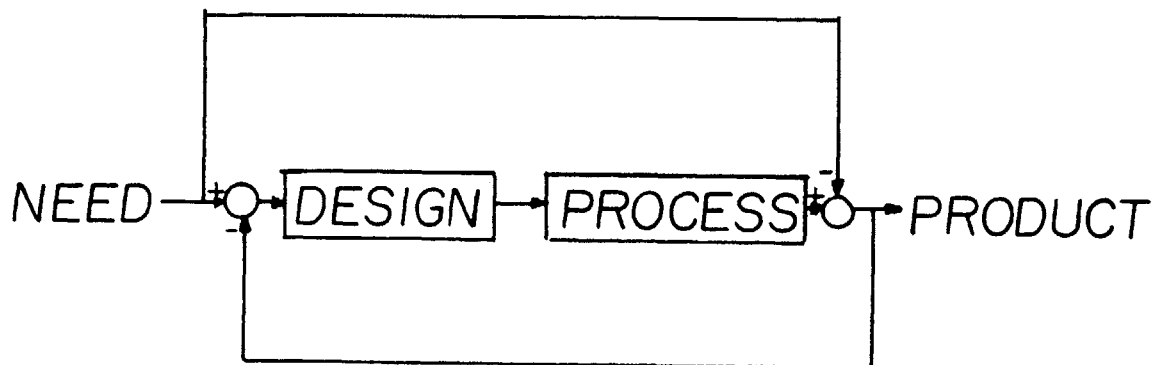
Figure 1-1: Block Diagram of Conventional Synthesis System

The theoretical models for the generation of molecular orientation and its effect on mechanical properties are also well established [14, 32, 69, 70, 76]. However, there are some important mechanical anisotropies which are not yet predicted quantitatively, although their phenomenological aspects are well understood. They are the strength of the weldline structure and the effect of crystallinity on the mechanical properties. In order to predict the mechanical properties of an injection molded thermoplastic part before the part is actually made, theoretical models for predicting these properties quantitatively *a priori* are needed.

However, there is a limit in applying theoretical models as the part shape becomes complex. This is because the injection molding process is inherently a non-Newtonian, non-isothermal system for which the rheological model cannot be established explicitly. Therefore, current tools of analysis are successful only for parts with simple geometry and can not be used to evaluate the design in general before the physical entity is made.

1.3 Goal and Tasks

The goal of this thesis is to develop a scientific method of designing an injection molded part and the molding process, which can increase the productivity of the process and to eliminate its dependence on empiricism [1]. It is mainly accomplished by constructing a computer-based consultation system which can evaluate the design and assist in generating alternative designs, interactively and quantatively (Fig. 1-2).

The success of design in injection molding depends on the moldability of the plastic part in the prototype tooling, the final mechanical properties of its product, and the appearance of the product. Since the appearance of the molded part is affected by the degree of heterogenity of the microstructure, the moldability and the mechanical performance must be the two principal criteria for decision making in this system. The following tasks are formulated to accomplish the goal of this thesis systematically.

1. Identification of the underlying mechanism which controls the thermomechanical properties and the microstructural anisotropies of
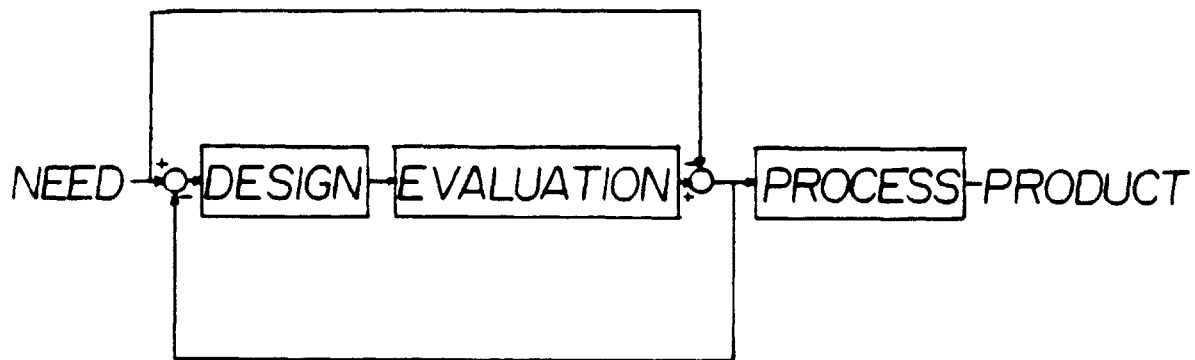
Figure 1-2: Computer-based Synthesis System

injection molded parts.

2. Prediction of the moldability and the mechanical performance of injection molded parts from known information at the design stage.

3. Knowledge-based synthesis, which makes use both of the expert's heuristic knowledge and the analytical knowledge based on process models.

The following chapters will elaborate on the above tasks.

In chapter 2, fundamentals of the injection molding process and related studies are reviewed. Most convincing theoretical and experimental models are examined and selected to simulate the process and to predict the consequent performances of the molded parts as delineated in accompanying chapters.

In chapter 3, filling of the mold cavity is simulated. An interactive cavity filling simulation program is developed which can produce results on a real time basis. Automatic input/output data processing is the key characteristic which enables the real time processing of the program and is essential to make a computer-based systhesis system at a later time.

In chapter 4, microstructural anisotropies are predicted quantatively based on the thermomechanical data which is generated during the cavity filling simulation. The generation of molecular orientation, the effect of orientation on the mechanical properties, and important unidentified phenomenological aspects of injection molding, such as weldline structure, are investigated and modelled theoretically. A microstructural data base is generated to predict the mechanical performance of the injection molded part when the expert system requests it.

In chapter 5, heuristic knowledge in injection molding is formalized *via* a production rule type system. A knowledge-based synthesis system is constructed by integrating the production system and the model-based analysis programs. The diagnosis of design and the generation of design alternatives are to be carried on easily and scientifically by the combination of the heuristics and the analytics.

In chapters 6 and 7, the overall concept is tested and summarized in a protype case study.

Chapter 2
Injection Molding Process

2.1 Fundamentals of Injection Molding

2.1.1 Introduction

Injection molding is a process by which plastic pellets or powders are melted and pressurized into a cavity to form a complex three dimensional part in a single operation.

Injection molding can be said to have started in 1872 with the filing of US Patent No. 133229, entitled "Processes and Apparatus for Manufacturing Pyroxiline", by I.S. and J.W. Hyatt [7]. But there was little development of the original process until World War II. Since that time, injection molding began to make rapid forward strides and became one of the major processing methods for polymeric materials. With the arrival of the reciprocating screw machine, the technology of injection molding advanced in two directions: in the size and control of the machine and in better understanding of the process.

Although the injection molding process can now produce complicated three dimensional parts of various molding compounds of better quality with the recent advancements in molding technology, such as, microprocessor-based process control, low thermal-inertia molding [40], about 95 percent of injection molded parts in the world are produced by the conventional injection molding process [7]. Therefore, only the conventional injection molding process is considered in this thesis.

2.1.2 Principles of the Process

Injection molding is a process whereby a polymeric molding compound is fed, in a solid state, into a cylindrical barrel where it is heated to a molten state and then forced under pressure into a mold. In the mold, it cools and hardens (thermoplastic) or cures and hardens (thermosetts) and in its hardened state can be ejected from the mold which can then be closed. The cycle of operation is then repeated. Although the topics discussed in later chapters are believed to be applicable to other molding compounds, only the molding of thermoplastics is considered in this thesis.

An injection molding machine consists of three basic components: a power unit, a plasticizing unit and a split mold. Depending upon the method of plasticizing and transferring of the material, there are two types of machines - the plunger type and the reciprocating screw type. The reciprocating screw machine, which was developed more recently than the plunger type, is widely accepted because it has many advantages in processing over the plunger type machine.

The lay-out of a typical reciprocating screw machine is shown diagrammatically in Fig. 2-1. A typical sequence of operations from start-up of the reciprocating screw machine is shown in Fig. 2-2.

In order to recharacterize the operational cycle with physical quantities, the typical melt temperature and pressure profile in the molding during one process cycle are shown in Fig. 2-3. It implies that a molded part experiences a complex thermomechanical history during the injection molding process. From the point of thermomechanical history, one operational cycle is characterized by the following four successive stages: plastification, filling, packing, and cooling.
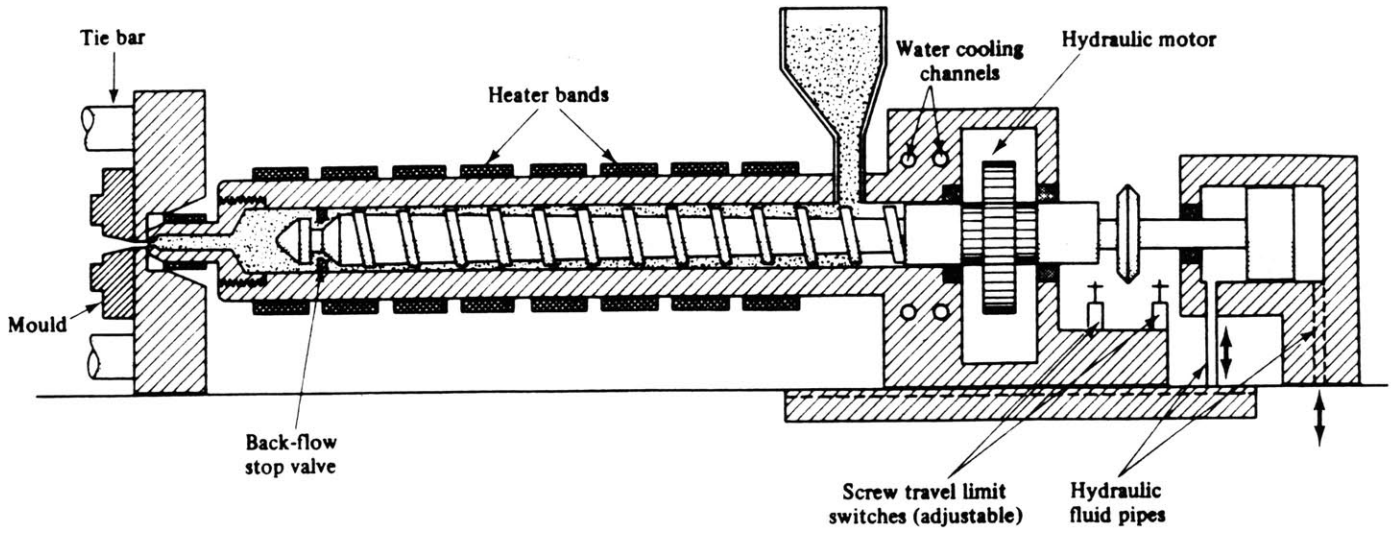
Figure 2-1: Reciprocating Screw Machine, excerpted from [7]
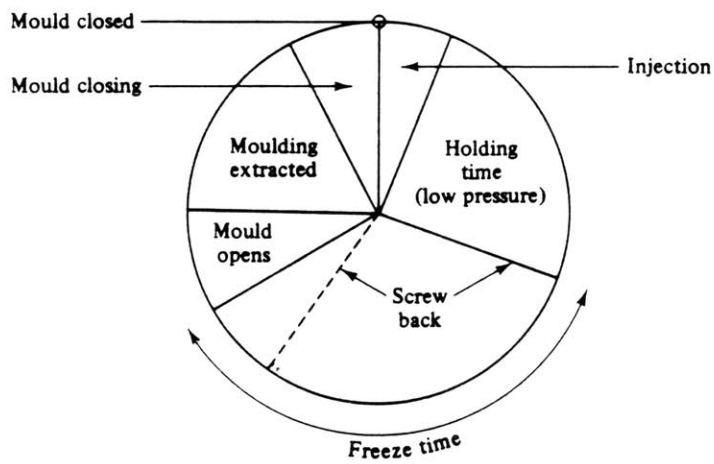
Figure 2-2: Cycle of Injection Molding Operations
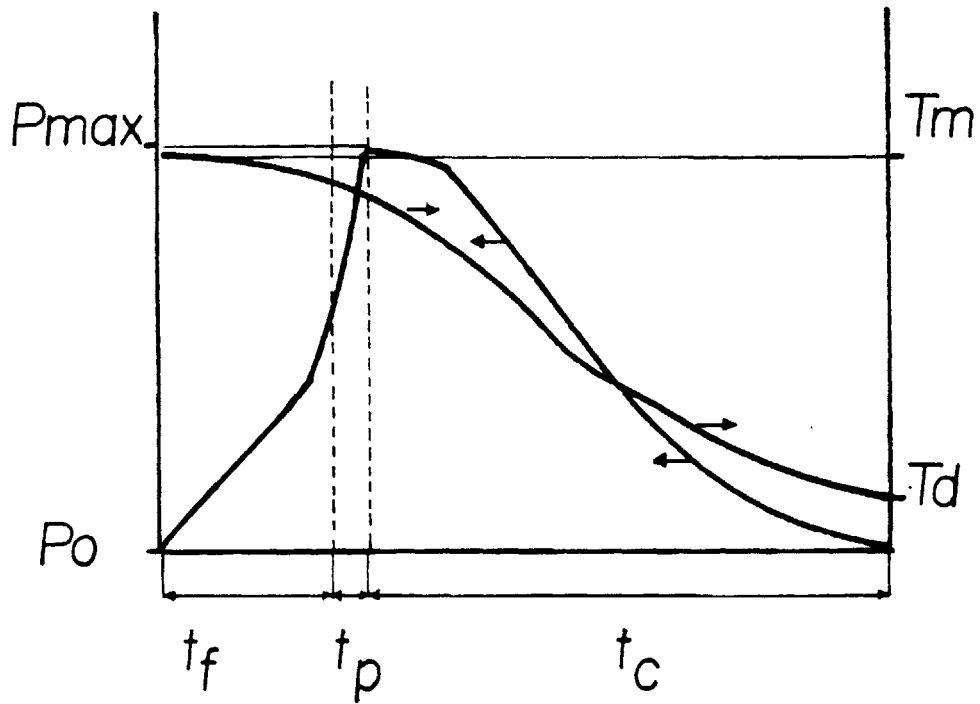
t_f: filling time

t_p: packing time

t_c: cooling time

Tm: melt temperature

Td: mold temperature

Figure 2-3: Typical Pressure and Temperature Profile of Polymer Melt in a Mold

1. <u>Plastification</u>:   Polymer pellets or powder are fed by gravity from the hopper to the rear flights of the screw which rotates, carrying material to the front of the cylinder. During its passage along the barrel, the solid material is plasticized to a molten state by the heat generated from the shear work done on the material and conducted from the electric heater bands which surround the barrel.

2. <u>Filling</u>:   The screw is pushed forward by the hydraulic cylinder at the rear of the screw. The molten polymer is pressurized into the mold to fill the cavity.

3. <u>Packing</u>:   After the mold is filled with molten polymer, the pressure rises rapidly and the material begins to cool from the surface. As the material cools, it shrinks slightly. More material is forced into the cavity to compensate for the shrinkage by holding the high pressure until the gate is closed.

4. <u>Cooling</u> <u>and</u> <u>Demolding</u>:   After the gate has frozen, the screw begins turning back to prepare for the next cycle. The molten polymer inside the cavity continues to cool and take on the shape of cavity. When the part has cooled sufficiently, the mold opens and the part is ejected. This finishes the cycle.

In summary, a complex pattern of thermomechanical history of the material results from the coupling of the flow and cooling of the melt during the process. It determines the spatial variations of microstructural anisotropies of the part and the consequent moldability of the design. Therefore, it is necessary to identify the process as a hydrodynamic and rheological model with which we can predict the thermomechanical history of the part.

2.2 Related Works in Process Simulation

In order to obtain some insight from the phenomenological aspects of the process and to establish the mathematical model for the process, a number of experimental and theoretical studies have been carried out. In an effort to predict the thermomechanical history of the molded part which is determined mainly by the three stages of the injection molding process - filling, packing and cooling, mathematical models for the process are reviewed in this section.

2.2.1 Filling Stage

During the filling stage, the molten polymer is introduced into the mold cavity through the delivery system.

The delivery system consists of the nozzle region, the runner system, and the gate. The sprue, usually, a short, diverging, conical channel, is the main pathway to the mold, connecting the nozzle and the runner system. The function of the runner system is to deliver the hot melt to the cavity with minimum pressure drop. Relatively slow cooling is also important to avoid premature solidification. The gate controls the flow of melt in the cavity depending on its shape and location. A narrow

gate is desirable in order to facilitate the demolding of the cooled part.

Models developed by Williams and Lord [77], Tadmor and Gogos [64] have dealt with the flow in delivery channels. The Cornell Injection Molding Program [70] and Moldflow [50] developed design packages for designing delivery systems having balanced filling in the case of family molds or multiple gated molds. Although the delivery system is important to get the mold be filled, it does not affect the flow behavior of the melt after it passes through the gate. Therefore, this thesis focuses on melt flow behavior inside the mold cavity.

Beginning with the experimental work of Spencer and Gilmore [58, 59, 60], various analyses of the filling stage have been reported. Spencer and Gilmore [58] studied the filling process visually and derived an empirical equation for the determination of the filling time. More flow visualization experiments were reported [24, 34, 35].

Then, in order to explain some of the observations from the flow visualization studies, many approaches of fluid mechanical analyses have been reported. Some authors began to analyze the moldfilling as a problem of combined transport of momentum and energy. Harry and Parrott [26] coupled one dimensional flow analysis with a heat balanced equation for a rectangular cavity in one of the first transport phenomena models.

Kamal and Kenig [34, 35] published a model of the filling process and associated experimental tests. Their model predictions for spreading radial flow of a power law fluid are in fair agreement with their experiments.

Wu, Huang and Gogos [79] developed a model based on different assumptions. They presented simulation results for PVC molding that show the effect of mold

temperature and filling time on the temperature distribution through the cavity.

Richardson [55] suggested that the lubrication theory may be applied in many mold filling situations. Recently, the fully developed creeping flow model (Hele-Shaw flow) has been used in mold filling simulation by White [75], Kuo and Kamal [44] and implicitly by Gutfinger, Broyer and Tadmor [22]. The application of the fully developed Hele-Shaw type flow for the modelling of the filling process gave rise to errors in the entrance region and is also unsatisfactory in the melt front region.

Ibrahim, Hieber and Shen [70] employed the generalized Hele-Shaw flow for the modelling of the two dimensional cavity filling problem. They simulate the problem based on a finite element/finite difference scheme in which the planar coordinates are described in terms of finite elements and the gapwise and time derivatives are expressed in terms of finite differences. They assumed that inertial effects, streamwise conduction and gapwise convection are all negligible. But they employed a non-Newtonian flow under non-isothermal conditions with shear viscosity which has a power-law shear rate dependence and an Arrhenius-type temperature dependence.

Austin [50] commercialized a simplified flow simulation program which predicts the pressure drop along the expected pathline using a Newtonian flow model. Although the program can attain the result quickly by being integrated with the SDRC's[2] graphic software, the detailed process model of the program is not well known.

---

[2]Structural Dynamics and Research Corporation

2.2.2 Post Filling Stages

After the mold cavity is filled completely, an additional amount of material is forced into the cavity to compensate for shrinkage which is due to the partial cooling of the melt. Rapid increase of pressure is observed during this packing stage.

Spencer and Gilmore [58, 59] reported an approximate equation for the calculation of the maximum pressure in the mold during packing. They combined an equation of state and an empirical equation for determining the filling time. They also proposed a state equation to relate the temperature, pressure and specific volume of polymeric materials through measurable material properties [61].

One of the first works considering the packing stage as a transport phenomena problem has been reported by Kenig and Kamal [38, 39]. Later on, Kuo and Kamal [44] extended the theory of the Hele-Shaw flow problem for the analysis of the packing stage associated with a non-Newtonian fluid in a thin rectangular cavity.

The gate freezes after the filling and packing stage. During this cooling stage, no additional material enters the cavity, and thus, there is no global fluid motion except some possible secondary flows due to the difference in local cooling rate. This often results in the sinkmarks on the surface of the part. On the other hand, different degrees of crystalization result in complex patterns of morphology in the case of semi-crystalline polymers.

Dietz [17] developed a model to represent the nonsteady heat transfer phenomena accompanied by a phase change during cooling. Kenig and Kamal [38, 39] solved the problem as a transient heat conduction model between two cooling plates. In their analysis, they account the effect of crystallization during cooling. Recently, Tan, Kamal and Lafleur [37, 65] proposed a prediction model for the degree of

crystallinity in injection molded parts.

2.3 Related Works in Microstructure Prediction

A complex pressure and temperature profile of polymer melt is developed at each location of the cavity as shown in Fig. 2-3. Depending upon the complex pattern of thermomechanical history which a molded part experiences during the process, diverse spatial variations of the microstructure are generated inside the part. The resulting microstructure shows mixed states of under-relaxed, stretched and crystallized (semi-crystalline polymers) molecular configurations. It also often contains weak-bonded structures at the interface of two merging melt fronts. This is known as a weldline which is regarded as one of the most detrimental defects of injection molded parts.

From a rheological point of view, the visco-elastic nature of polymeric materials results in the development of shear and normal stresses, and large elastic deformation during the filling stage with subsequent relaxation during the cooling stage. In this respect, a number of studies are reported to have predicted the resulting microstructure based on mathematical process simulation.

Jackson and Ballman [31] wrote an article which discussed the effect of molding conditions on molecular orientation and the effect of orientation on the mechanical properties of the injection molded part. They reported the strong influence of molecular orientation on the tensile and impact strength of the product.

Ballman and Toor [6] measured the gapwise birefringence in injection molded polystyrene strips and reported the relation between the magnitude of birefringence at different locations and processing conditions.

Curtis [14] measured the fracture surface energy for both stretched PMMA[3] and polystyrene and experimentally determined the relationship between the tensile and impact strength of those materials as a function of molecular orientation.

Menges and Wubken [48] studied the effect of processing conditions on the molecular orientation in injection molding. They concluded that the major direction of orientation in planar shaped moldings coincides with the flow direction. They also found that the state of orientation is biaxial at the surface of the molding.

Wales [69] measured the steady shear flow birefringence in all three planes of the part and experimentally determined the dynamic and steady shear rheological properties. Their work has drawn attention because their model included the rheological properties of the material while most of the previous experimental work had been carried without considering them.

Tadmor [63] proposed a semiquantitative model to predict the magnitude of molecular orientation in molded parts in terms of birefringence. The bead and spring theory of macromolecules was used to calculate the orientation arising from the steady elongational flow in the advancing melt-front region.

Menges, Thienel and Wubken [49] published a study on the relaxation of molecular orientation in plastics. They proposed a method to estimate the relaxation of molecular orientation from the knowledge of the time-temperature history of the material.

Bakerdjian and Kamal [5] studied the anisotropic properties of injection molded parts. They reported the three dimensional variation of density, heat

---

[3]Polymethylmethacrylate

shrinkage, birefringence and tensile strength. The lowest shrinkage value, for example, was found near the center of the molding, where the polymer chains have the greatest chance to relax and resume a more random configuration.

Hoare, Linda and Hull [28] studied the effect of orientation on the mechanical properties of injection molded polystyrene. They regarded the molding as a composite structure of materials with different degrees of anisotropy and orientation, but the same elastic modulus. They concluded that the crazing and cracking behavior of the amorphous polymers can be predicted from the measurement of the molecular orientation.

Janeschitz-Kriegl [32] developed a dynamic model for determining the frozen layer thickness of polymer melt during the molding process. His model involved a global energy balance in terms of transient heat conduction together with thermal convection and viscous heating. His model was compared favorably with the experimental results.

Dietz and White [16] developed a theoretical model to predict the distribution of molecular orientation in injection molding of amorphous polymers. Their method is based on the calculation of the solidification layer thickness in the wall region and the use of an isothermal power law fluid model in the core region. They also assumed that the stress-optical law can be used in the molten state of the polymer to get the frozen-in birefringence at the solid boundary. Although they employed some *ad hoc* assumptions in deciding the relaxational behavior of the flow stresses, their results compared well with some experimental results.

Recently, Isayev and Hieber [30] employed the visco-elastic constitutive equation for the prediction of the residual stresses, orientation and birefringence in

all planes, taking into account the effect of unsteady, nonisothermal flow during the filling stage and nonisothermal stress relaxation during the cooling stage. They have chosen the recently developed constitutive equation, the Leonov model, which is based on the irreversible thermodynamic theory. Therefore, their model was able to describe well the rheological behavior of the polymer melt under arbitrary elastic deformation.

Tan and Kamal [65] observed that there are four different morphological zones developed during the molding of semi-crystalline polymers. They are the skin layer which exhibits a non-spherulitic structure and has a high degree of orientation, the near-wall region which has a fine asymmetric structure, the near core region which consists of asymmetric oblate spherulites, and the core region which contains randomly nucleated spherulites. They predicted the crystallinity-time relationship in a nonisothermal injection molding process.

2.4 Summary

The principles of the injection molding process and key theoretical models for the process are reviewed in an effort to identify the relationships among the ultimate properties of the molded article, rheological resin properties, processing parameters and the part design. The nature of the injection molding process is defined as a visco-elastic, non-Newtonian flow under nonisothermal conditions and subsequent unfinished relaxation of flow-induced stresses under nonisothermal conditions. Some of the theoretical models are found to be qualitatively meaningful, but not sufficiently quantatively established to be used in this thesis.

In order to take the goal of this thesis to its final conclusion, a mathematical

tool for evaluating designs must be developed. The evaluation of design can be attained *via* process simulation and microstructure prediction. Two theoretical models, one for the cavity-filling simulation and the other for microstructure prediction, will be constructed in the following chapters based on the materials reviewed in this chapter. Most of the convincing mathematical models and numerical schemes reviewed in this chapter will be investigated, modified and collated to form an integrated process analysis system.

Chapter 3
Cavity Filling Simulation

3.1 Introduction

The ultimate properties of injection molded parts depend on the thermomechanical history developed during the process cycle as discussed in Chapter 2.2. Therefore, it is necessary to simulate all stages of the injection molding process to predict rigorously the resulting thermal, rheological and hydrodynamic properties of the part.

In order to achieve the goal of the process simulation effectively, which will form an analysis part of the integrated synthesis system, it is assumed that the filling stage is responsible for the most significant and substantial physical changes of the polymer melt. Although some important qualitative aspects of the part are determined during the post filling stages, the effect of packing and cooling is not considered in this thesis. The flow through the delivery system, from the nozzle to the gate, is also not included in the process simulation by assuming that the uniform, hot pressurized melt can be delivered to the gate with careful design of the delivery system.

Injection molded parts have thin, quasi-three dimensional shapes, which can be unfolded to appropriate two dimensional layflats, due to the following topological characteristics. It should have a proper opening for ejection from the mold. Due to the relatively low thermal conductivity of polymer melts, the thickness of the part

should be sufficiently thin for the melt to be cooled in a short time. Furthermore, the thickness should be as uniform as possible to avoid sink marks, distortion, cooling stresses and jetting phenomena. Therefore, it is possible to use a two dimensional flow model in the filling simulation for quite complicated geometry of molds by making an approximated two dimensional layflat for the part. Recently, the Cornell Injection Molding Program [70] has developed an automatic layflat generating software, which is a useful preprocessor to apply the two dimensional flow analysis for the filling of general quasi-three dimensional mold cavities.

Although the shape of a mold can be approximated as a two dimensional cavity, the resulting thermomechanical properties and resulting microstructures are distributed not only in planar coordinates but also in the gapwise coordinate. In order to obtain the three dimensional distribution of microstructural anisotropies, a decoupled flow analysis is proposed to predict the three dimensional distribution of the thermomechanical properties from the approximated two dimensional mold cavity as follows.

For an approximated two dimensional geometry of a cavity, the two dimensional flow analysis is carried out to get the planar distribution of thermomechanical properties. Then a one dimensional simple shear and elongational flow model is applied along each streakline to get the gapwise distribution of necessary thermomechanical properties as shown in Fig. 3-1. The theoretical model and numerical schemes of two dimensional cavity filling simulation will be discussed in this chapter. One dimensional streaklinewise flow analysis will be discussed as a part of microstructure prediction in Chapter.4.

STREAM LINE

GATE

MELT
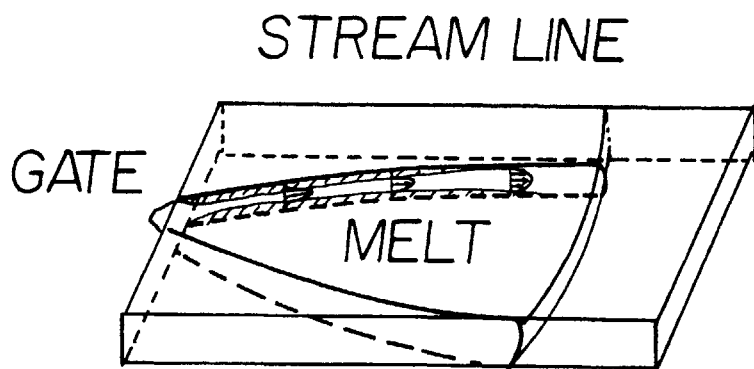
Figure 3-1: Decoupled Flow Simulation for Quasi-Three Dimensional Part

3.2 Two Dimensional Cavity Filling Problem

Ibrahim, Hieber and Shen [70] developed a two dimensional flow simulation program for the nonisothermal filling of a thin cavity with variable thickness. It is assumed in their modelling that inertial effects, streamwise heat conduction and gapwise heat convection are negligible. The fluid is taken to be inelastic, but non-Newtonian under nonisothermal conditions with the shear viscosity assumed to have a power-law shear rate dependence and an Arrhenius-type temperature dependence. The numerical computation is based on a finite element/finite difference scheme in which the planar coordinates are described in terms of finite elements and the gapwise and time derivatives are described in terms of finite difference.

Their simulation results compared favorably with their own experimental results, but the inclusion of the user's judgment at each time step to handle the

moving boundary problem requires large amounts of data preparation time. Therefore, their flow simulation program can not be used as part of a design system which requires a real time simulation result.

As part of the decoupled flow analysis which is proposed in the previous section, the flow model and basic numerical schemes developed by CIMP[4] are used in this thesis[5] for the two dimensional cavity filling simulation. The program is then modified and supplemented so as to be used as an interactive, real time process simulation program.

3.2.1 Governing Equations

The Hele-Shaw flow model for a fully developed viscous flow in a thin cavity as shown in Fig. 3-2 is generalized for an inelastic non-Newtonian fluid under nonisothermal conditions to have following governing equations.

<u>Continuity</u>;

$$\frac{\partial}{\partial x}(b\overline{U}) + \frac{\partial}{\partial y}(b\overline{V}) = 0 \tag{3.1}$$

where b is the half gap thickness at a location (x,y), $\overline{U}$ and $\overline{V}$ denote gapwise averaged velocity components in x and y coordinate.

<u>Momentum</u>;

---

[4]Cornell Injection Molding Program

[5]Courtesy of Prof. K. K. Wang (Director, CIMP)
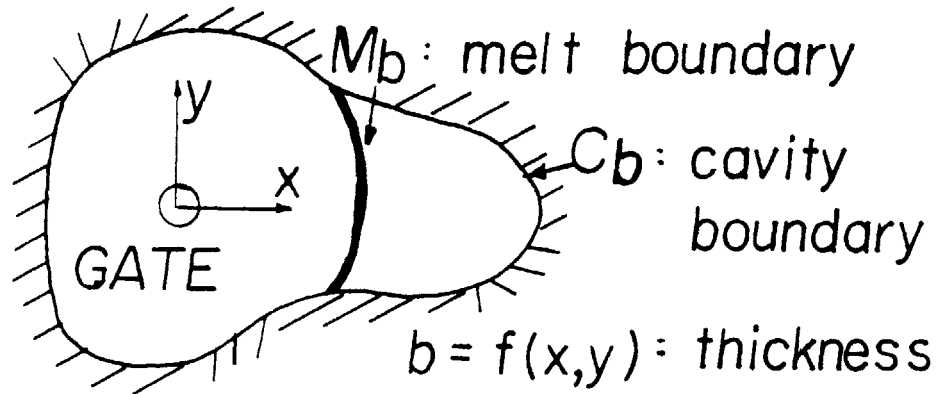
Figure 3-2: Two Dimensional Cavity with Varying Thickness

$$\frac{\partial}{\partial z}(\eta\frac{\partial U}{\partial z}) - \frac{\partial P}{\partial x} = 0 \qquad (3.2)$$

$$\frac{\partial P}{\partial y} - \frac{\partial}{\partial z}(\eta\frac{\partial V}{\partial z}) = 0 \qquad (3.3)$$

where the inertial effects and the z- axis velocity component are neglected.

Energy;

$$\rho C_p(\frac{\partial T}{\partial t} + U\frac{\partial T}{\partial x} + V\frac{\partial T}{\partial y}) = k\frac{\partial^2 T}{\partial^2 z} + \eta\dot{\gamma}^2 \qquad (3.4)$$

Consistent with the above governing equations, approriate boundary conditions in the z-direction can be given by,

$$U = 0$$
$$V = 0$$
$$T = T_w, \text{ at } z = b \tag{3.5}$$

and

$$\frac{\partial U}{\partial z} = \frac{\partial V}{\partial z} = \frac{\partial T}{\partial z} = 0, \text{ at } z = 0 \tag{3.6}$$

The shear viscosity, η, will have a relation with the shear rate, $\dot{\gamma}$ and the melt temperature, T, as follows.

$$\eta(\gamma, T) = m(T)\dot{\gamma}^{n-1} = m_o g(T)\dot{\gamma}^{n-1} \tag{3.7}$$

$$\dot{\gamma} = \sqrt{(\partial U/\partial z)^2 + (\partial V/\partial z)^2} \tag{3.8}$$

$$m_o = A exp(\frac{T_a}{T} - \frac{T_a}{T_o}) \tag{3.9}$$

where n is the power law index, $g(T)$ is a function arising from temperature dependence of viscosity and A, T_a and T_o are constants for the shear viscosity.

3.2.2 Numerical Solution

Fig. 3-3 shows the functional steps of numerical solution with the governing equations in two dimensional cavity filling simulation. Since the finite element/finite difference formulation to solve the governing equations in this thesis is a proprietary program of CIMP, the detailed numerical scheme is not presented here except the algorithm for the moving boundary problem, which will be changed in this thesis to make a user transparent, realtime running flow simulation program.

As noted in Fig. 3-3, the advancement of the melt front is the key step in

INITIAL INPUT DATA

GOVERNING
EQUATIONS

PRESSURE
DISTRIBUTION

VELOCITY
DISTRIBUTION

TEMPERATURE
DISTRIBUTION

ADVANCE MELT FRONT

FINISH
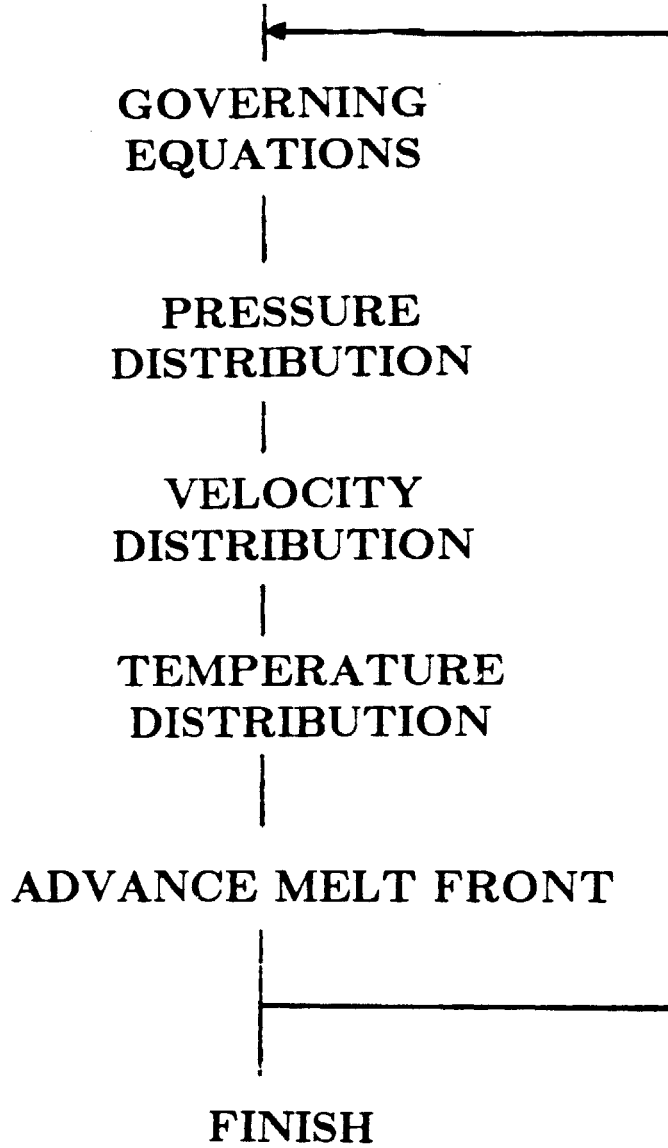
Figure 3-3: Schematic Representation of Numerical Steps for Filling Simulation

solving a moving boundary transient flow problem. Once the pressure field has been converged *via* iterations of calculation, gapwise-averaged velocity components at each vertex node are evaluated. Based on the predicted velocities at the current melt front, the new melt front is predicted for a specified time step. Then the finite elements for the new melt front are generated, edited and added to the current input data file in order to calculate governing equations at the next time step. At each time step, the new melt front is predicted and corrected until the whole mold cavity is filled.

Sometimes, however, the predicted melt front boundary partly falls either outside or inside the cavity boundary because the physical boundary information for the next time step is not included in the current governing equations. Therefore, an user's judgment is employed to rearrange the advanced melt front at each time step as shown in Fig. 3-4. During this manual rearrangement, two conditions are considered to give the user's judgment physical meaning: mass conservation and orthogonality. Based on the two conditions, the melt front is regenerated to permit the nodes at the physical boundary to advance along the boundary as shown in Fig. 3-4(b).

The orthogonality condition is set by CIMP noting that the melt front stands orthogonal to impermeable boundaries. However, this can not be construed as a general fact because the contact angle between the solid boundary and the polymer melt is mainly determined by the wetability of the two materials and the surrounding gas. Although the orthogonality condition does not have a proper physical basis, some polymer melts show near orthogonal contact with the metal surface phenomenologically. In the case of using the orthogonality condition in the boundary impingement problem, it is allowed only in the region which is sufficiently
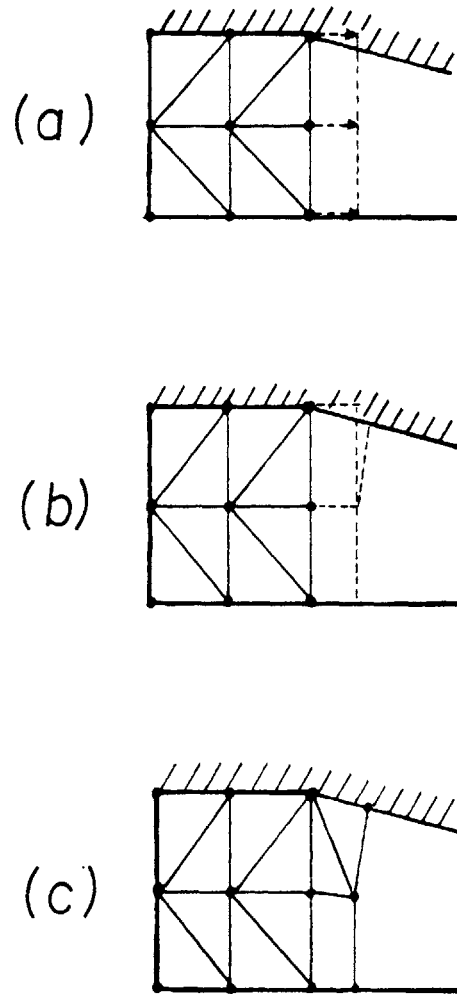
Figure 3-4: Manual Boundary Rearrangement Scheme [70]:
(a) Impingement, (b) Rearrangement, (c) Mesh genaration

close to the boundary. Therefore, from the author's point of view, the use of an *ad hoc* orthogonality condition, during the melt front prediction, is the major barrier prohibiting the automatic input/output data processing at each time step with the advancement of the melt front.

Since their approach to the boundary impingement problem requires the user's judgment at each time step, a tremendous data preparation effort is needed to complete the filling simulation even for a simple cavity geometry [70]. Therefore, it is necessary to develop an automatic melt front generation program which eliminates the inclusion of the user's judgment during the prediction and enables the mold filling simulation to be completed in real time.

3.3 Automatic Mesh Generation

In order to complete the filling simulation as a part the interactive design system, the generation of a new melt front and associated input data preparation should be done automatically without the user's judgement. In this respect, an automatic mesh generation program for the moving boundary problem is developed and discussed in this section.

3.3.1 Automatic Melt Front Advancement

Consider the current melt boundary $\overline{AB}$ in Fig. 3-5. The predicted melt boundary for the next time step is $\overline{A'B'}$ based on the calculated velocities at the current boundary nodes. However, the advanced boundary falls partly outside of the cavity boundary, which is not physically possible. This is because the forward boundary information is not included in the current calculation of nodal velocities.

Therefore, an effort is made to include the forward boundary information in the current calculation. For this purpose, the boundary-pressure-reflection method is derived in this thesis as follows.
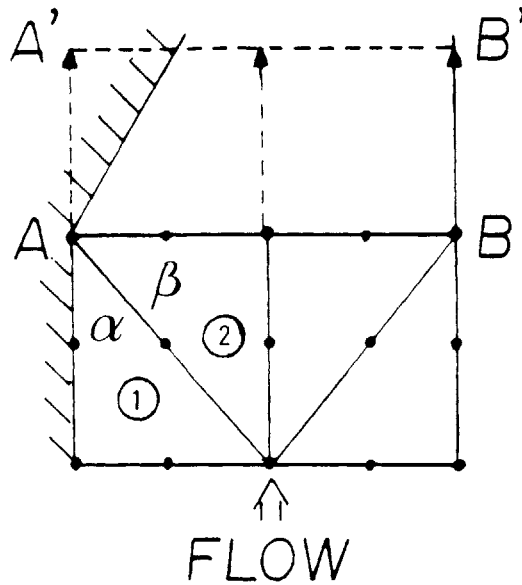
Figure 3-5: Boundary Impingement at the Predicted Melt Front

When the melt front impinges partly to the physical boundary, the pressure at nodes near boundary should be redistributed to allow the melt to flow within the cavity. In other words, it is assumed that there exists a virtual pressure at the physical boundary which partly reflects the current pressure distribution at the nodes near the boundary wall. The magnitude of reflection is dependent on the degree of impingement which represents the magnitude of penetration of the predicted melt front into the solid boundary based on the no-penetration condition. The degree of impingement is predicted and then reflected to the current pressure distribution near the boundary. Then the correct melt front is regenerated, based on the new pressure distribution. Thus the basic idea of the boundary-pressure-reflection scheme is to predict the physically acceptable melt front for the next time

step.

The velocity at the boundary node is calculated and compared with the physical boundary to determine the degree of impingement as follows. The velocity at node 1 in Fig. 3-6 (a) is calculated based upon the pressure drop from all elements containing node 1 (element 1 and element 2 in this case). The contributions are weighted on the basis of the subtended angle of each element, α and β.
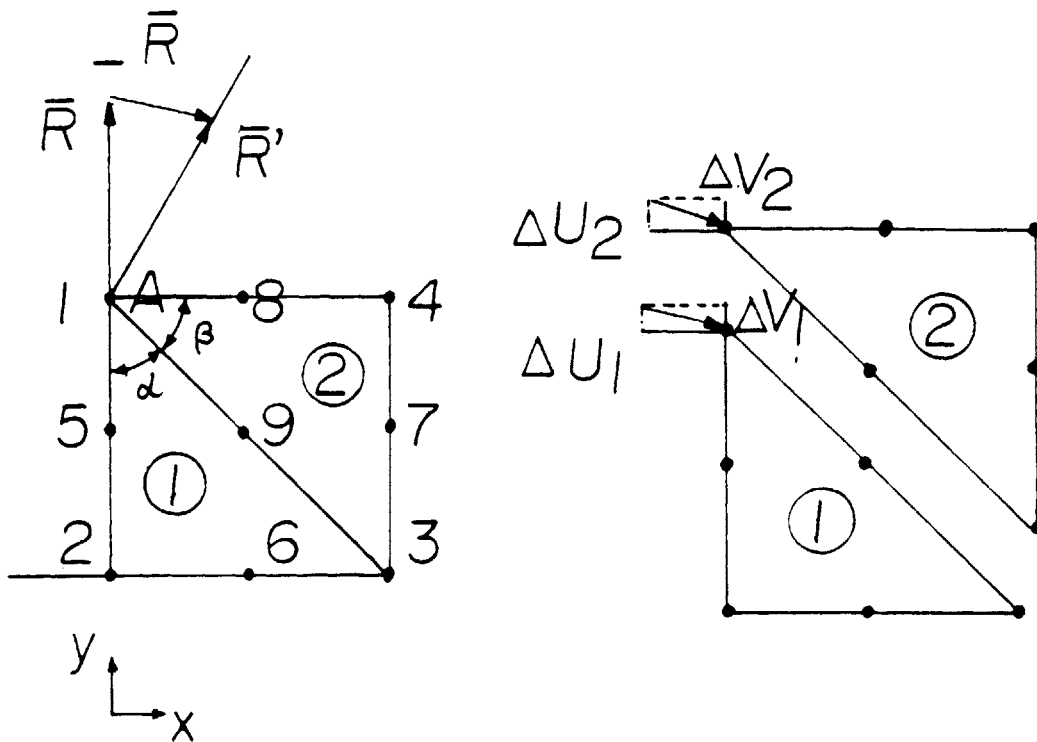
Figure 3-6: Pressure reflection for two elements containing the boundary node: (a) degree of impingement, (b) reflection to each element

For six-noded triangular element 1 and 2, the x and y velocity components can be written as follows [70]

$$\overline{U} = \frac{\alpha}{\alpha+\beta}(A_{11}P_{11}+A_{12}P_{12}+A_{13}P_{13}+A_{14}P_{14}+A_{15}P_{15}+A_{16}P_{16})+ \quad (3.10)$$

$$\frac{\beta}{\alpha+\beta}(A_{21}P_{21}+A_{22}P_{22}+A_{23}P_{23}+A_{24}P_{24}+A_{25}P_{25}+A_{26}P_{26})$$

$$\overline{V} = \frac{\beta}{\alpha+\beta}(B_{11}P_{11}+B_{12}P_{12}+B_{13}P_{13}+B_{14}P_{14}+B_{15}P_{15}+B_{16}P_{16})+ \quad (3.11)$$

$$\frac{\beta}{\alpha+\beta}(B_{21}P_{21}+B_{22}P_{22}+B_{23}P_{23}+B_{24}P_{24}+B_{25}P_{25}+B_{26}P_{26})$$

where $A_{1,i}$, $A_{2,i}$, $i=1,...,6$, are coefficients of linear interpolation function for pressure drop over each triangular element 1 and element 2 for x coordinate and $B_{1,i}$, $B_{2,i}$, $i=1,...,6$, are coefficients of linear interpolation function for pressure drop over each triangular element 1 and element 2 for y coordinate. $P_{i,j}$ is the pressure at j^{th} node of element i. α and β are subtended angles of element 1 and 2 for node 1 and $\overline{U}$ and $\overline{V}$ are gapwise averaged velocity component at node 1.

The resultant velocity is then multiplied by the specified time step, Δt, to get the displacement vector, $\overline{R}$ in Fig. 3-6 which is not lying on the boundary. Therefore, a compensating displacement vector, $\Delta\overline{R}$, is required to push the melt inside the cavity. Based on the compensating vector, $\Delta\overline{R}$, the amount of pressure reflection is calculated in reverse at every node of element 1 and element 2.

Reverse contributions of $\Delta\overline{R}$ to each element are distributed by the subtended angle, α and β, of each element. Let ΔU_1 and ΔU_2 be the x-axis components of the compensating vector for element 1 and element 2.

$$\frac{\Delta U_1}{\Delta U_2} = \frac{\alpha}{\beta} \qquad (3.12)$$

$$\Delta U = \frac{\alpha}{\alpha + \beta} \Delta U_1 + \frac{\beta}{\alpha + \beta} \Delta U_2 \qquad (3.13)$$

where ΔU is the x-axis component of the compensation vector $\Delta \overline{R}$.

From equation (3.12) and equation (3.13), the distribution of compensating displacement to each element in x coordinate is obtained as follows.

$$\Delta U_1 = \frac{1 + \beta/\alpha}{(1 + \beta/\alpha)^2} \Delta U \qquad (3.14)$$

$$\Delta U_2 = \frac{1 + \alpha/\beta}{(1 + \alpha/\beta)^2} \Delta U \qquad (3.15)$$

The same procedure can be applied to get ΔV_1 and ΔV_2 from ΔV for the y-axis components of compensation displacement as follows.

$$\Delta V_1 = \frac{1 + \beta/\alpha}{(1 + \beta/\alpha)^2} \Delta V \qquad (3.16)$$

$$\Delta V_2 = \frac{1 + \alpha/\beta}{(1 + \alpha/\beta)^2} \Delta V \qquad (3.17)$$

By matching the compensating displacement components, ΔU_1, ΔU_2, ΔV_1, ΔV_2, with each right hand term of equations from (3.10) to (3.11), four equations are made for the pressure reflection at nine nodes in Fig. 3-6 as follows.

$$\Delta U_1 = A_{11}\Delta P_1 + A_{12}\Delta P_2 + A_{13}\Delta P_3 + A_{14}\Delta P_5 + A_{15}\Delta P_6 + A_{16}\Delta P_9 \qquad (3.18)$$

$$\Delta U_2 = A_{21}\Delta P_1 + A_{22}\Delta P_3 + A_{23}\Delta P_4 + A_{24}\Delta P_9 + A_{25}\Delta P_7 + A_{26}\Delta P_8 \qquad (3.19)$$

$$\Delta V_1 = B_{11}\Delta P_1 + B_{12}\Delta P_2 + B_{13}\Delta P_3 + B_{14}\Delta P_5 + B_{15}\Delta P_6 + B_{16}\Delta P_9 \qquad (3.20)$$

$$\Delta V_2 = B_{21}\Delta P_1 + B_{22}\Delta P_3 + B_{23}\Delta P_4 + B_{24}\Delta P_9 + B_{25}\Delta P_7 + B_{26}\Delta P_8 \qquad (3.21)$$

where $A_{1,i}$, $A_{2,i}$, $i = 1,...,6$, are coefficients of linear interpolation function for pressure drop over each triangular element 1 and element 2 for x coordinate and $B_{1,i}$, $B_{2,i}$, $i = 1,...,6$, are coefficients of linear interpolation function for pressure drop over each triangular element 1 and element 2 for y coordinate. ΔP_1 to ΔP_9 are the pressure changes at nine nodes of element 1 and 2 in Fig. 3-6.

In order to solve the pressure reflections, $\Delta P_1,..., \Delta P_9$, five more equations are required for nine unknowns. Therefore, a linear interpolation function is assumed on five mid side nodes, such as:

$$\Delta P_5 = \frac{1}{2}(\Delta P_1 + \Delta P_2) \qquad (3.22)$$

$$\Delta P_6 = \frac{1}{2}(\Delta P_2 + \Delta P_3) \qquad (3.23)$$

$$\Delta P_7 = \frac{1}{2}(\Delta P_3 + \Delta P_4) \qquad (3.24)$$

$$\Delta P_8 = \frac{1}{2}(\Delta P_1 + \Delta P_4) \qquad (3.25)$$

$$\Delta P_9 = \frac{1}{2}(\Delta P_1 + \Delta P_3) \cdot \qquad (3.26)$$

The pressure reflections near the boundary region, $\Delta P_1,..., \Delta P_9$, are predicted by solving nine equations (3.18) - (3.26), for nine unknowns with the Gauss/maximum-pivot elimination method for linear equations.

After the calculation of pressure reflections, nodal velocities are recalculated and a correct advanced melt front is predicted based on the recalculated velocities as shown in Fig. 3-7. It is noted that the effect of pressure reflection propagates to neighboring nodal velocities when the nodes of the boundary element are included in the adjacent elements' quadratic shape functions.
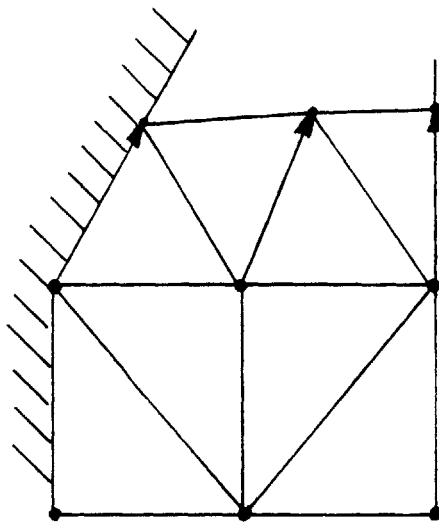
Figure 3-7: Automatically Generated Meltfront

In summary, the boundary-pressure-reflection scheme provides a theoretical basis for the prediction of new melt fronts at each time step. It does not require user's judgements during the regeneration of the melt front. The prediction is based on the correct nodal velocities in which calculation the forward boundary information is included. The case in which the boundary node has more than two elements is not considered in this formulation, which can be controlled during the mesh generation.

3.3.2 Mesh Editing and Data Formating

By advancing the melt front at each time step without manual judgments, automatic input data preparation for the whole numerical procedure becomes possible. Based on the predicted location of the melt front, new elements for the advanced front region are generated, numbered and added to the current finite element input data. Then, the input data for the next time step is generated in the matching format of the program by the flow simulation program itself. The numbering sequence for a 6-noded triangular element is shown in Fig. 3-8.

However, depending upon the shape of finite elements, the stability of the numerical calculation is significantly affected. Too much distortion or too high an aspect ratio of a generated element should be avoided in order to obtain an improved numerical stability [70]. Therefore, a proper mesh editing process is required to maintain the shape of newly generated elements as regularly as possible. For this purpose, the time step can be changed by the editing program to avoid too big-or too small-sized meshes. A birth/death function is also given to the editing program to split too slim elements or to merge too narrow elements as shown in Fig. 3-9.

On the other hand, the user can also control the mesh editing in order to handle possible singular boundaries during the flow simulation. The user's decision overrides that of the mesh editing program, at anytime, upon the user's request. The functional description of the automated flow simulation program is given in Appendix A.
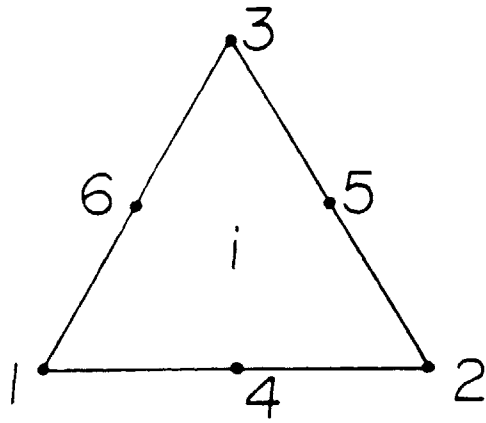
Figure 3-8: Six Noded Triangular Element
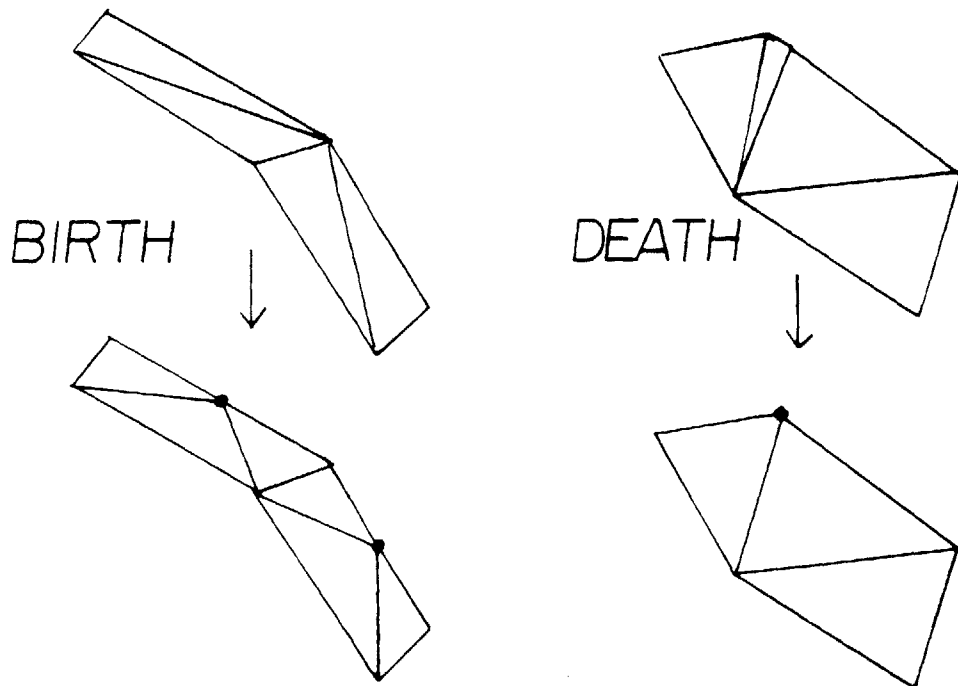
Figure 3-9: Birth and Death of Irregular Elements

3.4 Case Studies

3.4.1 Edge Gated Circular Cavity

In order to test the boundary-pressure reflection scheme and the automatic mesh generation program by comparing the result with that of the manual front rearrangement scheme [70], the same values as those given in Ref. [70] for the cavity geometry, processing parameters and the material are chosen.

The disk has a diameter of 4.446 cm and half gap thickness of $b = 0.0795$ cm. Melt enters the cavity through a point gate (origin) on the circumferential end. Due to symmetry, only half of the disk needs to be solved.

The calculation has been carried out for the following process conditions:

Melt Temperature: 528°K

Mold Wall Temperature: 341°K

Injection Rate: 2.705 cm^3/sec (per half circle, half gap)

Material: polystyrene

Material Constants for equation (3.5)-(3.9):

$\rho = 1.02$ gm/cm^3

$k = 1.84*10^4$ erg/(cm.sec.°K)

$C_p = 2.35*10^7$ erg/(gm.°K)

$A = 80.1$ gm.sec^{n-1} /(cm.sec)

$T_a = 3635$ °K

$n = 0.32$

The finite element calculation is initiated by assuming that, for a sufficiently

small initial time step, the cavity is filled essentially isothermally. In this case, nodal pressures on the initial elements (corresponding to t=0.03 sec) have been calculated analytically from the following equation [70].

$$P = P_0 - \frac{m_0}{(1-n)b}(\frac{2n+1}{2b^2 n})^n(\frac{Q}{1.4})r^{1-n} \qquad (3.27)$$

where r denotes the radial distance from the source and Q is the injection rate.

From the initial mesh configuration (Fig. 3-10.a), subsequent melt fronts are predicted and advanced until the most of the cavity is filled (Fig. 3-10.b - Fig. 3-10.d). Fig. 3-11 shows the predicted melt fronts at each time step. The results compare favorably with the result by CIMP [70], while consuming less than an hour of total simulation time. Most of the simulation time is the CPU time. This proves that the filling simulation with the automatic mesh generation program can be used as a part of a real time design evaluation system.

FILLING TIME : 0.00 SEC

FILLING TIME : 0.452 SEC
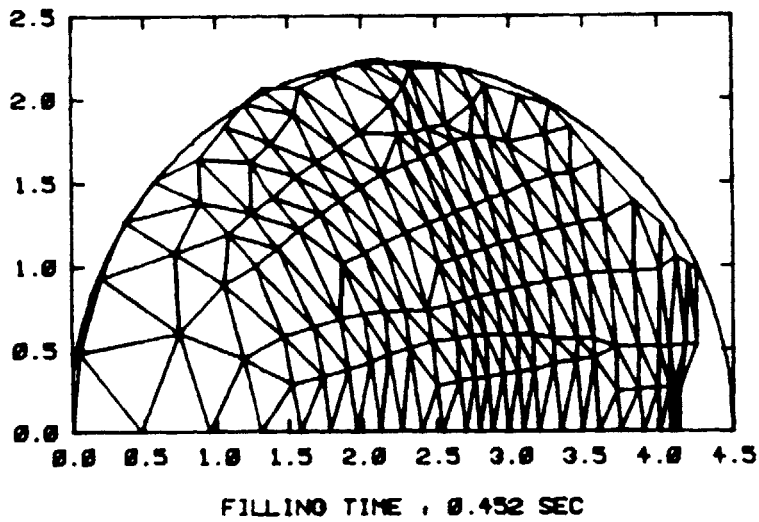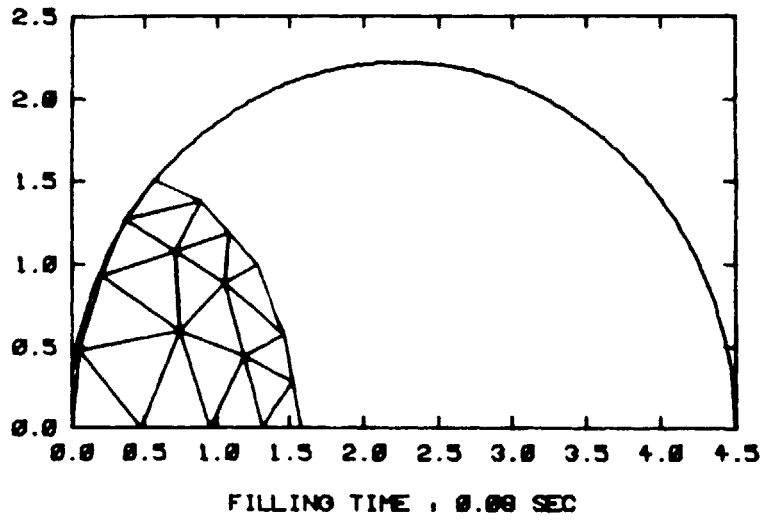
Figure 3-10: Mesh Configuration During the Filling Simulation
Case Study 1:Circular Cavity
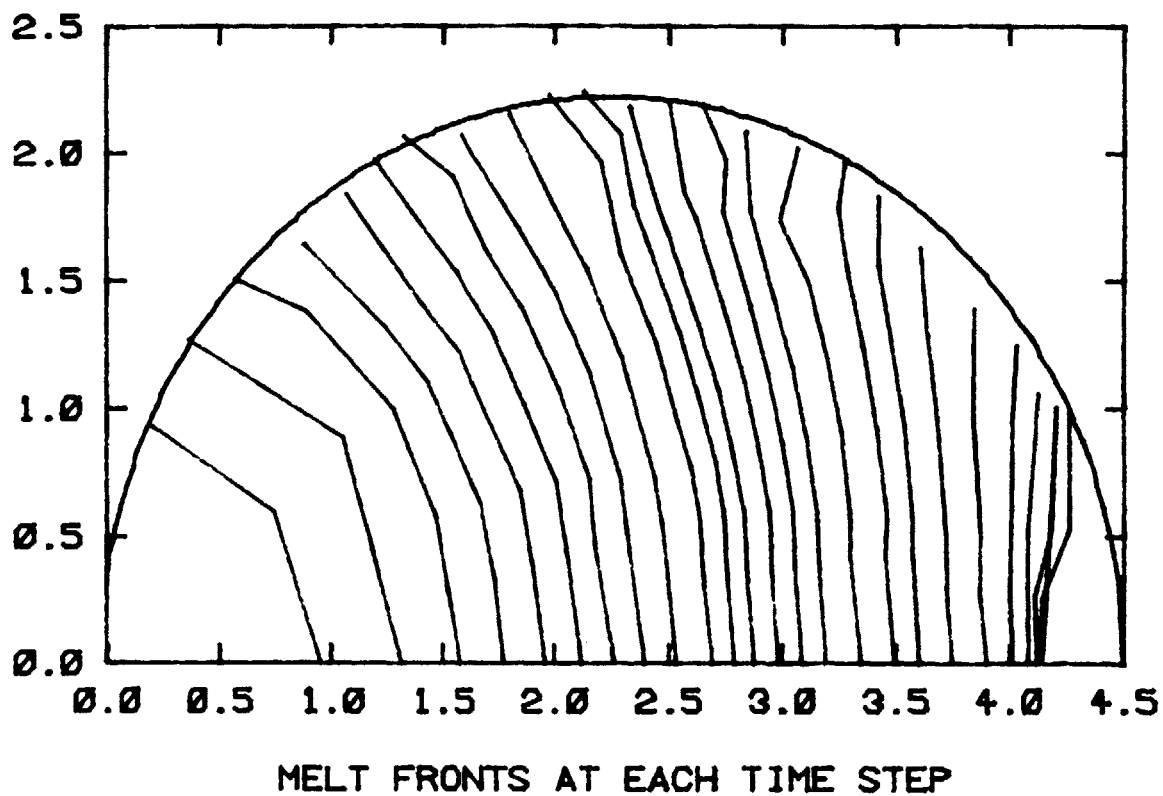
Figure 3-11: Predicted Melt Fronts at Each Time Step
Case Study 1: Circular Cavity

3.4.2 Fan Gated Rectangular Cavity with an Insert and Varying Thickness

For a more realistic case study, an L-shaped cavity with an insert at the center is designed as shown in Fig. 3-12.a. The part is then unfolded as a lay flat as shown in Fig. 3-12.b and the two dimensional cavity filling simulation is carried out with the approximated geometry.

Processing parameters and constants are as follows:

Melt Temperature: 493°K

Mold Wall Temperature: 303°K

Injection Rate: 10.0 cm^3/sec (whole cavity)

Material: polystyrene

All other material constants are the same as in the previous case study.

Initial input data for the finite element calculation is prepared based on the same assumption as in chapter 3.4.1 that the cavity is filled isothermally for a sufficiently short time (0.03 sec). Advanced melt fronts are generated automatically at each time step as shown in Fig. 3-13. Fig. 3-14 shows the predicted melt fronts at each time step. The simulation is carried out with the minimum of the user's judgment and completed in less than an hour, most of which is CPU time.

Due to the insert, a weld line is formed along the edge against the gate. Although a weld line can be handled as a movable boundary in the original numerical formulation, the generation of the weld line should be decided by the user. The automatic prediction of the weld line is not included in this thesis.

(a)

(b)

FAN
GATE

8.0

8 Cm

∅ 2.0

0.1

0.15
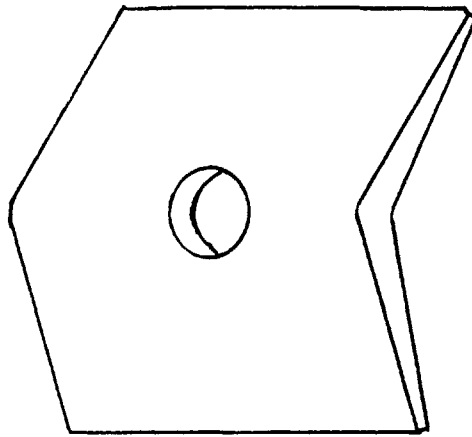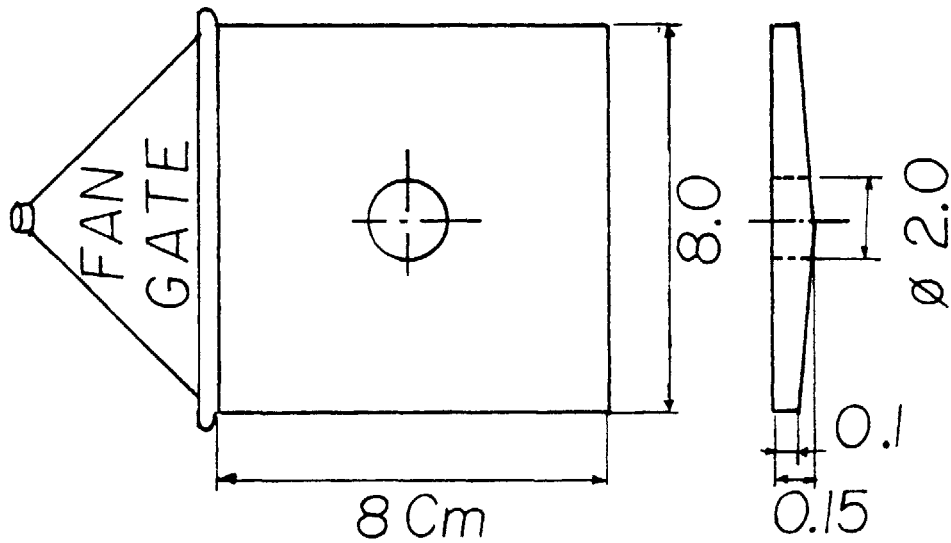
Figure 3-12: Fan Gated Rectangular Cavity with an Insert and Varying Thickness
(a) Part Shape, (b) Lay Flat Approximation
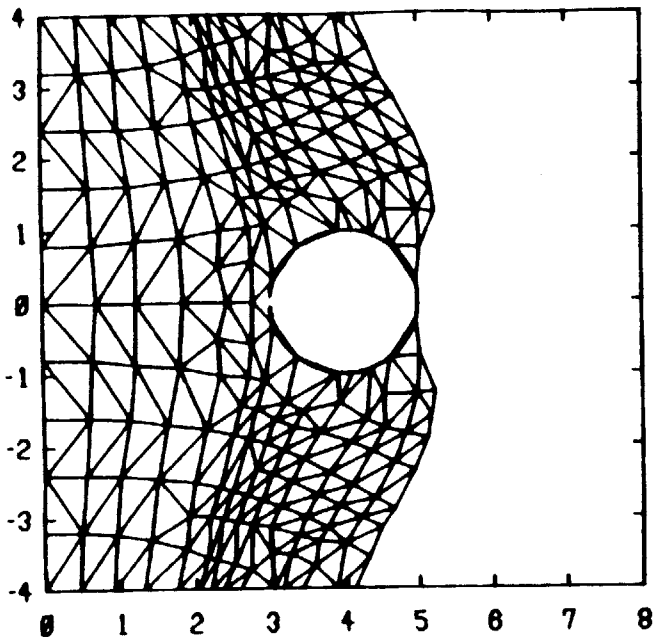
FILLING TIME : 0.402 SEC
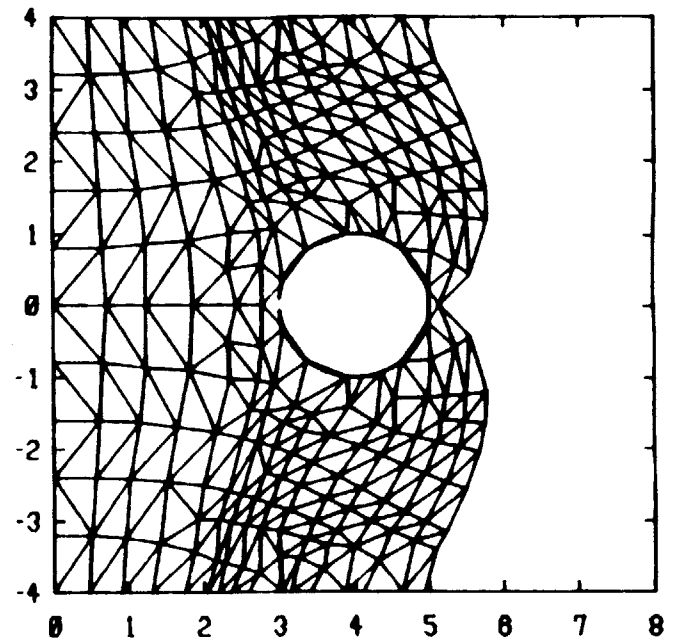
FILLING TIME : 0.48 SEC
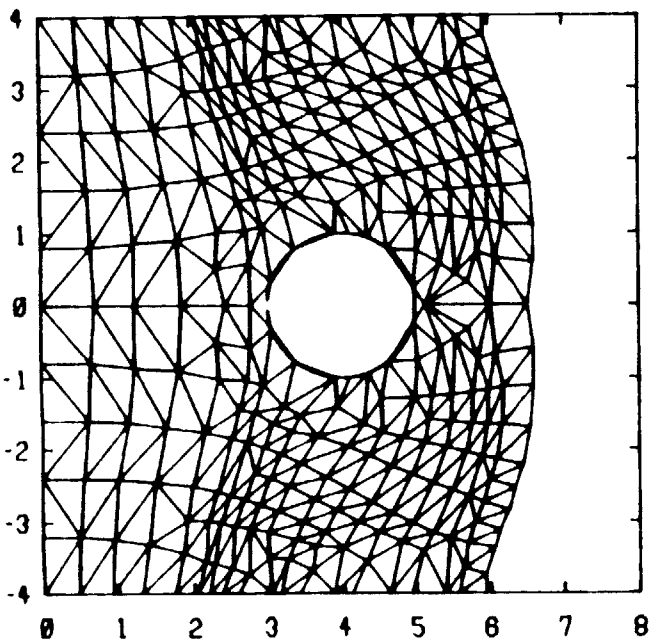
FILLING TIME : 0.548 SEC
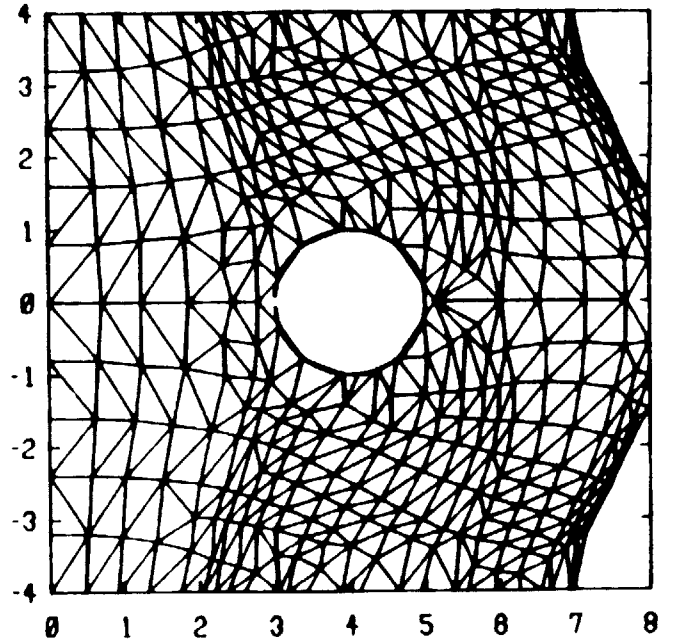
FILLING TIME : 0.883 SEC

Figure 3-13: Automatic Mesh Generation During the Flow Simualtion
Case Study 2: Rectangular Cavity with an Insert
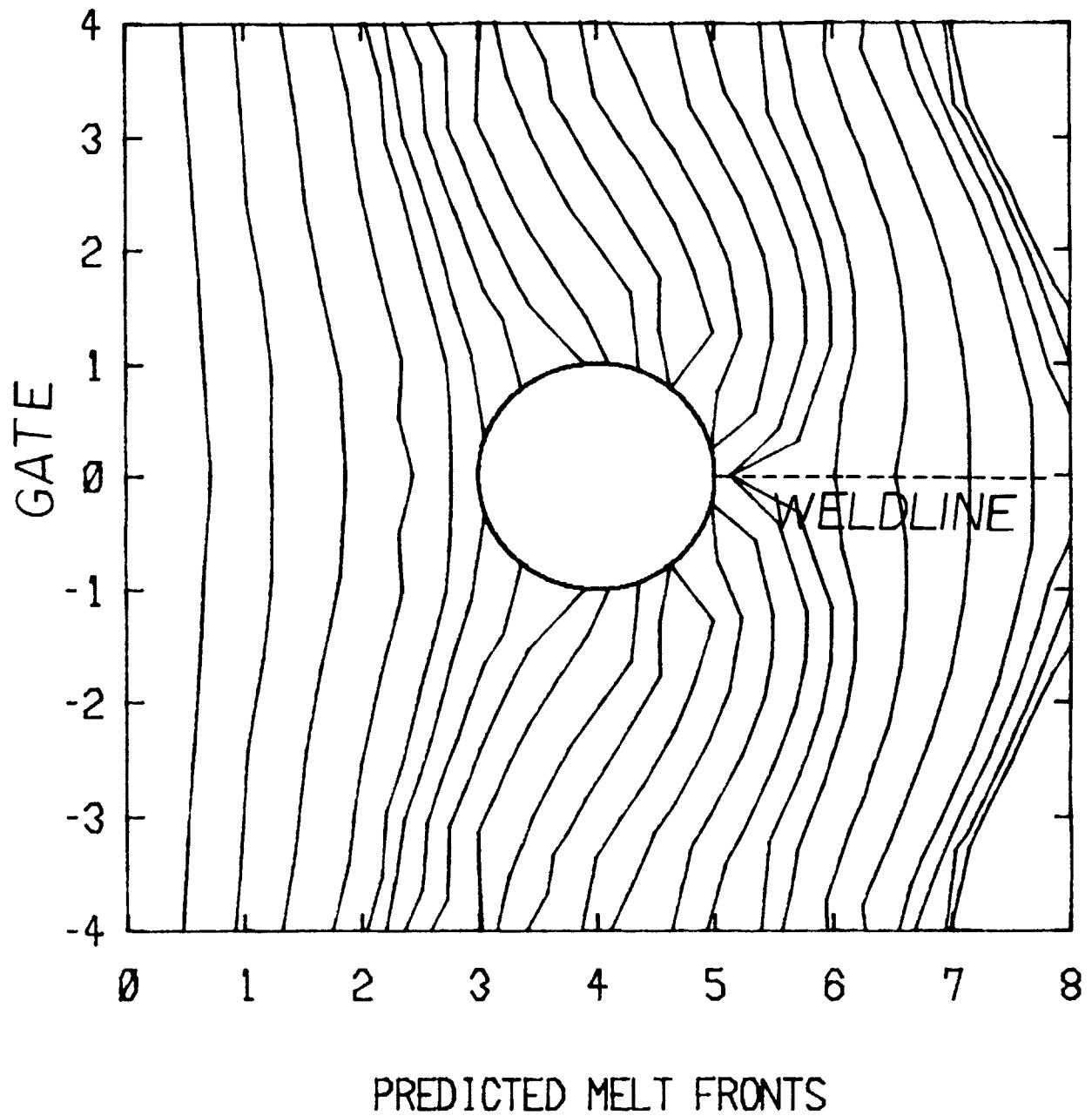
Figure 3-14: Predicted Melt Fronts at Each Time Step
Case Study 2: Rectangular Cavity with an Insert

3.5 Summary

Based on the FEM/FDM numerical analysis program developed by CIMP, a user transparent two dimensional cavity filling simulation program is developed in this thesis. An automatic mesh generation program is uniquely developed with the idea of the boundary-pressure-reflection scheme which enables the filling simulation to be completed in real time. Case studies proved that the program developed in this thesis can be used to simulate the filling stage of the injection molding quantatively.

As a part of quasi-three dimensional flow analyses, planar distributions of the thermomechanical properties are predicted from the two dimensional cavity simulation. A thermomechanical data base is constructed during the flow simulation as shown in Fig. 3-15. Based on this data base, a spatial distribution of microstructural anisotropies of the quasi-three dimensional injection molded part will be predicted in the following chapter.
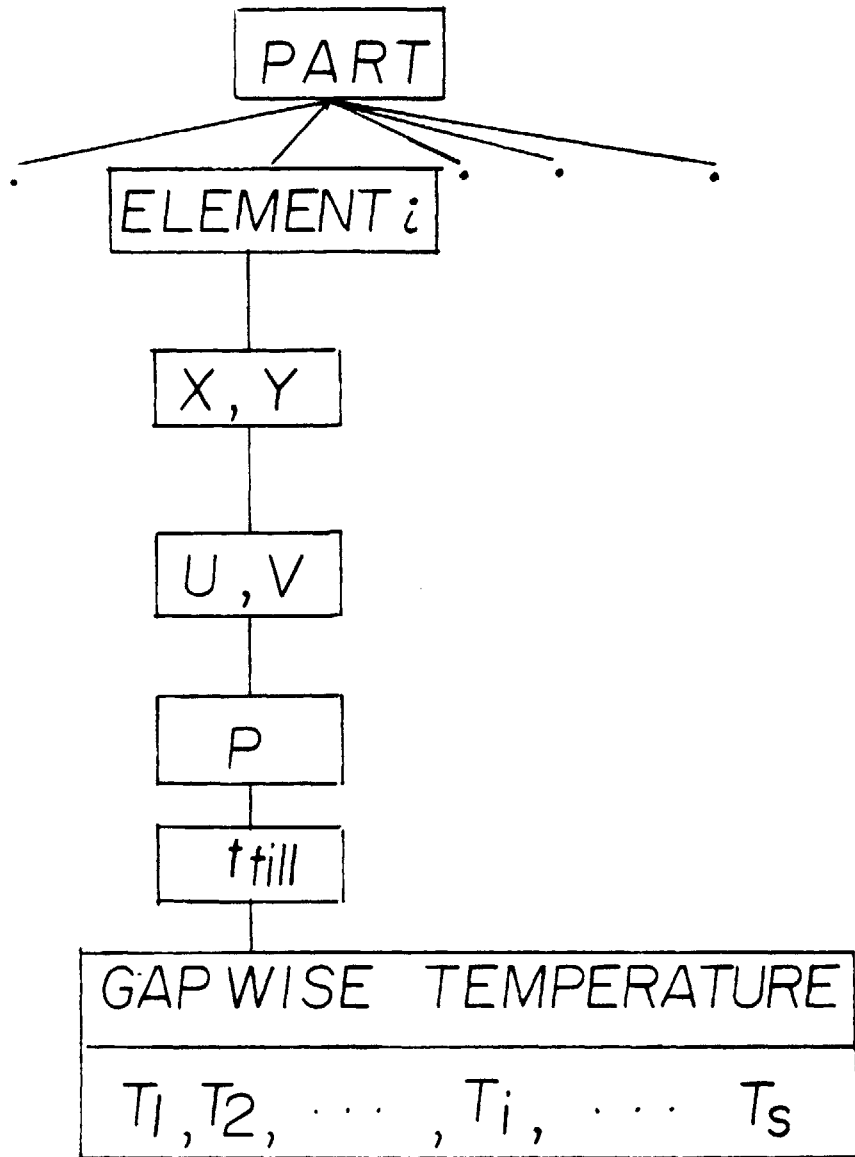
Figure 3-15: The Structure of the Thermomechanical Data Base

Chapter 4
Mechanical Anisotropies and Performance Prediction

4.1 Introduction

A thermomechanical data base is constructed by the cavity filling simulation. It contains a set of information which is necessary to predict the resulting three dimensional distribution of the microstructural anisotropies and the mechanical performance of a molded part. The moldability of the design can be readily predicted from the flow simulation by observing a necessary injection pressure during the filling simulation. When the necessary injection pressure does not exceed the limit of the machine's capacity, the design and associated toolings are thought to be feasible to produce a designed part. When the design is evaluated to be moldable, it becomes necessary to predict the mechanical behavior of the molded part.

The mechanical properties of injection molded parts are affected by the microstructural anisotropies within the part. These anisotropies are introduced during molding by a coupling of flow and cooling of polymer melt, which generates spatial variations of the molecular orientation and residual stresses within a molded part. This coupling further weakens the molded part *via* the formation of a weldline structure when melt fronts merge together inside the mold. These two factors, the molecular orientation and the weldline structure can adversely affect the mechanical behavior of the molded part unless the part and the mold are properly designed.

As part of the goal of this thesis which is to develop a computer-based rational design system for injection molding, the microstructural anisotropies of molded parts are theoretically predicted in this chapter based on the result of the cavity filling simulation.

4.2 Molecular Orientation

4.2.1 Background

The molecular orientation, which is often an unintentional accompaniment of polymer processing, has received considerable theoretical and experimental investigations [9, 18, 36, 45, 75]. The effect of molecular orientation on the mechanical properties of a molded part is most likely to be deterious, revealing themselves in the form of crazing under stress, or the loss of strength with respect to transverse stresses.

McGarry and Broutman [9] observed a reduction in energy for crack propagation with the increasing orientation for PMMA[6] and polystyrene. Curtis [14] measured the fracture surface energy for both PMMA and polystyrene, and experimentally determined the relationship between the tensile and impact strength of those materials as a function of molecular orientation as shown in Fig. 4-1. He used birefringence as a measure for different degrees of molecular orientation.

The phenomenological aspects of molecular orientation have been well characterized by many workers. They have confirmed that the prediction of the

---

[6]Polymethylmethacrylate
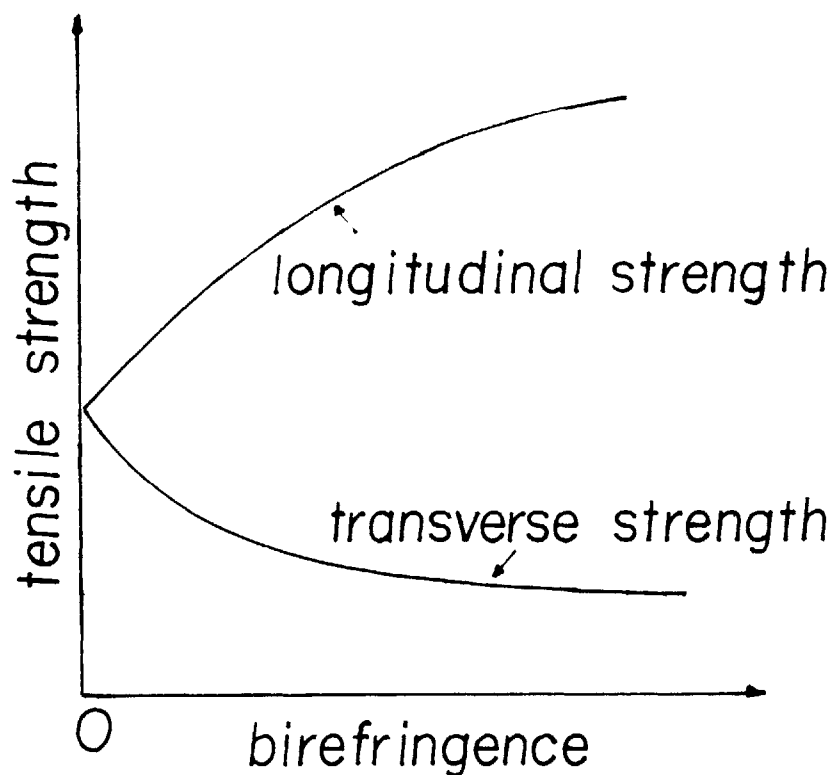
Figure 4-1: The relation between tensile strength of polystyrene and the
birefringence [14]

molecular orientation is essential to determine the mechanical properties of a
polymeric part.

In recent years, two research groups reported fairly convincing results in
theoretical prediction of the molecular orientation from a simple one dimensional
flow model. Isayev and Hieber [30] used an idealized one dimensional injection
molding problem to study the influence of processing variables on frozen-in flow
stresses and accompanied birefringence due to incomplete relaxation of the residual
stresses. They employed the Leonov's viscoelastic constitutive equation, which is
based on the irreversible thermodynamics theory, for the prediction of flow stresses

and subsequent relaxation. Although their theoretical model is better grounded than any other model at the present time, there is still a some discrepancy observed between the predicted values of orientation and the experimental measurements. This is, probably, due to the complex nature of the process which requires simplifying assumptions in deriving mathematical models.

On the other hand, Dietz and White [16, 76] developed a prediction model for the molecular orientation based on reasonable assumptions. They assumed that the state of the polymer melt consists of an isothermal core region and solidified layers in the wall region. They used an isothermal power-law flow model model in the core region and calculated the birefringence at the melt-solid boundary where the generated orientation is about to freeze-in by the subsequent cooling of the melt. The successive calculations with the growth of the frozen-layer thickness continue until the whole cavity is filled. After the cessation of flow, they consider nonisothermal stress relaxation by means of a simple Maxwellian-type model in which the relaxation time is not a function of shear rate, but only a function of temperature. In general, their predictions compared well with some experimental results, while consuming much less computation effort than the rigorous models do [70].

A local minimum gapwise birefringence has been observed between the surface of a part and the position of the local maximum birefringence as shown in Fig. 4-2. This observation was explained by Tadmor [63] and Menges [49] pointing out that there are two major sources of orientation in injection molding, such as, the elongational flow at the advancing melt front and the shear flow behind it. Tadmor [63] proposed that the surface birefringence is originated from the extensional flow at the melt front (fountain flow) and freezes in as soon as it
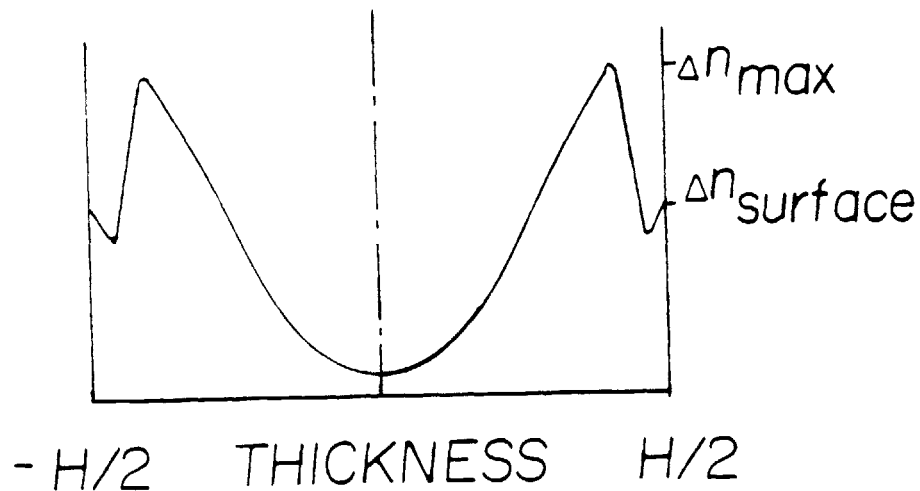
Figure 4-2: Typical Distribution of Gapwise Molecular Orientation
in Injection Molded Part

contacts the cold mold wall. In order to calculate the magnitude of the surface birefringence, a two dimensional simple extensional flow model was used.

4.2.2 Streaklinewise One Dimensional Shear Flow

In order to predict three dimensional distribution of the molecular orientation, a quasi-three dimensional flow analysis was proposed in Chapter 3. From the two dimensional cavity filling simulation, a planar distribution of thermomechanical properties of the melt during the process is calculated, except the temperature profile which is calculated in both the planar coordinates and the gapwise coordinate.

One dimensional flow analysis is applied along the streakline to get the gapwise distribution of molecular orientation as shown in Fig. 4-3. Due to the rapid increase of the viscosity in the solidifying layer, the velocity in that region is assumed to be
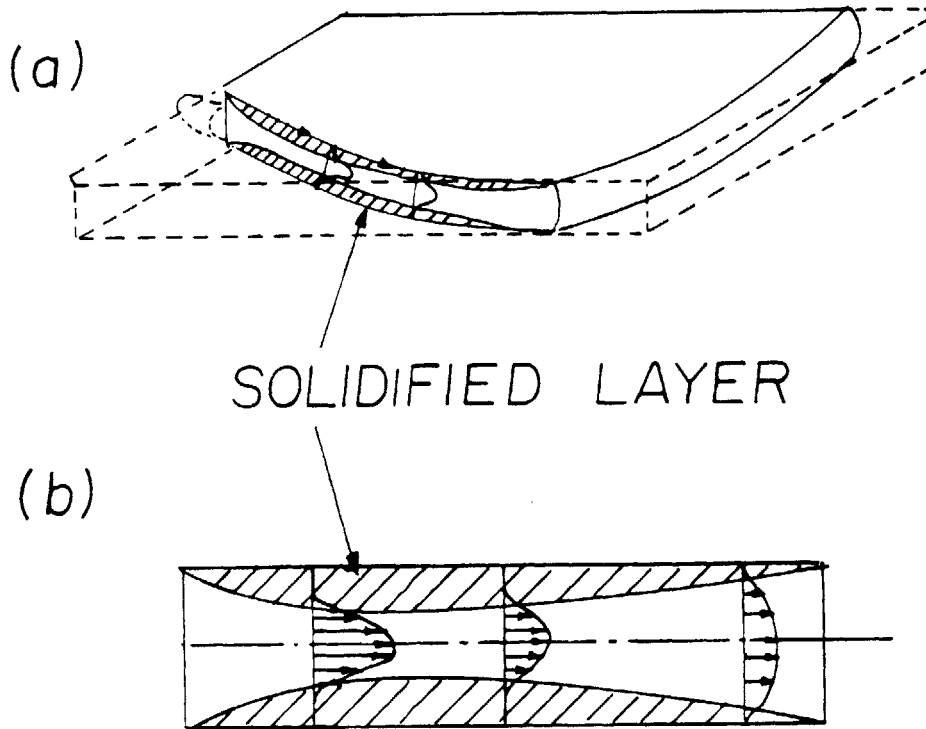
Figure 4-3: Quasi-Three Dimensional Flow Analysis for a Injection Molded Rectangular Cavity: (a) 2-D Filling Simulation (b) 1-D Streamwise Flow

neglible. The flow of melt which is confined between two thickening solidifying layers is idealized as an isothermal flow with a uniform melt temperature, Tc.

The assumed uniform core temperature, T_c, which differs from the initial melt temperature, T_m, is calculated by averaging the gapwise temperatures between the two cooled layers, which are obtained from the two dimensional cavity filling simulation.

$$T_c = \frac{1}{(H\text{-}H_s)} \int_0^{H\text{-}H_s} T(y,t)\,dy \qquad (4.1)$$

where H is the half gap thickness and H_s is the solidified layer thickness.

The thickness of the solidified layer is readily predicted from the result of the cavity filling simulation. The predicted thickness of the solidified layer along a typical streamline from the case study in section 3.4.2 is shown in Fig. 4-4, which is compared favorably with the experimental results [32]. As a vitrification temperature, $T_s = 130^\circ C$ is used for polystyrene.

As a result of the increase in cooled layer thickness, the average velocity of the isothermal melt in the core region increases as follows.

$$V = U\frac{H}{H\text{-}H_s} \qquad (4.2)$$

where U is the streamwise initial average velocity and V is the increased melt velocity between two solid layers.

Until the cessation of flow, the frozen-in shear stress and the accompanying birefringence increase with the growth of the solidifying layer. From the power-law flow model, shear stress at the solid-melt boundary is,

$$\tau_{12} = m_c\dot{\gamma}^n \qquad (4.3)$$

$$\dot{\gamma} = \frac{2n+1}{n}\frac{V}{H\text{-}H_s} \qquad (4.4)$$

where m_c is the shear viscosity, $\dot{\gamma}$ is the shear rate at $y = (H$ - $H_s)$, and n is the power law index.

The shear viscosity is assumed to have an Arhenius type temperature dependence, such as;

$$m_c = m_{ref}e^{-\alpha(T_c\text{-}T_{ref})} \qquad (4.5)$$

where material constants are same as in the ref. [16], such as:
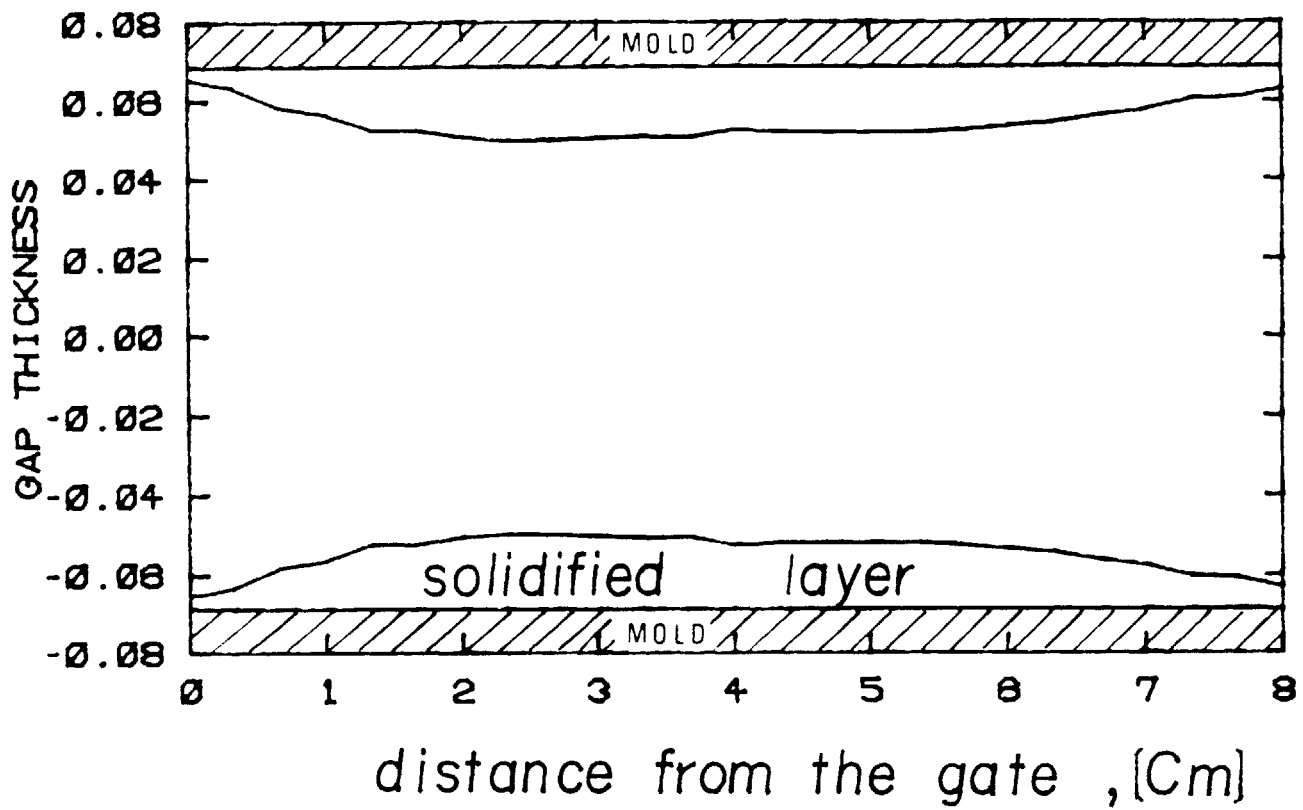
Figure 4-4: Predicted Solidified Layer Thickness along a Typical Streamline in Rectangular Cavity: from the case study in section 3.4.2

$$n = 0.36 \qquad \alpha = 0.025/^\circ K$$

$$T_{ref} = 463^\circ K$$

$$m_{ref} = 1.14*10^5 \ gm/cm.sec/sec^{0.64}$$

In order to calculate the first normal stress components, Dietz and White [76] employed an *ad hoc* procedure to correlate the normal stress to the shear stress on the basis of experimental steady shear data. Although there is a room for arguments in using the *ad hoc* procedure, the associated first normal stress components in this study are evaluated from the calculated shear stress using the experimentally determined correlations [16].

$$\tau_{11} - \tau_{22} = a\tau_{12}^{\ \alpha} \qquad\qquad (4.6)$$

where a and α are experimentally determined constants as follows.

$$a = 3.50*10^{-4} \ (\frac{dyne}{cm^2})^{1-\alpha}$$

$$\alpha = 1.685$$

if $\tau_{12} < 3.91*10^5 \ dyne/cm^2$

$$a = 1.29*10^{-6} \ (\frac{dyne}{cm^2})^{1-\alpha}$$

$$\alpha = 2.12$$

if $\tau_{12} > 3.91*10^5 \ dyne/cm^2$

The corresponding birefringence is then calculated by multiplying the stress optical coefficient to the calculated pricipal stress difference on the basis of the stress optical law [76].

$$\Delta n = C\sqrt{4\tau_{12}^2 + (\tau_{11} \text{-} \tau_{22})^2} \qquad\qquad (4.7)$$

where C is the stress optical coefficient. For polystyrene, the stress optical coefficient, $C = 4.9*10^{10}$ $cm^2/dyne$ as measured by Wales [69].

Until the cessation of flow, the above procedure is repeated. The calculated frozen-in birefringence increases as the flow channel narrows due to the growth of solidified layer. Therefore, the maximum birefringence due to the shear flow occurs at the melt-solid interface when the melt stops to flow. From the mold filling simulation, the filling time is predicted. Thus the position and the magnitude of maximum birefringence are readily determined by combining the one dimensional shear flow analysis and the two dimensional cavity filling simulation.

In subsequent cooling, there is no more melt flow and shear stresses. The stress relaxation continues until the whole melt cools to a solid. The stress relaxation after the filling stage is not included in this thesis by employing a reasonable approximated model for predicting the gapwise pattern of birefringence.

4.2.3 The Fountain Flow at the Melt Front

Tadmor [63] observed that the source of the frozen-in orientation at the skin layer is the central region of the melt front where the shear rates are negligible. This is known as a *fountain flow* effect as shown in Fig. 4-5. A two dimensional elongational flow model was proposed by Tadmor [63] to calculate the molecular orientation at the skin layer. The velocity profile of a two dimensional extensional flow in Fig. 4-6 is given by;
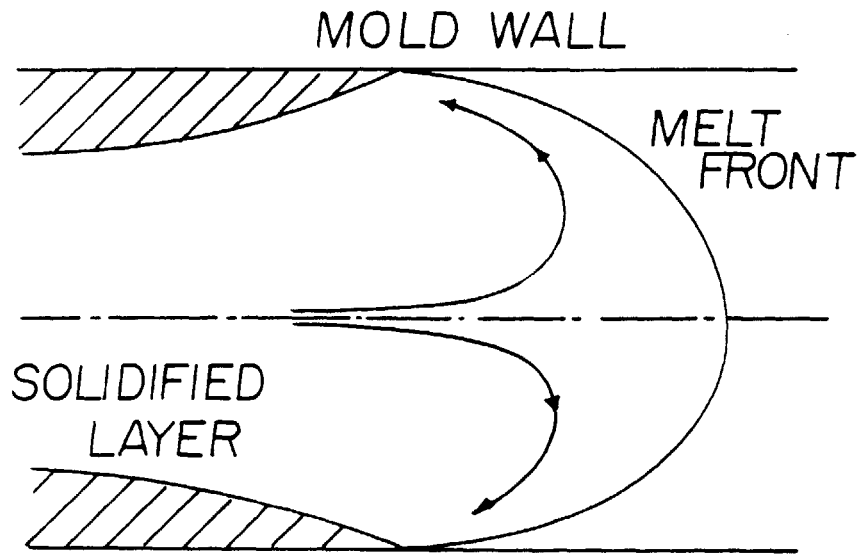
Figure 4-5: Schematic Representation of the Flow Pattern at the Advancing Melt Front between two Parallel Plates
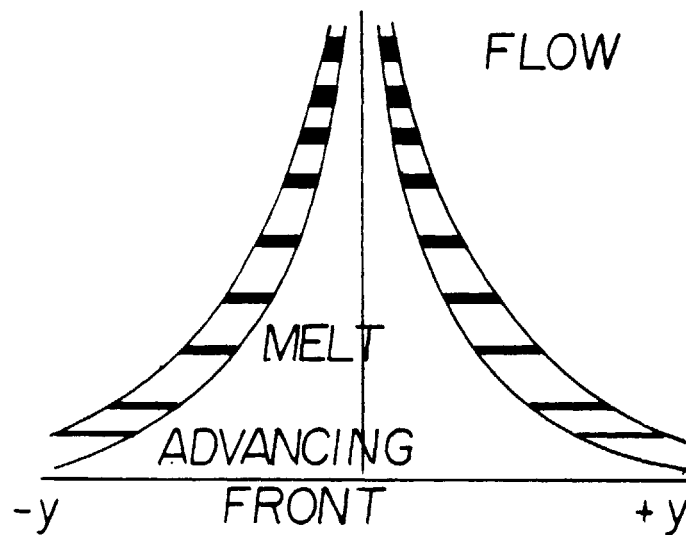
Figure 4-6: Two Dimensional Approximation of Fountain Flow

$$v_x = 0$$

$$v_y = \dot{\epsilon}\, y$$

$$v_z = -\dot{\epsilon}\, z \tag{4.8}$$

where $\dot{\epsilon}$ is the rate of elongation.

An experimentally determined extensional viscosity of polystyrene was used by Dietz and White [16] to calculate the principal stress difference, $\Delta\sigma_o$, at the flow front as a product of the rate of elongation and the extensional viscosity. This can be written as;

$$\Delta\sigma_o = \Psi_e \dot{\epsilon} \tag{4.9}$$

where Ψ_e is the extensional viscosity of the melt.

For the calulation of the surface birefringence, equation(4.8) and equation(4.9) are used in this thesis without further arguments.

4.2.4 Approximation

In previous sections, quantitative models to explain the gapwise distribution of the molecular orientation was discussed. By comparing the experimental measurements of birefringence with the theoretical models, following similitudes in the pattern of gapwise birefringence are observed.

(1) There is a local maximum of birefrtingence at the surface which is mainly determined by the elongational flow at the melt front. As soon as the advancing melt front which spills from the center toward the wall touches the cold mold wall, the elongational stress is frozen-in to the surface without relaxation.

(2) There is a local maximum of birefringence at the location which coincides with the thickness of the solidifying layer at the instant of complete filling. This can be calculated by applying the simple shear flow model along the streamline with known temperature profiles and the filling time which have been predicted from the filling simulation.

(3) There is a local minimum point between the surface and the internal maximum point. This is resulted by overlapping of the increasing shear stress on the diminishing elongational stress which was originated from the advancing melt front.

(4) The magnitude of birefringence inside the core region is dependent on the cooling rate which usually determined by the thickness of the part and the temperature of the mold. Incomplete relaxations of the shear stresses remain as residual stresses which can be approximated as quadratic distributions.

In summary, there are four local min/max points in the magnitude of cross sectional molecular orientation. Their locations are the surface, the immediate skin layer, the melt/solid boundary at the end of filling, and the center which has more time to relax its orientation. In order to simplify the prediction, the similar patterns of the birefringence are characterized by the four min/max points.

It is observed that the local minimum location is very close to the surface in most cases. Therefore a linear interpolation is employed between the surface birefringence and the internal maximum birefringence. The quadratic approximation is used between the maximum birefringence and the center of the core region which is assumed to be fully relaxed.

Based on this approximation, the gapwise distribution of orientation is predicted by calculating the maximum birefringence from the shear flow analysis and

the surface birefringence from the elongational flow analysis. In order to compare the result of approximated prediction which is derived in this thesis with other experimental and theoretical data, a rectangular cavity, as shown in the Table. 4-I, is chosen and the simplified procedure is applied to it.

inj speed cm/s	melt temp °k	mold temp °k	half gap thickness cm	width cm	length cm
12	503	323	0.1	7.5	30

Table 4-I: Rectangular Cavity Specifications

Curve (a) in Fig.4-7 is the experimentally measured birefringence by Wales [69]. Curve (b) is the predicted birefringence pattern by Dietz and White [16]. Curve (c) is calculated by Isayev, Shen and Hieber [70]. Curve (d) is the pattern predicted in this thesis with simple approximation between characteristic points.

In general, the approximation employed in this thesis is proved to be a reasonable method to predict the gapwise pattern of molecular orientation, while reducing the computation effort enormously. With the thermomechanical data base from the cavity filling simulation, this approximate prediction method is applied along each streamline to predict the three dimensional distribution of the molecular orientation. The detailed numerical steps for the prediction are discussed in Appendix. A.
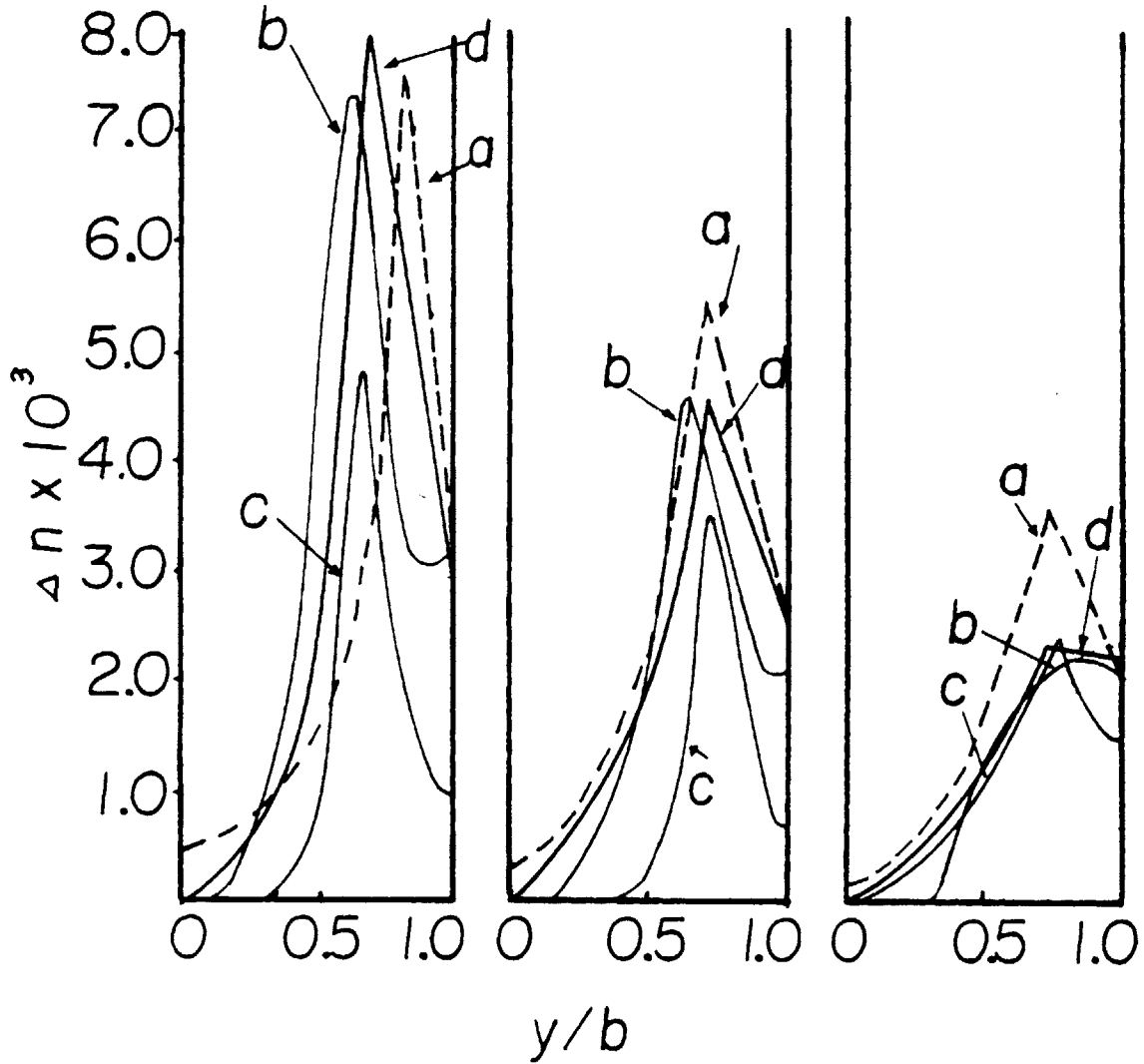
Figure 4-7: Gapwise Birefringence Pattern in Rectangular Cavity:
(a) Experimantal Measurement [69], (b) Prediction Ref. [16]
(c) Prediction Ref. [70], (d) Prediction in this thesis

4.3 Strength Ellipse

A spatial variation of the molecular orientation within a molded part is obtained by a simple and reasonable method. The objective of the microstructure prediction is to evaluate the mechanical performance of a molded part. The effect of orientation on the mechanical properties of a molded part has been well characterized experimentally [9, 14, 28]. Among these works, Hoare and Hull [28] regarded a molded part as a composite structure of layers with different degrees of anisotropies and orientation as shown in Fig. 4-8.
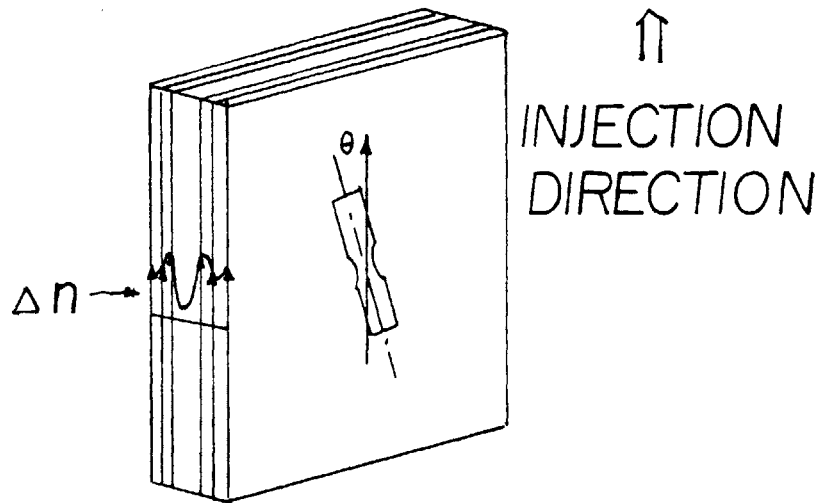
Figure 4-8: Injection Molded Part as a Composite Structure [28]

Although they did not quantatively predict the mechanical properties from the measured birefringence, they suggested a possibility of theoretical prdiction on the

basis of predicting the molecular orientation.

Consider a sufficiently small planar element as an orthropic laminae. It is assumed that the laminae represents the local distribution of the microstructure at a certain location of a thin injection molded part. It is also assumed that the major orientation occurs along the flow direction [48] and the averaged molecular orientation along the thickness represents the magnitude of the anisotropic strength of the laminae as shown in Fig. 4-9.
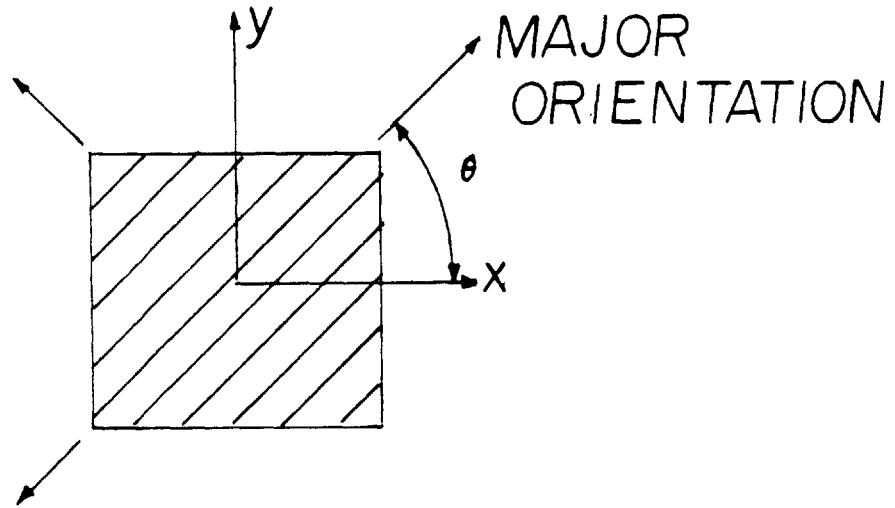
Figure 4-9: An Orthotropic Laminae

For the idealized orthropic laminae under a plane stress condition, the Tsai-Hill failure criterion [29] is applied to determine the strength locus at different angle as follows.

$$(\frac{\sigma_L}{\sigma_L^*})^2 - (\frac{\sigma_T \sigma_L}{\sigma_T^{*2}}) + (\frac{\sigma_T}{\sigma_T^*})^2 + (\frac{\tau}{\tau^*})^2 = 1 \tag{4.10}$$

where σ_L^* is the tensile strength of the material along the orientation, σ_L is the longitudinal tensile stress. Likewise, σ_T^* is the transverse tensile strength, σ_T is the

transverse tensile stress, τ^* is the shear strength of the laminae and τ is the shear stress.

The shear strength, τ^*, can be obtained *via* off-axis tests [29]. As an effort to determine the relation between the shear strength and the molecular orientation, the experimental results of tensile test by Hoare and Hull [28] are used in place of the off-axis test. However, due to the mixed mode fracture in the range of angle, $20^\circ < \theta < 70^\circ$, the shear strength can not be obtained from the experimental results as the orientation increases. Therefore, the explicit form of the Tsai-Hill criterion can not be used in this application. However, it has been proved experimentally that the longitudinal tensile fracture occurs in the range of angle, $0^\circ < \theta < 20^\circ$, and the transverse tensile fracture occurs in the range of angle, $70^\circ < \theta < 90^\circ$.

A simplified form of strength ellipse is proposed in order to represent effectively the spatial distributions of anisotropic properties within a molded part and to compact the microstructural database of them.

$$(\frac{\sigma_L}{\sigma_L^*})^2 + (\frac{\sigma_T}{\sigma_T^*})^2 = 1 \tag{4.11}$$

The major axis of the ellipse by equation(4.11) represents the major direction of the molecular orientation. The intercept on the major axis represents the longitudinal tensile strength and the intercept on the minor axis represents the transverse strength as shown in Fig. 4-10. In a graphical form of a strength ellipse, the magnitude and the direction of the molecular orientation within a molded part and its effect on the mechanical strength of the part are represented comprehensively.
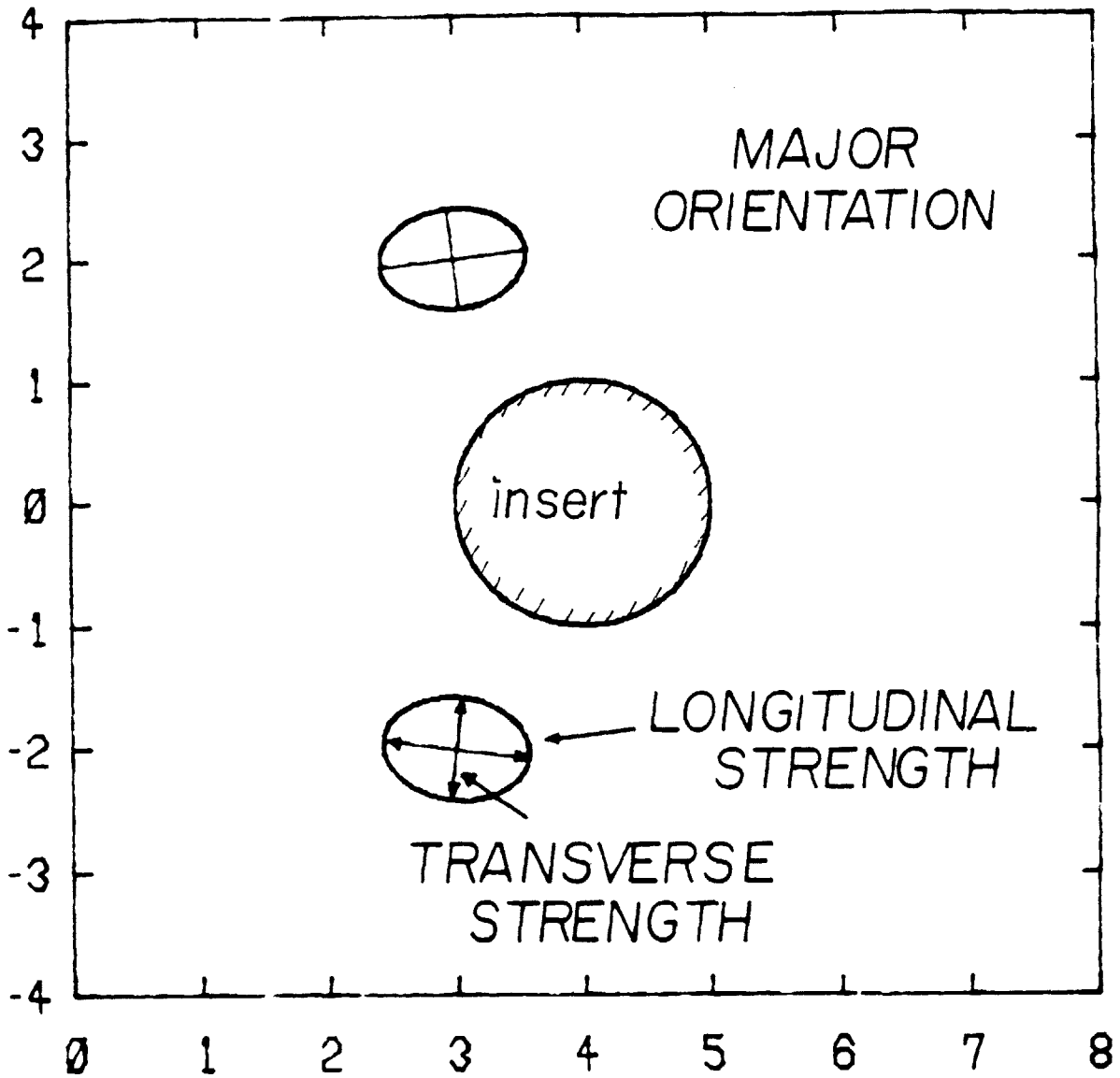
Figure 4-10: The Strength Ellipse

4.4 Weldline

4.4.1 Introduction

The presence of a weldline generally reduces the mechanical strength of injection molded parts. A typical remedy to eliminate the problem of weak weldline structure has been to increase the melt temperature. This, however, is not an acceptable solution in some situations. A general solution to the weldline problem requires an in-depth understanding of the thermomechanical history of the injection molding process. In this section, a theoretical model for the strength of weldlne is presented, which provides a comprehensive physical insight of the bonding process at the weldline interface. The model is based on the self-diffusion of molecular chains across the polymer-polymer interface and the frozen-in orientation which remain parallel to the interface. Both factors are analyzed separately and then superimposed to predict the strength of weldlines from known processing conditions and geometry. Experimental results show good correlation with predictions.

4.4.2 Origins of Weldline Weakness

The development of molecular orientation during flow and its effect on the strength of molded parts are reasonably well understood in the previous sections. However, the strength of weldlines cannot be predicted *a priori* based on the processing information using the models developed in the past [23, 25, 46], although the phenomenological aspects of the weldline formation are well known.

Weldlines form due to the presence of cores, pins and multiple gates. They also form when jetting occurs due to an abrupt change in geometry, such as near a gate. It has been observed that the presence of weldlines generally reduce the

strength of injection molded parts. In order to eliminate this problem, a number of remedies has been investigated. Experimental results showed that the strength of the weldline structure increased as the melt temperature was raised [46]. However, the strength of very thin parts with weldlines decreases with an increase in the melt temperature in some temperature range [25]. These contradictory results show that the weldline strength cannot be predicted based solely on experimental results. The purpose of this section is to present a theoretical model for the strength of weldlines by identifying and analyzing the causes of weldline weakness. The strength of the weldline is predicted from known processing conditions and geometry for amorphous glassy thermoplastics which do not undergo crystallization and morphological changes.

Hagerman [23] investigated the tensile strength of weldlines under different molding conditions and observed that the the weakness of a weldline can be attributed to the following three factors (Fig. 4-11):

1. A lack of mixing at the interface of the two melt fronts.

2. The frozen-in molecular orientation which is caused by the fountain flow effect at the melt front and remains parallel to the interface.

3. The existence of V-notches around the weldline surface, caused by entrapped air or contaminants.

It is reasonable to assume that these are three major factors that determine the strength of a weldline of an amorphous polymer, although they have not been analyzed quantitatively vis-a-vis the strength of weldlines. In the case of crystalline polymers, the size and distribution of the crystalline structure also determine the strength of semicrystalline polymers.

In this thesis, the effect of morphology on strength is not considered, since this
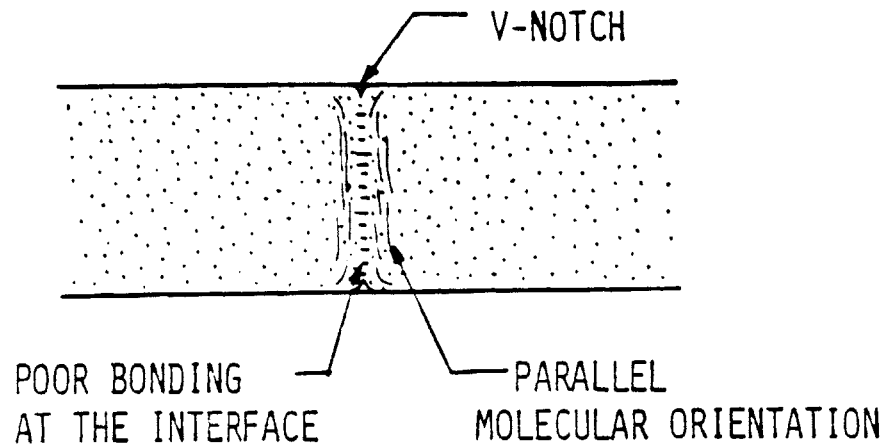
Figure 4-11: Origins of Weldline Weakness

analysis is applied only to amorphous glassy polymers. The effect of V-notches is also disregarded, because they are not generated as a direct consequence of the thermomechanical history of the injection molding process, and because they can be eliminated by special processing techniques [46]. This thesis does consider the effect of poor bonding at the interface and the effect of parallel molecular orientation. They are analyzed in a decoupled way, neglectng the interaction between these two factors. Molecular orientation at the interface may have an effect on the chain interdiffusion across the polymer-polymer interface depending on the direction of the orientation. This coupled phenomenon is not considered here, although it can have important second order effects.

4.4.3 Bonding at the Interface of Melt Fronts

Consider the interface of homogeneous polymer melt fronts which just came into contact. Initially, there are no molecular chains bridging the interface, since no gross mechanical mixing due to the flow instability can be present in typical injection molding process. However, at the instant of contact, the molecules at the melt front are highly oriented because of the extensional and shear deformation that exist at the melt front during the filling process. Consequently, the free energy at the melt front interface is different from elsewhere. This free energy gradient can cause self-diffusion of molecules across the interface, gradually randomizing the molecular orientation and bridging the interface with long chained molecules. The bonding strength at the weldline increases with the degree of diffusion of molecules. Therefore, the bonding strength is affected by all the factors that control the diffusion rate.

The chain diffusion at the interface of homogeneous polymer is a special type of mass transfer and has been studied at the level of chain dynamics under the restriction of entanglements [33, 41, 78]. However, those microscopic descriptions of the motion of macromolecules can not relate the processing variables of injection molding to the macroscopic properties of the weldline structure. An alternative approach to the healing of a homogeneous polymer interface at the weldline is to model it macroscopically using a Gibb's free energy approach.

For the purpose of modelling, consider the healing process. When two melt fronts meet together for the first time, there are no molecular chains bridging the interface. If whole molecular chains can move freely across the interface, perfect bonding can be obtained immediately, where there is no difference in spatial

distribution of the chain density between the melt interface and the bulk. When the melt temperature drops below T_g before a sufficient number of molecular chains cross the interface and are randomized, various intermediate degrees of bonding occur (Fig. 4-12). The bond strength is proportional to the density of molecules crossing the interface. For simplicity, the intermediate stage of bonding may be idealized as consisting of one unbonded area and the other fully bonded area. If we denote the unbonded area where there is no molecular chain across the interface, as A, and the fully bonded area where the chain crossing density is equal to that of the bulk material, as A_o-A, where A_o is the initial cross-sectional area of the interface, then the strength of the weld interface, σ_w, may be expressed as:

$$\sigma_w = \frac{A_o\text{-}A}{A_o}\sigma_b \qquad (4.12)$$

σ_b is the tensile strength of the bulk without any orientation.

The degree of bonding which is defined as the ratio, $\dfrac{\sigma_w}{\sigma_b}$, can be obtained from equation (4.12) by calculating the unbonded area at the instant when the melt temperature drops below T_g.

The free energy difference, ΔG, between an intermediate degree of bonding and the perfect bonding is the driving potential for diffusive bonding at the weldline. The self-diffusion constant D represents the degree of activation to overcome the energy barriers on the way to the stable equilibrium state. Then, the decreasing rate of no-bonding area can be represented as a special type of mass transfer using Fick's first law.

$$\frac{dA}{dt} = C\frac{D\Delta G}{kT} \qquad (4.13)$$

A. NO BONDING

C.PERFECT BONDING

B.INTERMEDIATE STAGE
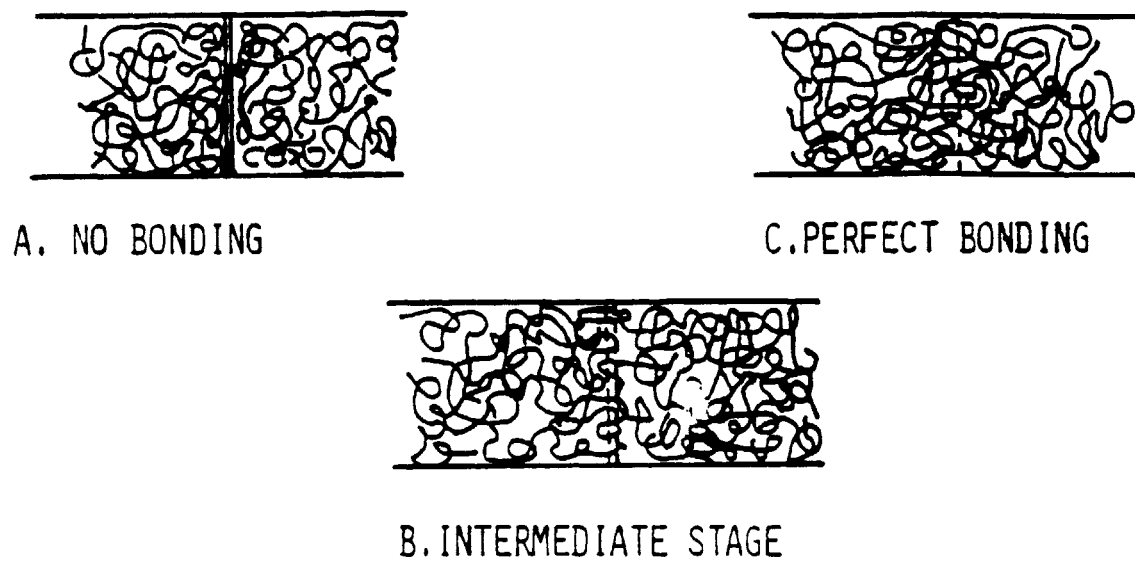
Figure 4-12: Stages of Diffusive Bonding at the Interface of
Homogeneous Amorphous Polymer Melt Fronts

Here, C is a constant which can be determined from the condition that the rate of interfacial area change, $\dfrac{dA}{dt}$, is zero at the glass transition temperature T_g.

The free energy difference can be written as the sum of surface energy of the remaining interface and the configurational entropy of mixing;

$$\Delta G = -2\gamma A - T\Delta S_m \qquad (4.14)$$

The surface energy of a polymer melt can be measured at various melt temperatures, and the entropy of mixing, ΔS_m, can be calculated by applying the Flory-Huggins Lattice Theory for a finite volume element and integrating over the entire volume of penetration at the interface [21]. It is assumed here that the combinatorial entropy, which is due to the geometrical rearrangement of the mixing molecules, is the major contributor to the entropy of mixing. For a small volume element δV which has δn_o lattices, the possible number of arrangements for m segments of long molecular chains into this element may be written as;

$$\Omega_{\delta v} = \left\{\frac{m}{(\delta n_o - m)!}\right\} \left\{\frac{Z-1}{\delta n_o}\right\} m \qquad (4.15)$$

The combinatorial entropy of mixing in δV is given by Boltzman's equation,

$$\Delta S_m|_{\delta v} = k \, \ln\Omega_{\delta v} \qquad (4.16)$$
$$= -k \, \delta n \, \ln v$$

Then the total change of entropy of mixing at the interface of area A is obtained by integrating equation (4.16) over the volume of penetration as :

$$\Delta S_m = -kA \, \delta x \, \delta n_o \, \ln\left(\frac{1}{2}\right) \qquad (4.17)$$

The rate of chain diffusion is determined by the self-diffusion constant at a given free energy difference. In low molecular weight liquids, the self-diffusion

constant is obtained by considering the total number of jumps molecules make to occupy neighboring holes [68]. However, long molecular chains cannot move as a single unit; instead, a small portion of a molecular chain will jump from one position to another constrained by the entanglements of the molecule with the segments of its neighboring molecules [12, 68]. Alternatively, the self-diffusion constant of amorphous high polymers (including the effect of entanglements) can be calculated in terms of the viscoelastic parameters of the material as follows [11, 12]:

$$D = \frac{\rho kT \, N_A \, R^2}{36 \, \eta \, M_w}$$

(4.18)

R^2/M_w, is the ratio of the square of mean end-to-end distance of molecular chains to the molecular weight. It is essentially a constant for a bulk polymer, and can be readily determined from light scattering data. Therefore, it is possible to predict the self-diffusion constant D if the bulk viscosity η is known. Experimental measurements confirm the calculated values of D within an experimental error [11].

From equations (4.13)-(4.18), the rate of the unbonded area change may be expressed as an integrable form:

$$\frac{1}{A} \, dA = - \frac{CD}{kT} \left(2\gamma - \frac{0.98}{\sqrt{2}} \, kT \, \delta x \, \delta n_o \right) \, dt$$

(4.19)

By integrating equation (4.19) and substituting it into equation (4.12), the degree of bonding due to the molecular interdiffusion across the interface may be expressed as a function of time and temperature:

$$\frac{\sigma_w}{\sigma_b} = 1 - \frac{A}{A_o}$$

(4.20)

$$= 1 - exp\left\{ - \frac{CD}{kT} \left(2\gamma - \frac{0.98}{\sqrt{2}} \, kT \, \delta n_o \, \delta x \right) t \right\}$$

4.4.4 Effect of Molecular Orientation

In highly oriented polymers, the deformation mechanism of molecules along the direction of orientation is the backbone-chain stretching or angle opening of a folded chain. Hence, the strength in the direction of orientation is greater than that of the orientation-free structures. On the other hand, the strength perpendicular to the orientation is less than that of the orientation-free polymers, since the deformation along this direction occurs when the weak intermolecular bond forces are overcome [14].

During mold filling, the melt front is subject to the so called "Fountain Flow", which is an elongational flow [63]. Molecular chains at the melt front are stretched parallel to the weld plane as a result of this flow. Some of this orientation is relaxed during solidification and the rest is frozen in. This molecular orientation which remains parallel to the interface makes the weldline structure weak when forces are appied perpendicular to the weldline.

The strength of the weldline can be predicted based on the assumption that the two melt fronts make perfect bond at the weldline interface and that only the orientation affects the bond strength. This can be done since the degree of orientation for amorphous poystyrene can be quantified by the birefringence index via the stress-optical law [16], and the tensile strength perpendicular to the orientation can be predicted from the experimental strength-orientation curve. The calculated average birefringence index in thickness direction of the weldline will be used as a measure of orientation.

Tadmor [63] modeled the melt front which flows through a thin rectangular cavity as an elongational flow. White [76] calculated the initial principal stress

difference, $\Delta\sigma_o$, at the flow front as a product of the rate of elongation, $\dot{\epsilon}$, and the extensional viscosity of the melt, Ψ_e, which was determined experimentally. This may be written as:

$$\Delta\sigma_o = \Psi_e \, \dot{\epsilon} \qquad (4.21)$$

During mold filling, the melt front spills from the center toward the wall, and the initial orientation freezes-in without relaxation as soon as the melt touches the cold mold wall. The initial principal stress difference may be related to the initial magnitude of the frozen-in birefringence index as:

$$\Delta n_o = C_o \, \Delta\sigma_o \qquad (4.22)$$

Here, C_o is a stress optical coefficient for a polymer melt.

In case of weldline formation, it is assumed that there is no more flow right after the two flow fronts meet together, and that the initial orientation generated by the fountain flow is uniform along the weldline interface. The initial orientation begins to freeze-in from the surface as soon as the melt temperature drops below T_g. But the molecules in the interior have more time to relax their orientation before they are frozen-in than those near the mold surface due to the low thermal conductivity of polymer melts. The frozen-in orientation may be characterized using a single integral constitutive equation for the calculation of stress relaxation [45], as:

$$\Delta\sigma(y,t) = \Delta\sigma_o \, exp(-\tau_r(y,t)) \qquad (4.23)$$

$$\tau_r(y,t) = \frac{1}{\tau_o}\int_0^t \frac{dt^*}{a_T(t^*)} \qquad (4.24)$$

Here, τ_r is the weighted relaxation time and the shift factor a_T can be obtained from the WLF equation.

The one dimensional unsteady heat conduction equation can be used to obtain the thicknesswise temperature history, which may be written as:

$$\frac{\partial T(y,t)}{\partial t} = \alpha \frac{\partial^2 T(y,t)}{\partial y^2}$$

$$T(y,0) = T_m$$

$$T(\frac{L}{2},t) = T_d$$

(4.25)

Here, T_m is the initial melt temperature and T_d is the mold temperature. The actual melt temperature at the melt front may be a little bit different from the melt temperature measured at the nozzle due to the partial cooling at the melt - air interface and due to the frictional heat generation. In this analysis, the nozzle temperature is used as T_m.

By solving equation(4.25), the solidification time which is the duration for the melt temperature to drop below T_g can be determined as a function of thickness. By substituting it into equations(4.22) (4.24), the amount of relaxation and the thicknesswise frozen-in birefringence index can be obtained. Then the averaged birefringence, $\Delta \underline{n}$, along the depth direction of the weldline may be written as:

$$\Delta \underline{n} = \frac{\int_0^L C_o \, \Delta\sigma_o \, exp(-\tau_r) \, dy}{L}$$

(4.26)

For the case of general purpose polystyrene, the tensile strength in the direction perpendicular to the orientation was read from the experimental strength-birefringence diagram (Fig. 4-13) with the averaged birefringence index along the weldline calculated from equation(4.26). The curve (B) of Fig.4-16 is the predicted tensile strength of this material with weldline, considering only the effect of molecular orientation frozen-in parallel to the weldline interface.
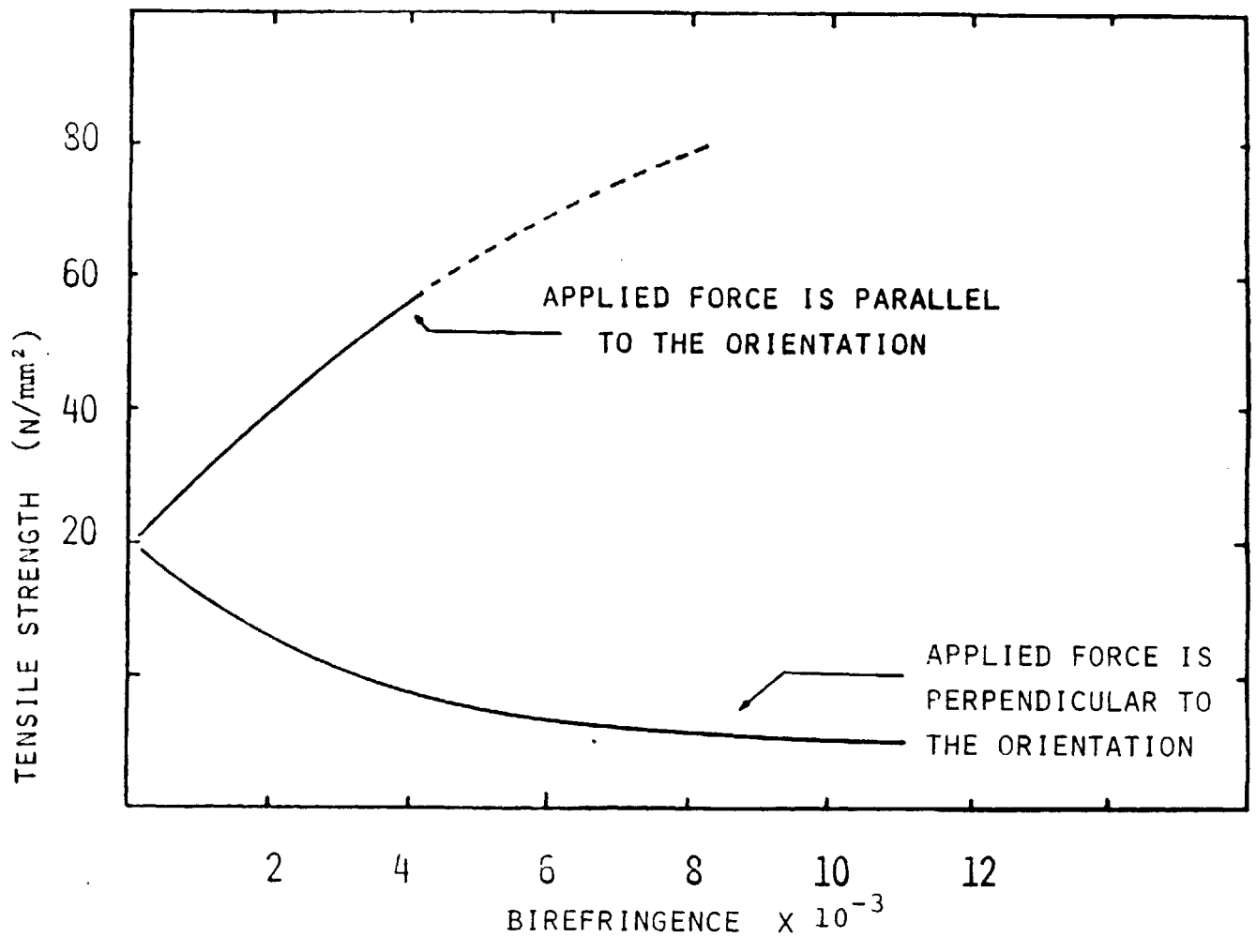
Figure 4-13: Strength - Birefringence Curve of General Purpose Polystyrene [14]

4.4.5 Predictions and Experimental Results

In order to compare the theoretical prediction with the experimental results, weldlined specimens were prepared by injecting general purpose polystyrene (DOW STYRON 678) at four different melt temperatures into a two gated mold. The same material and processing data in the experiments were used in the theoretical prediction. From equation (4.20), the degree of bonding is plotted as a function of time on the basis of the chain diffusion model for bonding (Fig. 4-14). It is noted from this figure that almost instantaneous bonding can be obtained above the melt temperature of $190^{\circ}C$. This means that the molecular chains have sufficient energy to move across the weldline interface. This temperature coincides with the "liquid to liquid transition temperature ($T_{l,l}$)" of polystyrene, which is a second order transition temperature where translational chain movement can occur while rotational chain movement can occur at T_g [8, 66]. In the actual injection molding process, the degree of bonding is a function of melt temperature rather than a function of contact time. This is because melt fronts cannot remain above T_g for long. Therefore, the degree of bonding from equation (4.20) is plotted as a function of melt temperature at a fixed time window (10 sec) (Fig. 4-15).

By calculating the average birefringence from equation (4.26), the tensile strength perpendicular to the orientation can be predicted from the tensile strength-birefringence relation for general purpose polystyrene (Fig. 4-13) at different melt temperatures. The ratio of the predicted tensile strength to that of the orientation free polystyrene is plotted as curve B in Fig. 4-16. Then Fig. 4-15 is superimposed on Fig. 4-16 as curve A and the final prediction of weldline strength is obtained by taking the lower value of either curve A or curve B of Fig. 4-16. The solid line in
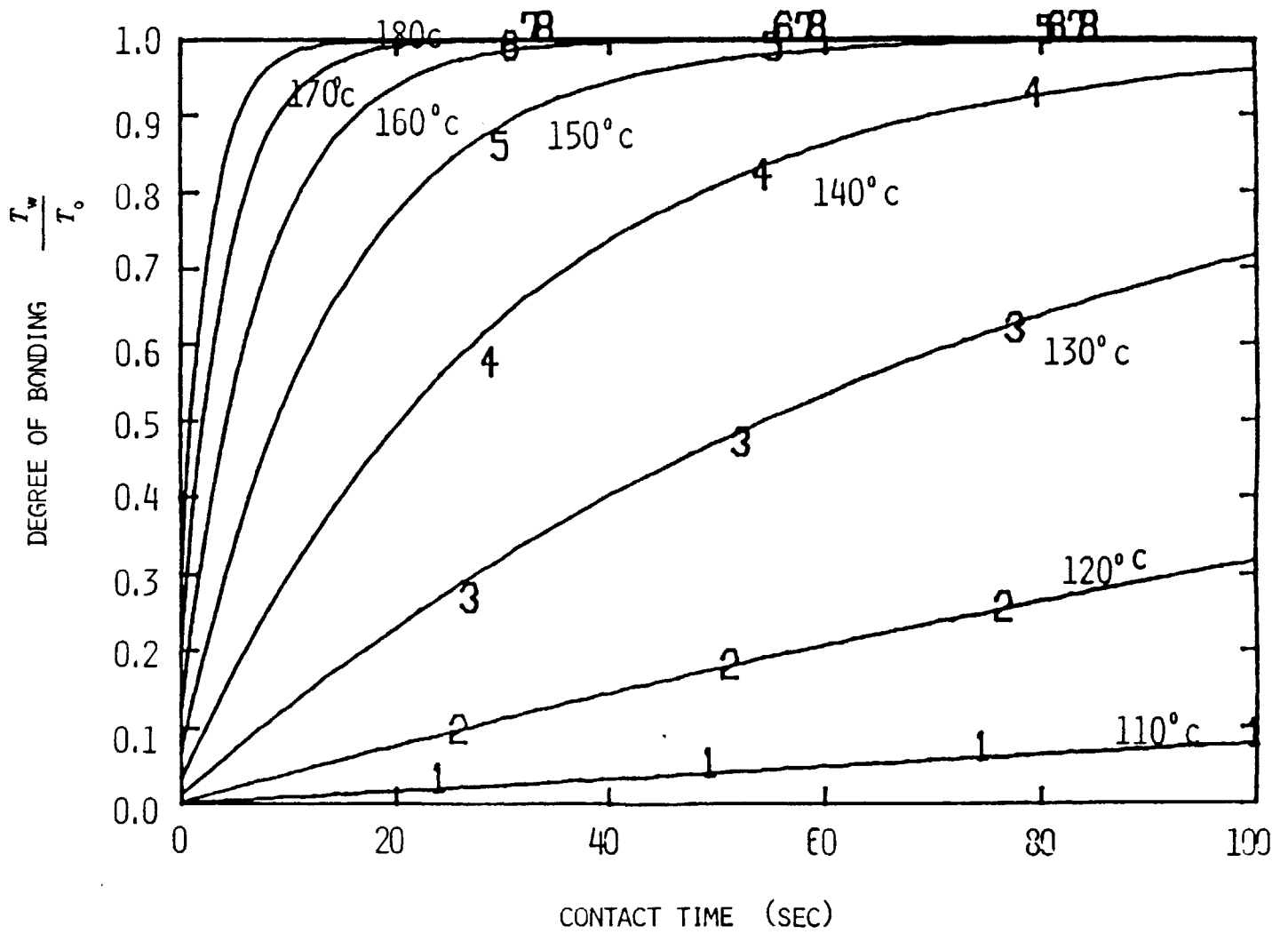
Figure 4-14: Degree of Bonding as a function of contact time at different melt temperatures: general purpose polystyrene
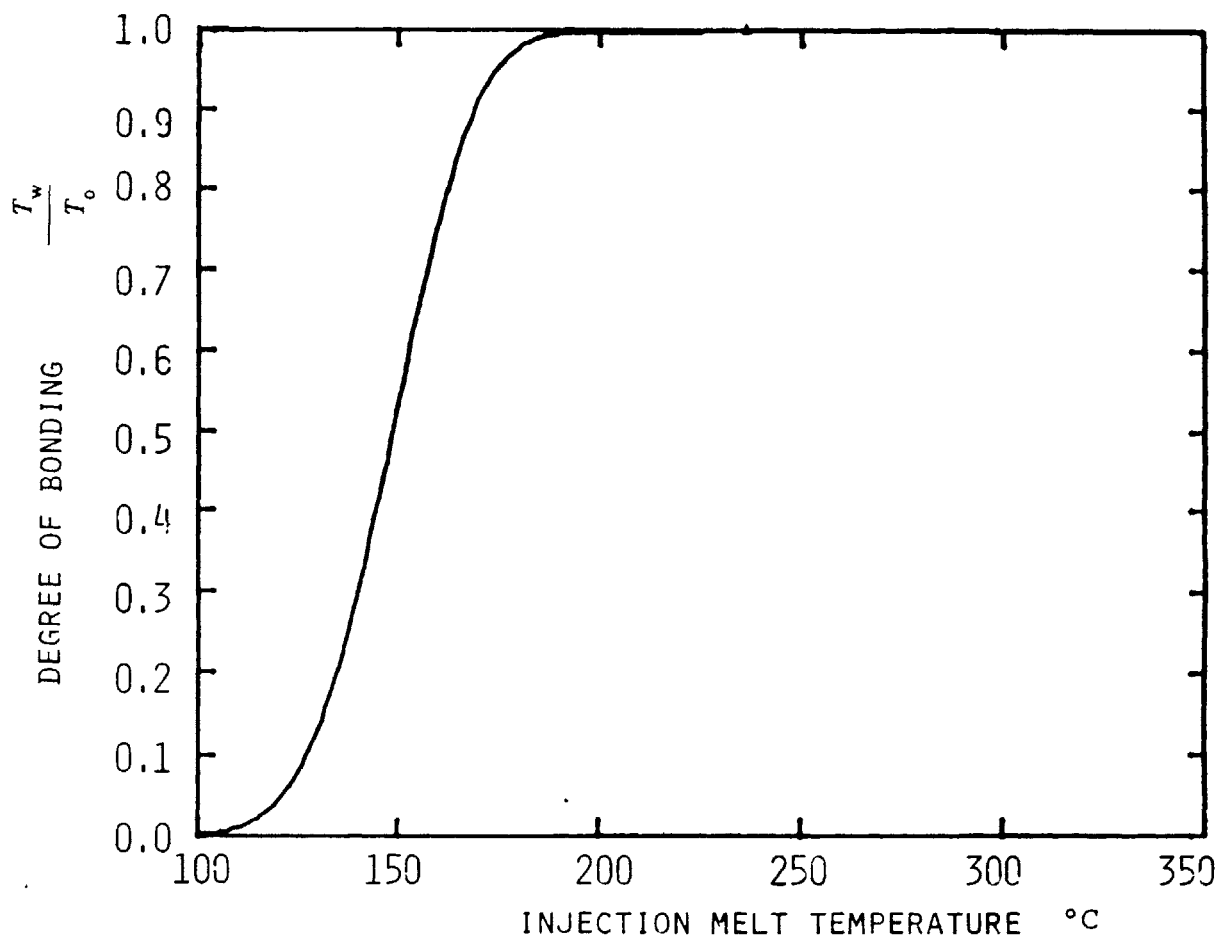
Figure 4-15: Degree of Bonding as a function of melt temperature at a fixed contact time (10 sec)
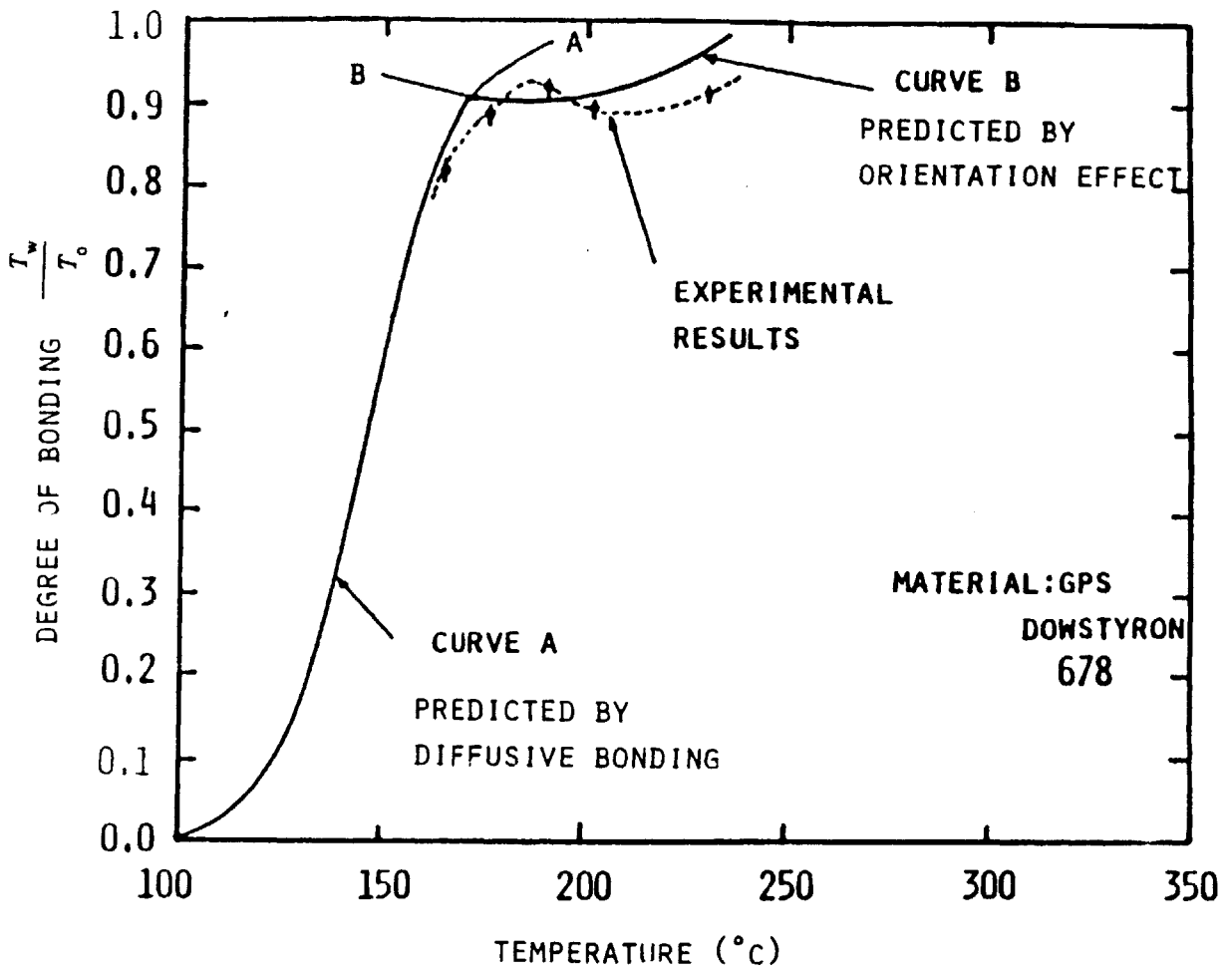
Figure 4-16: Theoretical Prediction and Experimental Results of the Tensile Strength at the Weldline of Amorphous Polystyrene

Fig. 4-16 is the predicted strength of amorphous polystyrene with weldline, which is plotted as a ratio of the tensile strength of weldline to that of the orientation free polystyrene.

DOW STYRON 678 was injected at four different melt temperatures into a two gated mold cavity of a thin rectangular shape (0.75 in x 5 in x 0.125 in). The surface of specimens were polished in order to remove V notches around the weldline. The specimens were cut to shape according to ASTM D638, and tested using an INSTRON machine. The ratios of the tensile test results to the tensile strength of general purpose polystyrene are plotted as a dotted line in Fig. 4-16. Experimental results show very good agreement with the theoretical predictions except for a small shift on the temperature axis. This is because the actual melt temperature is different from the melt temperature measured at the nozzle of the machine [56]. If the actual melt temperature at the melt interface can be predicted accurately, the theoretical model developed in this paper becomes more convicing in spite of some simplications made during the derivation.

4.5 Summary

A weldline structure is one of the most serious defects which must be considered in the design of an injection molded part. By analyzing the effect of molecular orientation at the weldline region and the effect of chain diffusion at the interface of homogeneous polymers, the tensile strength of injection molded amorphous polystyrene with a weldline is predicted using known processing variables. The experimental results show good correlation with the theoretical prediction except for a small shift on the temperature axis. This temperature lag is mainly due to the difference between the actual melt temperature at the flow front and the temperature measured at the injection nozzle.

The origins of molecular orientation and its effect on the mechanical strength are well characterized. By employing a reasonable approximation with convincing mathematical models of one dimensional shear and two dimensional elongational flow, the spatial variations of molecular orientation and accompanying mechanical strength are successfully predicted. The direction of major orientation and the magnitude of longitudinal and transverse tensile strength are effectively represented by a simple form of strength ellipse. The shape of the strength ellipse can be used as an intuitive design index which represents the state of microstructural anisotropies within a molded part.

Chapter 5
Knowledge Based Synthesis System

5.1 Introduction

The manufacture of injection molding includes the creation of the geometry of parts and molds, and the choice of processing parameters and materials. At the present time, this is done empirically, often involving iterative corrections and modifications by means of prototype tooling because it is difficult to predict the performance of the design before the physical entity is made. Therefore the empirically acquired knowledge has been the primary design guideline for the injection molding process. Although many good designs have made by human experts' experience and intuition, many poor designs have also resulted.

Designs which are based solely on human experts' knowledge have the following drawbacks. First of all, the success of a design can be confirmed only by prototype testings. This often requires expensive and laborious iterations of prototype tooling. Therefore, empirical approaches to design remain empirical unless a scientific tool for design evaluation is provided.

The second drawback is that expertise can be acquired only through trainings and experience. This is because there has been no proper system of knowledge which can absorb in an orderly fashion the empirically acquired heuristic knowledge to build a scientific base for design.

Theoretical models for predicting the moldability of the design and the

mechanical performance of the molded part have been formulated in previous chapters. A computer-based process simulation system, which is built in this thesis, can now determine the moldability of the design and the microstructural anisotropies of the molded part from known design parameters with real time simulation. Therefore, two of the most important aspects of design in injection molding can be evaluated without prototype testings and expensive mold making. This gives rise to the possibility that the empirical design can be tested and evaluated quantitatively.

Recently, scientific ways of formallizing heuristic knowledge are being introduced from the area of artificial intelligence. One of them is the *expert* system [4, 20]. The goal of an *expert* system is formalizing the experience of human experts and making it scientifically testable. Thus, the *expert* system can be used as a scientific base for design, by formalizing expert designer's knowledge of injection molding.

The goal of rational design in injection molding, the scientific evaluation of design and the intelligent generation of design alternatives, are embodied by constructing a knowlegde-based synthesis system in this thesis. Toward this end, valuable heuristic knowledge of injection molding is formulated into an expert system, which can communicate with the process simulation programs already developed in this thesis.

5.2 Expert Synthesis System

5.2.1 Expert System

Early work in artificial intelligence looked for simple and powerful reasoning techniques that could be applied to many different problems. A classic example is the work of Newell and Simon [52] on a program called GPS. Intended to be a general problem solver, GPS could prove theorems, solve puzzles and a wide variety of logical problems. However, attempts to apply general methods to large and coupled real-world problems were mostly unsuccessful.

In order to cope with real world problems, a kind of semi-logical method was introduced by exploiting the stack of human expert knowledge in the real world. An expert system is one that handles real-world, complex problems which require an expert's interpretation [73]. The expert system solves these problems by using a computer model of human expert's reasoning, reaching the same conclusion that the human expert would reach if faced with a comparable problem. The major goal of the expert system is to build a scientifically testable knowledge base from the human expert's experience.

Over the past decade, various research groups in artificial intelligence have built highly specialized expert systems containing the expertise needed to solve problems of medical diagnosis and treatments [57, 71], symbolic integration [51], chemical structure analysis [10, 62], geological exploration [19, 72], computer configuration selection and fault diagnosis [47], among others as shown in Table 5-I. Although these systems are very different and specific to each application, it has been gradually discovered that computer-based techniques for representing knowledge and reasoning with expertise can be quite general. One of general

Expert Systems

Expert System	Application	Developer
ACE	telephone cable maintenance	Bell Labs
AIRPLAN	air traffic planning	CMU/U.S.S. Carl Vinson
AL/X	general purpose expert system	Intelligent Terminals
CADUCEUS/INTERNIST	internal medicine diagnosis	Univ. of Pittsburgh
CALLISTO	large project management	CMU
CASNET	glucoma diagnosis/ therapy	Rutgers Univ.
DART/DASD	computer fault diagnosis	IBM/Stanford
DENDRAL	mass spectrocopy	Stanford
Dimeter Advisor	dipmeter well-log interpretation	Schlumberger
ELAS	well-log interpretation	Amoco/Rutgers
EMYCIN	a basic inference system derived from MYCIN	Stanford
EXPERT	a basic inference system to design an expert system	Rutgers Univ.
GENESIS	simulation of gene-splicing experiments	IntelliGenetics
HASP/SIAP	identification and tracking of ocean sonar signals	SCT/Stanford
ISIS	job shop planning	CMU
KAS	a knowledge acquisition system based on PROSPECTOR	SRI
KBVLSI	VLSI design	XEROX/Stanford
KM-I	an experimental knowledge-based management system	System Development Co.
MACSYMA	symbolic integration	MIT
MOLGEN	DNA analysis and synthesis	Stanford
MYCIN	antimicrobial therapy	Stanford
PROGRAMMER'S APPRENTICE	software construction and debugging	MIT
PROSPECTOR	geological exploration	SRI
PUFF	pulmonary function tests	Stanford/Pacific Medical Center
R1/XCON	VAX computer configuration	DEC/CMU
SACON	stress analysis advisor	Stanford
TATR	tactical air targeteering	RAND/U.S. Air Force

Table 5-I: Expert Systems

approach to represent knowledge and reasoning is the use of a production system [15].

A production system contains three major components: a set of production rules (knowledge base), a global data base and the inference engine (rule interpreter) as shown in Fig. 5-1.
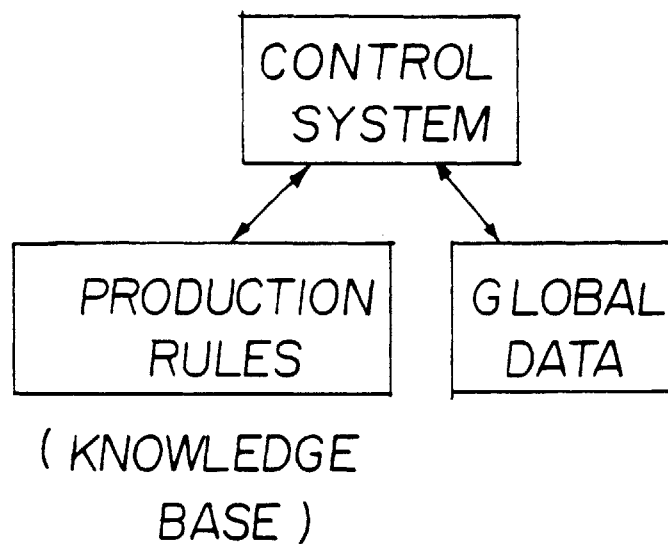
Figure 5-1: A Production System

The production rules have the following form:

IF: <antecedent 1>

.

<antecedent n>

THEN: <consequent 1>

.

.

<consequent m>

The antecedents can be thought of as patterns that can be matched against entries in the data base, and the consequence as conclusions that can be deduced. A set of production rules obtained from experts forms the knowledge base.

The role of the inference engine (rule interpreter) is to load the knowledge base into an internal representation form and use the knowledge base to guide an interactive consultation with the data base from the user. Depending upon the specific application of the expert system, different control strategies are developed to enhance the performance of the inference engine. A data-driven control strategy and a goal-driven control strategy are two typical strategies [20].

A data-driven strategy is to scan through the rules until the right rule is found whose antecedent matches assertions in the data base. The rule is applied, updating the data base, and the scanning resumes. This process continues until either a goal state is reached or no applicable rules are found. This strategy is also known as forward-chaining or antecedent reasoning.

A goal-driven strategies is to select a goal to be achieved and scan the rules to find those whose consequent action can achieve the goal. If the antecedents for a rule match existing facts in the data base, the rule is applied and the problem solved. If an unmatched antecedent is encountered, rearranging conditions to match that antecedent becomes a new subgoal, and the same procedure is applied recursively. If there are no rules to establish the new subgoal, the program asks the user for the necessary facts and enters them in the data base. This strategy is also known as backward chaining or consequent reasoning.

Since production rules are rather an elementary descriptive structure of expert systems, Weiss and Kulikowski [73] described expert systems in a way other than as

a pure production system. They proposed a classification model which selects a conclusion from a prespecified list of possibilities with associated observations (Fig. 5-2-a).

While a classification system may employ production rules, the form of the production system can be tailored to the classification model (Fig. 5-2-b). The knowledge base is organized as a classification model containing a list of conclusions, a list of observations and production rules. The control system determines how and in what order the production rules are to be evaluated. It also resolves conflicts between rules and may request for further information from the user. Many expert systems for diagnosis or interpretation have been developed successfully using the classification frame work [72, 73].

5.2.2 Multi-Level Expert System

The purpose of employing the expert system in this thesis is to interpret the result of the process analysis and to generate the best design alternative intelligently based on the human experts' knowledge. In this context, the classification model combined with the production system is considered to be a proper tool to represent and reason with the heuristic knowledge from injection molding experts. However, the decision rules for the design diagnosis in this thesis are based not only on heuristic knowledge, but also on the numerical process analyses. The expert system should be able to communicate and interact with the complex numerical analysis programs. At the present time, most expert systems mainly focus on logical reasoning, and can not handle the purely numerical analyses properly. Therefore a variant structure of the classification type expert system which can communicate with external numerical analysis programs is considered in this thesis.

(a)

```
┌─────────────┐
│ PRODUCTION  │
│   RULES     │
└─────────────┘
```

┌──────────────┐   ┌─────────────┐
│ OBSERVATIONS │   │ CONCLUSIONS │
└──────────────┘   └─────────────┘

(b)

```
┌──────────────────────────┐
│ CONTROL  SYSTEM          │
│                          │
│  • evaluation of         │
│    production rules      │
│  •evidence selection     │
└──────────────────────────┘
```

┌────────────────────┐   ┌────────────────────┐
│ KNOWLEDGE BASE   │   │ WORKING MEMORY   │
│   │   │   │
│ • conclusions   │   │ •recorded.   │
│   │   │   observations   │
│ •observations   │   │   │
│   │   │ •confidence in   │
│ •production rules │   │   conclusions   │
└────────────────────┘   └────────────────────┘
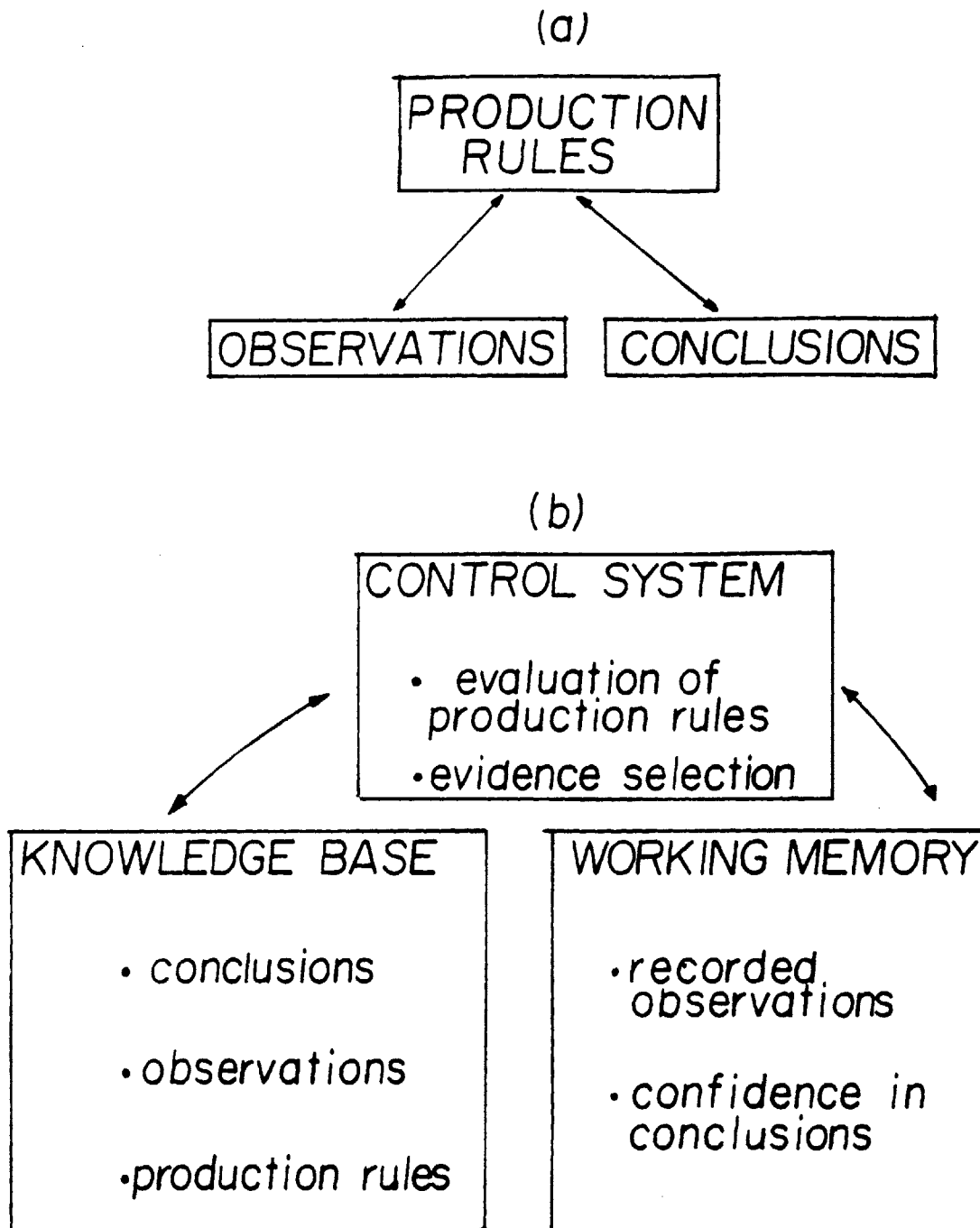
Figure 5-2: Classification System
(a) classification model, (b) a production system with a classification model

Hart [27] proposed a multi-level structure expert system to enhance the performance of expert systems. He contrasts the reasonings of surface-level models with deep-level models. The surface model is of the production rule type system, whereas the deep model is a purely mathematical description of the physical system.

Based on this concept, Weiss and Kulikowski [72] reported a multi-level expert system, *ELAS*, for well-log[7] analysis. They build an expert advice system based on the knowledge and reasoning methods of an expert log analyst. The advice system is integrated with AMOCO's[8] large scale well-logging data analysis software, *INLAN*. By combining an advisory system with the existing complicated software, the use of the analysis programs and the interpretation of their results become easier for a wide variety of expert and non-expert users. The integration of the analysis programs and the classification type expert system is the key characteristic of the multi-level expert system, *ELAS*, which is also suitable for the application in this thesis.

An expert consultation system is built in this thesis to allow a multi-level structure as follows. Flow simulation programs and microstructure analysis programs which are developed in this thesis form the deep reasoning model, while a classification model combined with the production system forms the surface reasoning model of the system as shown in Fig. 5-3.

Based on the heuristic rules from expert designers and the process analysis results, the proposed expert system can diagnose designs and generate optimal

---

[7] Well logs are the various electromagnetic, sonic and nuclear signals obtained from instruments placed down hole in a well which characterizes the properties of the rock and fluid formation below the surface.

[8] American Oil Co.
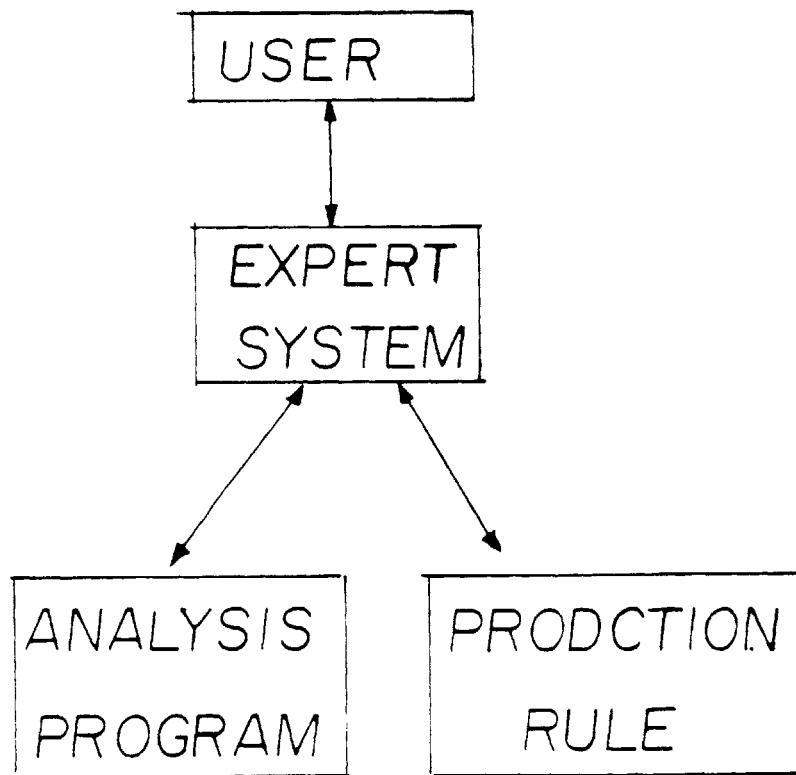
Figure 5-3: Multi-Level Structure Expert Synthesis System for Injection Molding

redesign tips to the designer. Furthermore, the expert system frees the designer from acquiring detailed knowledge of hydrodynamics, rheology, polymer science and numerical analysis which are necessary to run and interprete the results of the analysis programs.

5.3 Expert System for Injection Molding

A prototype consultation system for designing injection molded parts is built based on the production rule scheme of the *EXPERT*.

EXPERT is a general purpose expert system design tool developed by Weiss and Kulikowski [73]. It is one of the simpler systems and is specialized for classification problems. It is written in *FORTRAN*, which makes communication between the expert system and the external analysis programs relatively straightforward. For schemes which require extensive list processing, back tracking or recursion, a logic-oriented language such as *LISP* or *PROLOG* is preferable. Thus, most of the current expert systems such as *EMYCIN* [67], *PROSPECTOR* [19], are written in *LISP*[9] or *PROLOG*[10] [20]. However, due to the ease of communication with the analysis programs, which are written in *FORTRAN*, and due to the ease of model design, *EXPERT* is used in this thesis to design a prototype system.

Heuristic design rules for the injection molding process are formalized and implemented as production rules according to the *EXPERT*'s language structure [74].

---

[9]List Processing Language

[10]Logic Programming Language

5.3.1 Knowledge Formalization

5.3.1.1 Design Evaluation

The moldability of a design and the microstructural anisotropies can be quantitatively predicted by the analysis programs developed in this thesis. The global mechanical behavior of the designed part can be readily determined by doing straightforward stress analysis, if the microstructural anisotropies for the whole geometry can be calculated. However, this requires an immense amount of computation time and data storage, while producing not much improvement as paid for. Although global analysis is required for designing a part which receives great and complicated stresses, most of the injection molded parts do not require rigorous stress analyses due to their typical small load applications. A heuristic method is introduced to avoid brute force analysis for evaluating designs.

Mechanical failures occur first when the stress concentrations are imposed on the weakest directions of mechanical anisotropies. For arbitrary loading situations, stress concentrations occur at holes, corners, edges and thin sections. Therefore the distribution of microstructural anisotropies at these regions are critical in determining the critical mechanical behavior of the part. From the above observations, a rule is deduced for evaluating designs with respect to the mechanical performance of molded parts.

- Mechanical Acceptability: An adverse combination of microstructure and geometry mainly deteriorates the mechanical performance of an injection molded part.

A local prediction scheme which detects only the critical aspects of the design

is developed in this thesis based on this rule. The microstructures and accompanying anisotropic properties are predicted at limited regions where stress concentrations possibly occur and are judged by the production rules to determine the acceptability of the design.

Moldability of a design is an important criterion for the evaluation of design, which can be readily determined from the flow simulation. When the injection pressure during the flow simulation exceeds the limit of the employed machine, it can be concluded that a closed contour of flow path is blocked by the solidified polymer. This results in the short shot of the mold and the design is not moldable. A second rule for design evaluation is set in this respect.

- Moldability: When the required injection pressure exceeds the limit of the machine's capacity, short shot occurs and the design is not moldable.

Beside the above two rules, more rules can be added easily to the current rule base in order to evaluate design more successfully in many aspects of injection molding. The possible defects and relevant heuristic cures of injection molded parts at the present time are listed in Table 5-II. The useful candidates are rules for jetting, sinkmark, warpage, among others. But they will not be included in this expert system until they can be proved to be scientifically testable.

5.3.1.2 Design Alternative Generation

Human experts have developed simple and intuitional redesign tips based on the prototype testing results. Table 5-II shows some of them. In the previous section, the moldability and the mechanical acceptability are chosen as criteria for the evaluation because they become scientifically testable in this thesis. Therefore,

Faults and Empiricl Remedies

Fault	Genaralized Cause	Possible Cures
Short Molding Sinks and Voids Weld and Flow Marks Poor Surface Finish	Cavity not filling properly	Increase injection pressure Increase injection rate Increase melt and mold temperature Increase feed Improve mold venting Increase Size of gate, spruc and runner
Burn Marks	Lack of mold venting	Improve mold venting
Mechanical Sticking Flash Warping	Over-pressurization of cavity	Reduce injection pressure Use minimum hold-On pressure and time Fill more quickly
Silvering and Splash Marks Decomposition	Overheating of material	Reduce cylinder temperature Reduce effects of mechanical heating
Distortion	Ejecting too hot	Increase cooling time Eject over large areas
Jetting	Linear velocity of melt too high	Reduce velocity or break up stream of melt
Lamination, crazing Surface Cracking	Frozen-in stresses	Ensure rapid filling at lowest possible pressure

Table 5-II: Heuristic Rules for Curing Defects of Injection Molding

heuristic rules of treatment for the cases, when either of the above two rules is invoked, are studied and formalized in this section.

There are three major causes for the incomplete filling of the mold, which is known as a short shot. One of them is the use of a machine having insufficient power capacity, or improper processing parameter settings, which can be readily determined by comparing the necessary injection pressure and the machine's capacity. Considering that the necessary power for the injection molding is calculated by multiplying the specified injection rate by the necessary injection pressure, a comparison is easily made between the necessary injection power and the maximum power of the machine. In this case, the problem can be simply solved by changing to a larger machine or by choosing an optimum injection rate to allow the injection pressure to fall within the machine's power capacity.

Another cause of short shot is the build-up of back pressure inside the cavity by the trapped air or gas. However, this is regarded as a result of poor mold design, especially poor vent design. Considering that the part design is the major concern in this thesis, mold design case is not included in this study.

Therefore the main cause of short shot is considered to be the build-up of backpressure by the pre-solidification of the melt. Empirical treatments for this problem are simply increasing the melt temperature, mold temperature or injection speed. However these processing parameters are also important variables in deciding the resulting microstructure of the part. Hence, the treatments for the short shot are to be discussed together with the treatments for mechanical unacceptability.

The possible cause of the mechanical failure during the general uses of injection molded parts is the adverse combination of microstructure and geometry. There are

some empirical remedies to prevent this kind of bad microstructure, such as, addendum of reinforcements or secondary shapers to the primary part shape, changing the location or the shape of the gate and adjusting processing parameters [7, 13, 53, 54]. From the analytical point of view, these empirical remedies are intended to prevent the weakest direction of the microstructural anisotropy from being imposed on the possible stress concentrations, which has already been identified as a rule of mechanical acceptability. In this respect, those heuristic rules of treatment have a sound theoretical basis to be used in this study.

As an effort to formalize the empirical remedies as production rules, the causal relationship between the design variables, thermomechanical properties, and the resulting microstructural anisotropies are studied. Fig. 5-4 shows the schematic causal relationships based on the experimental and theoretical works by many researchers [6, 7, 9, 18, 28, 42, 43]. Although the individual relationship can not be identified explicitly due to the strong coupling among them, a general causality is observed as follows.

- General Causality:

    * The direction of the anisotropy is mainly dependent on the geometrical variables, such as, the primary part shape,the secondary part shape, gate geometry and the locations.

    * The magnitude of the anisotropy and the moldability is mainly dependent on thermal and temporal variables of the process, such as, melt and mold temperature, injection rate, (part thickness).

Although this is not a fact which is induced purely theoretically, it can be effectively used in generating design alternatives. This is because the regenerated design can be easily tested by means of real time process simulation programs

| THERMOMECHANICAL HISTORY | MICROSTRUCTURAL ANISOTROPY | DESIGN VARIABLES |

PRESSURE

TEMPERATURE

VELOCITY

MOLECULAR ORIENTATION
- direction
- magnitude

WELDLINE
- direction
- magnitude

SHORT SHOT

GEOMETRY

GATE
- location
- shape

PROCESSING PARAMETERS
- Tm
- Td
- Inj. Speed
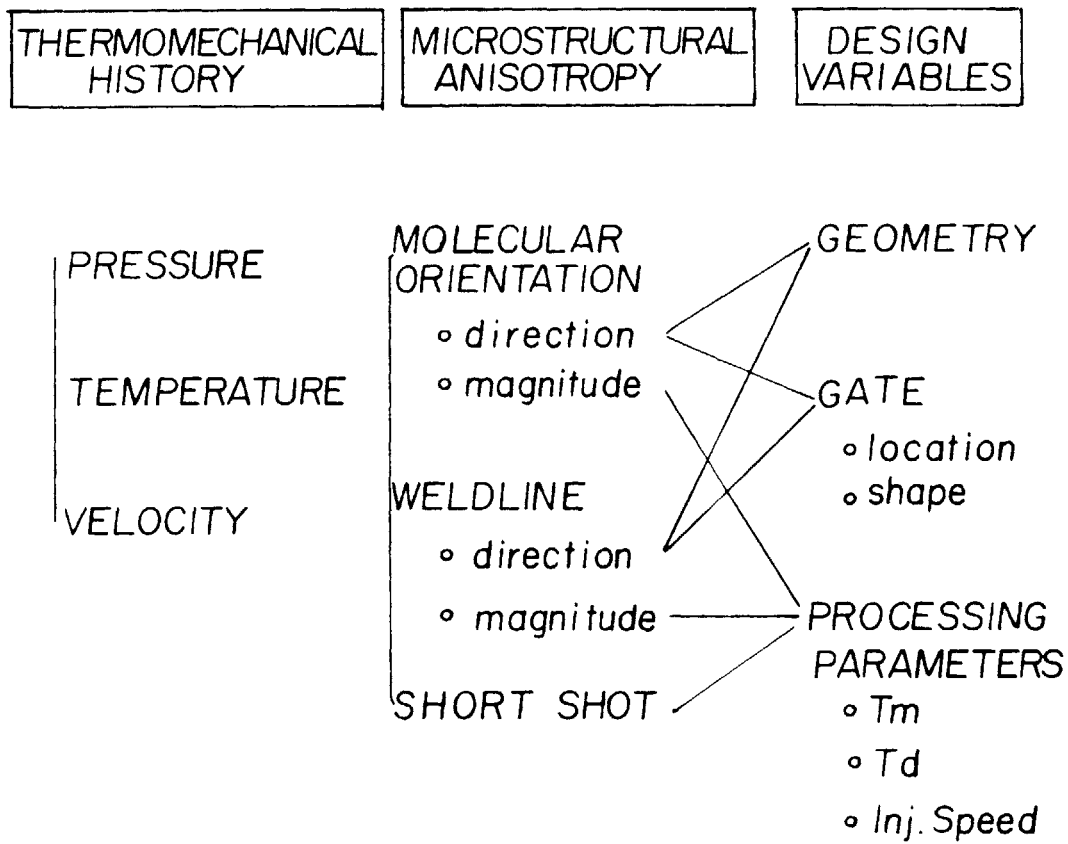
Figure 5-4: Causal Relationships Between Design Variables and Process Variables

without any costly prototype tooling.

In summary, heuristic knowledge discussed in this section is formalized as production rules which is illustrated schematically in Fig. 5-5. A prototype expert consultation system is built based on the production rules which are formalized in this section.

5.3.2 Knowledge Representation

In the $EXPERT$[11] language format, three representational components for describing the formalized heuristic knowledge are used to design a classification model.

- Hypotheses (Conclusions): Hypotheses are the set of conclusions that may be inferred by the system. A measure of uncertainty may be associated with a hypothesis to control the priority of a decision.

- Findings (Observations): Findings are the results of analysis programs or the user's inputs. They are reported in the form of logical, numerical or unavailable responses to questions.

- Reasoning (Decision Rules): The reasoning rules are expressed as production rules as discussed in section 5.2.1.

The simple description of findings and hypotheses in $EXPERT$ is somewhat

---

[11]An expert system design tool developed by Rutgers University.

proposed design → filling simulation → moldability test ? —ok→ general application? —y→ edge? → weldline? → stress concentration?

no

no

stress analysis

strength ellipse prediction

bad microstructure?

yes

no

mold machining

change processing conditions

change gate & geometry

injection molding process

PRODUCT
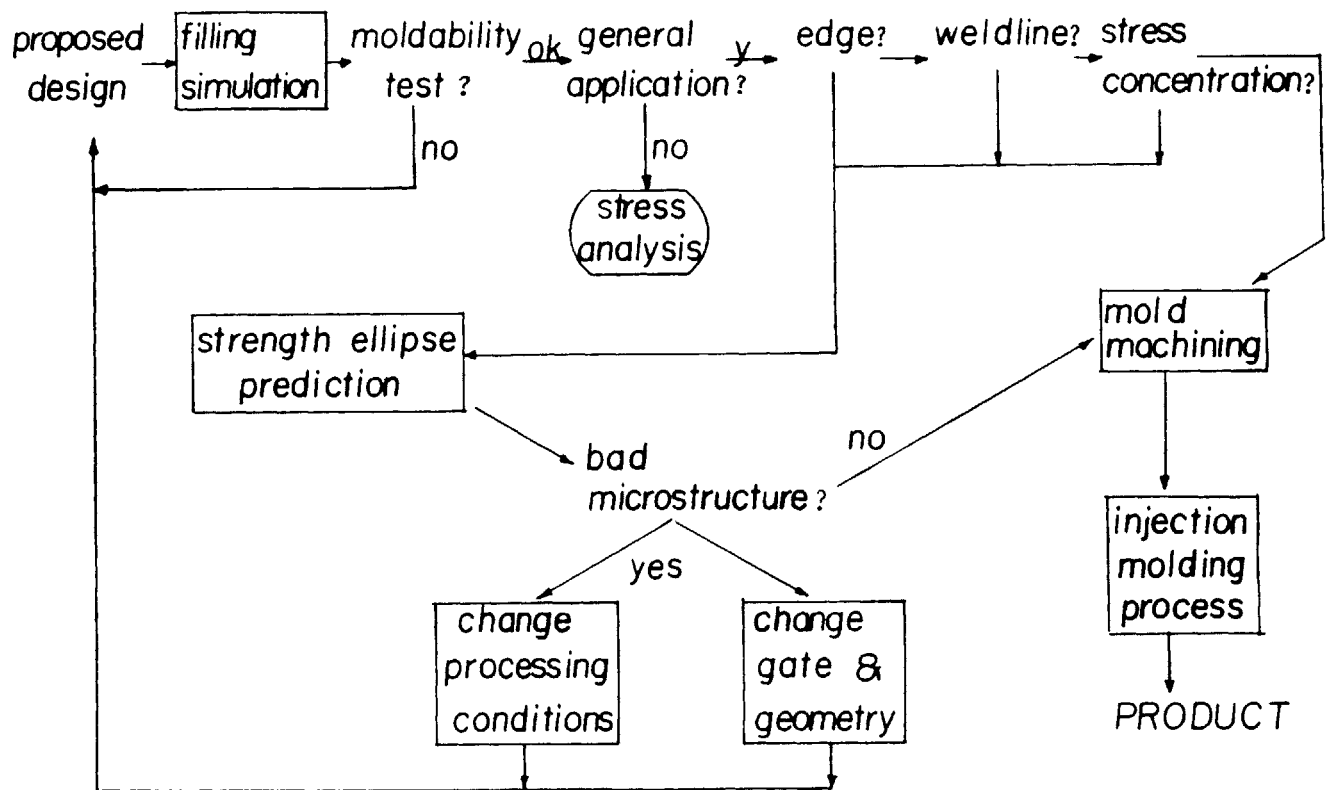
Figure 5-5: Conceptual Representation of the Decision Rules for Design Diagnosis and Redesign

primitive in comparison to the triples[12] description of hypotheses or findings in other systems, such as *EMYCIN* or *PROSPECTOR*. Thus *EXPERT* works mostly at the simpler propositional logic level, whereas *EMYCIN* or *PROSPECTOR* can include many rich expressions of the predicate logic level. However, the simple logical structure of *EXPERT* does not impose any difficulty in designing a expert system in this thesis. This is because the process-oriented decision rules can be formalized in a simple logical structure.

Based on the representational scheme in *EXPERT*, heuristic knowledge and analytical results from process simulation are classified and coded as listed in Appendix B. Fig. 5-6 shows the functional description of each area of knowledge representing a component which is implemented on the expert consultation system designed in this thesis.

5.4 Knowledge Based Synthesis System

A prototype knowledge-based synthesis system is constructed by combining the process simulation programs and the expert consultation system for the injection molding process.

An ideal knowledge-based synthesis system is proposed to reach the ultimate goal of this thesis, which is establishing a rational design system for injection molding. It also aims to make an user transparent synthesis system which enables an inexperienced designer to design expertly. The structure of the system is illustrated in Fig. 5-7.

---

[12]objective, attribute and value

```
┌─────────────────────────────────────────────────────────┐
│ HYPOTHESES                                              │
│                                                         │
│     ○ CONCLUSIONS OF  DESIGN EVALUATIONS                │
│                                                         │
│     ○ TREATMENTS FOR DESIGN ALTERNATIVES                │
└─────────────────────────────────────────────────────────┘


┌─────────────────────────────────────────────────────────┐
│ FINDINGS                                                │
│                                                         │
│     ○ ANALYTICAL RESULTS FROM THE                       │
│         PROCESS SIMULATION                              │
│                                                         │
│     ○ USER OBSERVATIONS                                 │
└─────────────────────────────────────────────────────────┘


┌─────────────────────────────────────────────────────────┐
│ RULES                                                   │
│                                                         │
│     ○ FINDING TO FINDING  RULES                         │
│                                                         │
│     ○ FINDING TO HYPOTHESIS RULES                       │
│                                                         │
│     ○ HYPOTHESIS TO HYPOTHESIS RULES                    │
└─────────────────────────────────────────────────────────┘
```

Figure 5-6: Knowledge Representation component in the Expert System for Injection Molding
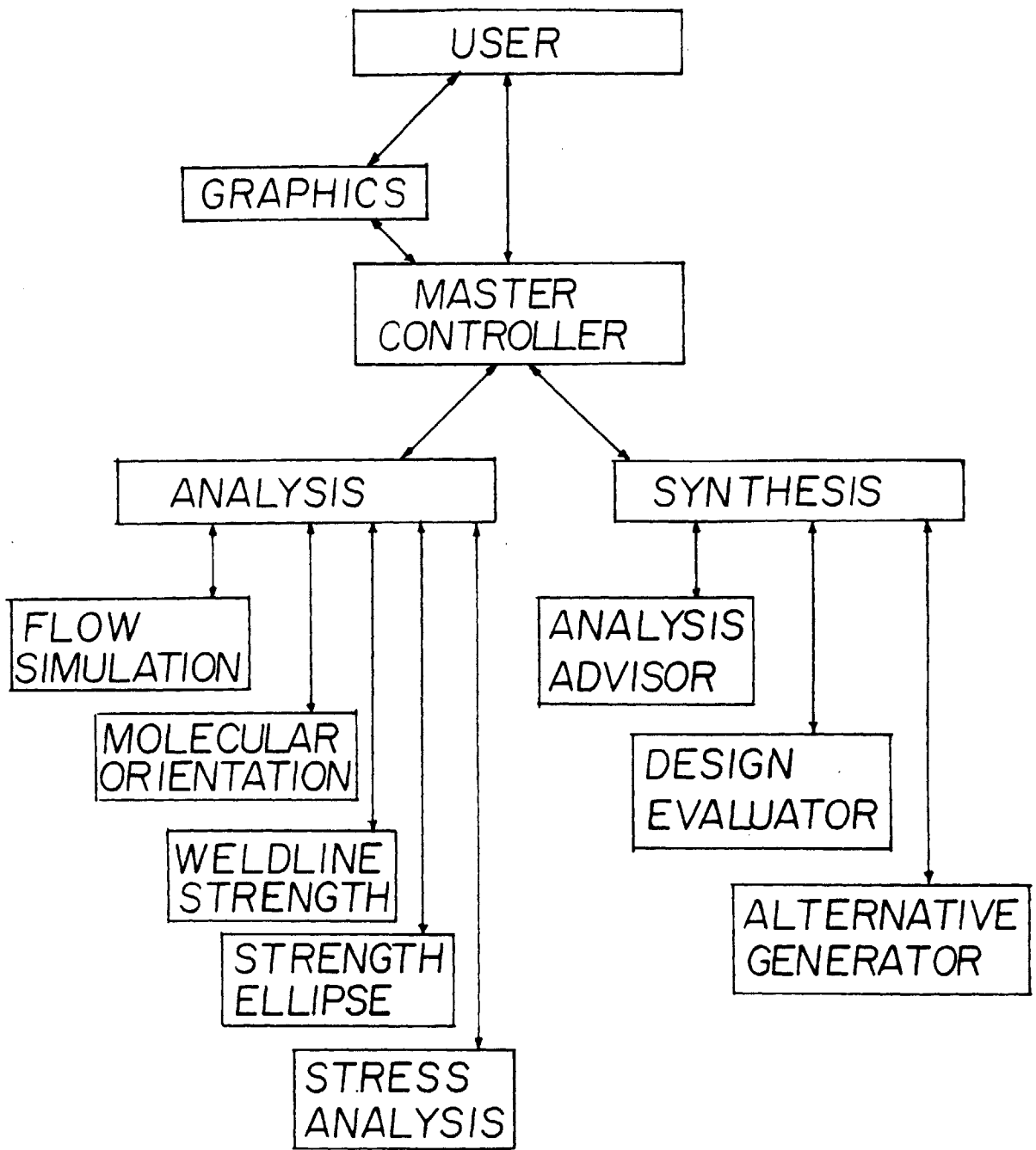
Figure 5-7: Ultimate Structure of a Knowledge-Based Synthesis System
in Injection Molding

The system has two terminal configuration, a raster-scan color graphic terminal system with a data tablet and a video terminal. The user provides the necessary information and the geometric data to the master controller interactively through the two terminals.

The master controller receives initial information from the user and triggers the expert system to request advice for the next action. Depending upon the decision from the expert system, the controller either executes the analysis program or returns the decision of the expert system to the designer for additional questioning or conclusions.

The expert system has three major functional blocks, such as, data retrieval and synthesis control, design evaluation, and design advice. Based on the information supplied by the master controller, it interpretes the data and decides the necessary action for the controller. If the information is not sufficient to evaluate the design or to confirm the conclusion, the expert system requests the controller to take relevant action to obtain more data either from the user or from the analysis programs. After retrieving sufficient information to evaluate the design, it diagnoses the design and generates proper alternatives.

The analysis system has five functional blocks as shown in Fig. 5-7. Flow simulation is the core of the analysis system because it generates a necessary thermomechanical data base for further analyses. Therefore, it is executed whenever a new design diagnosis is requested. Moldability is readily predicted from the result of the flow simulation. Mechanical performance prediction programs are executed only when the expert system requests the running of the specific program among them.

Within the limits of available hardware and software, a practical system is built to include most of the key functions devised in the ideal system. The structure of the system is shown in Fig. 5-8.

Instead of the color graphic facility, a Digital's VT-240 monochrome graphic terminal is used as an input-data/output-display device.

For a given design task, the flow simulation program is first executed to build a thermomechanical data base. Then the expert consultation program is initiated. Based on the decision from the expert system, a part or the whole of the microstructure analysis programs are executed. The expert system's request with relevant data for a specific analysis program is transmitted to the microstructure analysis system *via* communication programs between the expert system and the microstructure analysis program. The result of the analysis, then, automatically returns to the expert system to diagnose the design. If the design is not acceptable, the user generates an alternative on the basis of expert system's advice. This design cycle is repeated until the acceptable design is made.

In order to have more insights into the system, a detailed case study is provided in chapter 6.

5.5 summary

A knowledge-based synthesis system is built to embody the integration between two domains of knowledge for injection molding. Heuristic knowledge of design is formalized as production rules and combined with analytical knowledge from the process simulation. The overall structure of the expert system, as designed, is based on *EXPERT*, which is an expert system designing program, and linked
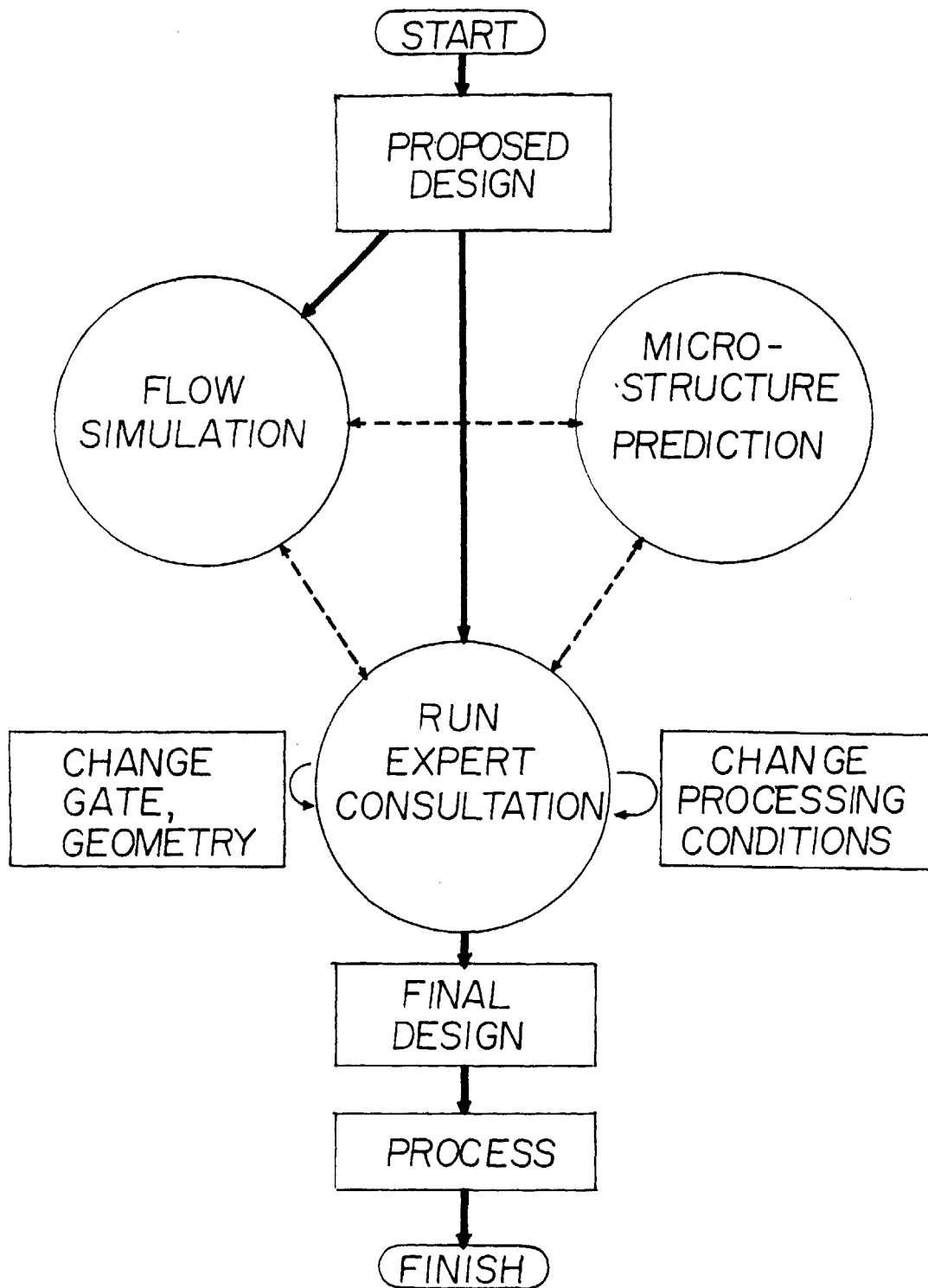
Figure 5-8: A prototype knowledge-based systhesis system built in this thesis.

together with analysis programs to have a multi-level reasoning structure.

At the present time, this system is not equipped with a sophiscated graphic input/output facility. Therefore a practical system is built within this hardware availability. However, future inclusion of the full graphic facility will enhance the performance of the system to embody the ultimate goal of this thesis.

The current knowledge base contains decision rules and mathematical models only in respect to moldability and mechanical acceptability of the design. More knowledge about the injection molding process are urged be added to the current knowledge base to evaluate and modify designs in every aspect of injection molding, such as, sinkmarks, jetting, warpage, and mold design, among others.

Chapter 6
Case Study

The overall scheme of the knowledge-based synthesis system is illustrated in this chapter by means of a case study. An L-shaped part with a hole at the center has been designed. It will be made of general purpose polystyrene by injection molding. A fan-shaped gate will deliver the melt to the cavity uniformly. The shape and dimensions are shown in Fig. 6-1.

The material constants and chosen processing parameters are as follows;

Processing Conditions:

Melt Temperature: 200°C

Mold Temperature: 30°C

Injection Rate: 10.0 cm³/sec

Material Constants: same as listed in Chapter 3.4.2

Pump Capacity of the machine: 20 HP

In order to approximate the shape of a two dimensional cavity, the L-shaped part is unfolded as shown in Fig. 6-2.

Then cavity filling simulation is initiated. The initial input data is prepared following the method described in Chapter 3.4. There is no need for the user to interpret the output and prepare the input data for the following time steps, because all the necessary input/output data is prepared by the program itself after the initial
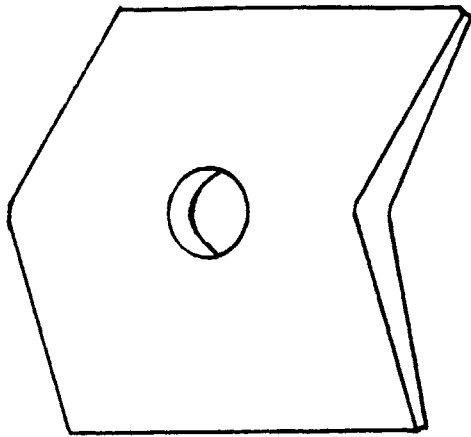
Figure 6-1: L-Shaped Injection Molded Polystyrene
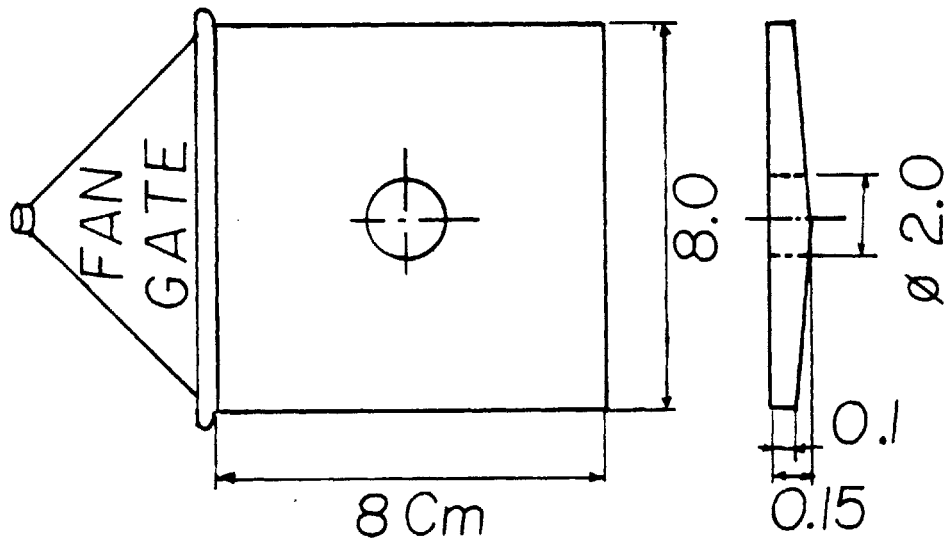
Figure 6-2: Lay Flat Approximation

- 124 -

time step.[13]

Advanced melt fronts for the next time steps are predicted based on the boundary-pressure-reflection scheme developed in this thesis. Then melt front elements are meshed in 6 noded triangular elements, numbered and added to the input data file for the next time step automatically. In order to keep the mesh geometry as regular as possible, birth, death and time step change functions are provided in the automatic mesh generation program. The user can override the mesh editing program to handle possible singular boundary conditions. Predicted melt fronts at some key instants are shown in Fig.6-3 - Fig. 6-11.

The thermomechanical data base contains averaged velocity components, pressure distribution, planar and gapwise distribution of temperature and time history at each nodal point. By the end of the cavity filling simulation, a thermomechanical data base is constructed and ready to be used by the expert consultation system. Then the consultation session begins as follows.

The expert system will ask questions of the user to gather information for design diagnosis. If there is a need to have analytical results from the thermomechanical or microstructural data base, the expert system will ask the user to run the relevant analysis program within the control of the expert system. The results of the analysis return to the expert system automatically and change the value of associated findings. Data interpretation, design diagnosis and recommendations will be presented to the user by the expert system.

---

[13]In this case, 0.03 sec
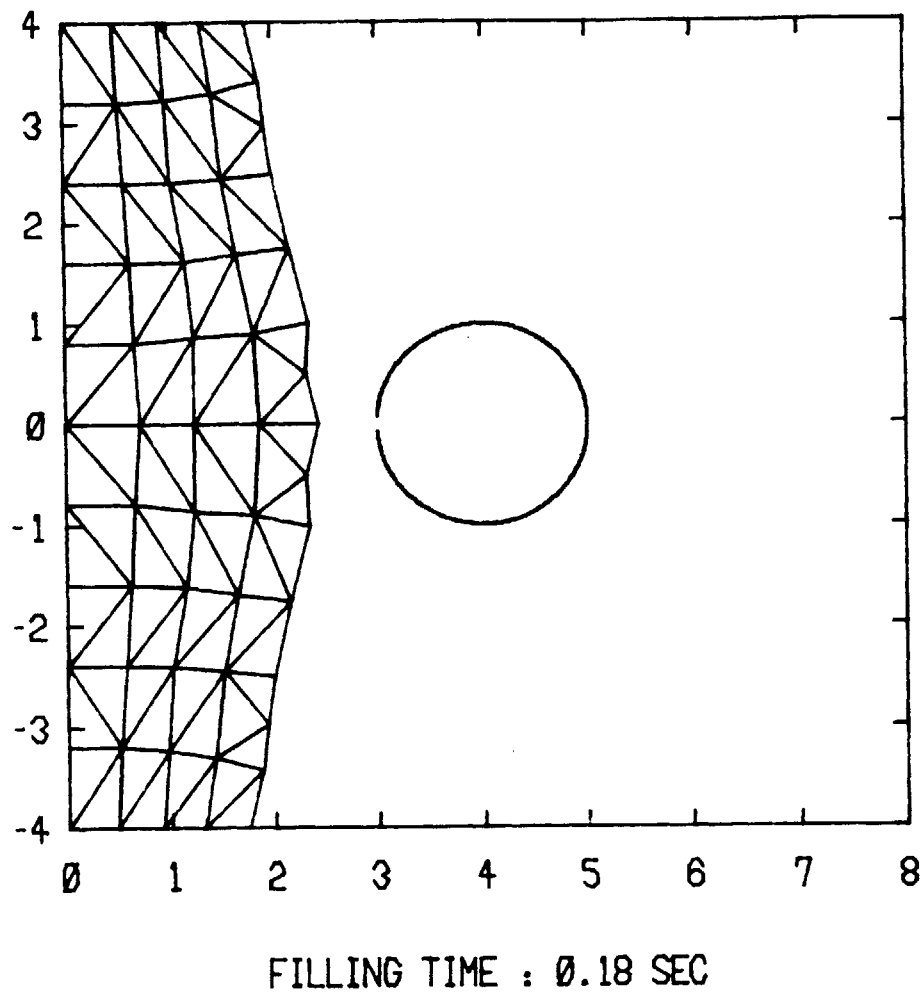
Figure 6-3: Cavity Filling Simulation; Mesh Generated at 0.18 sec.
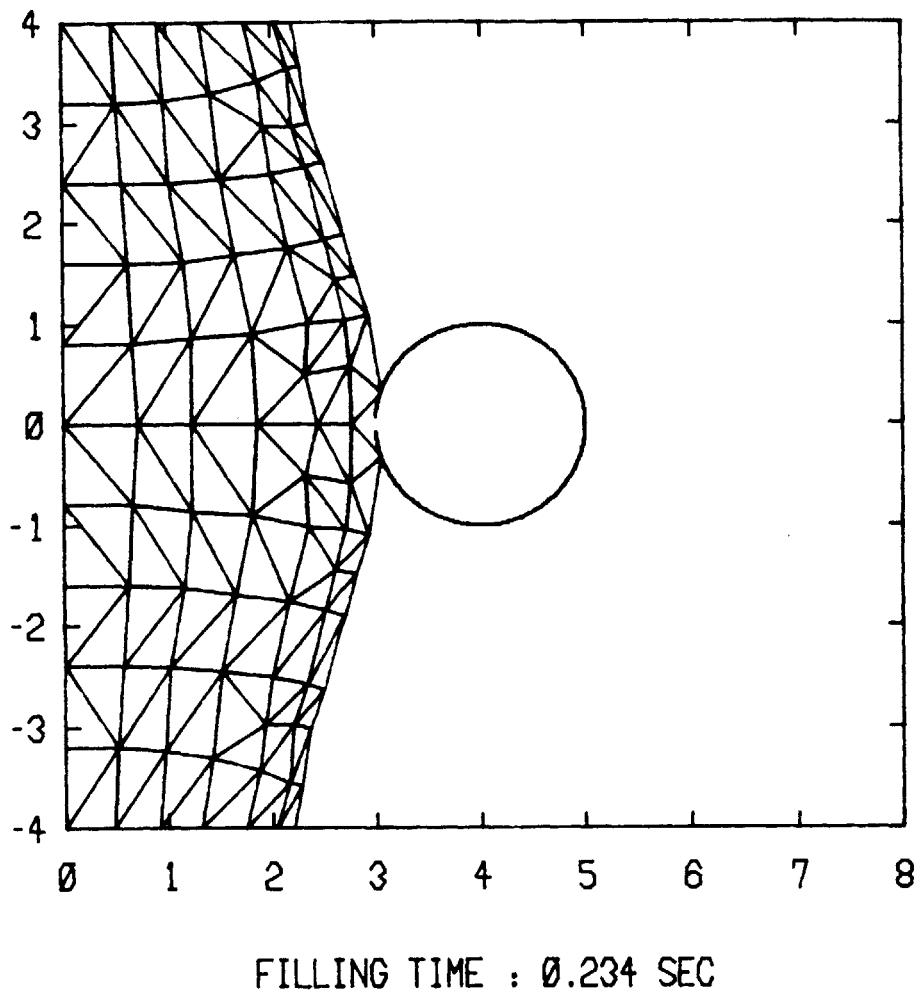
Figure 6-4: Cavity Filling Simulation; Mesh Generated at 0.234 sec.
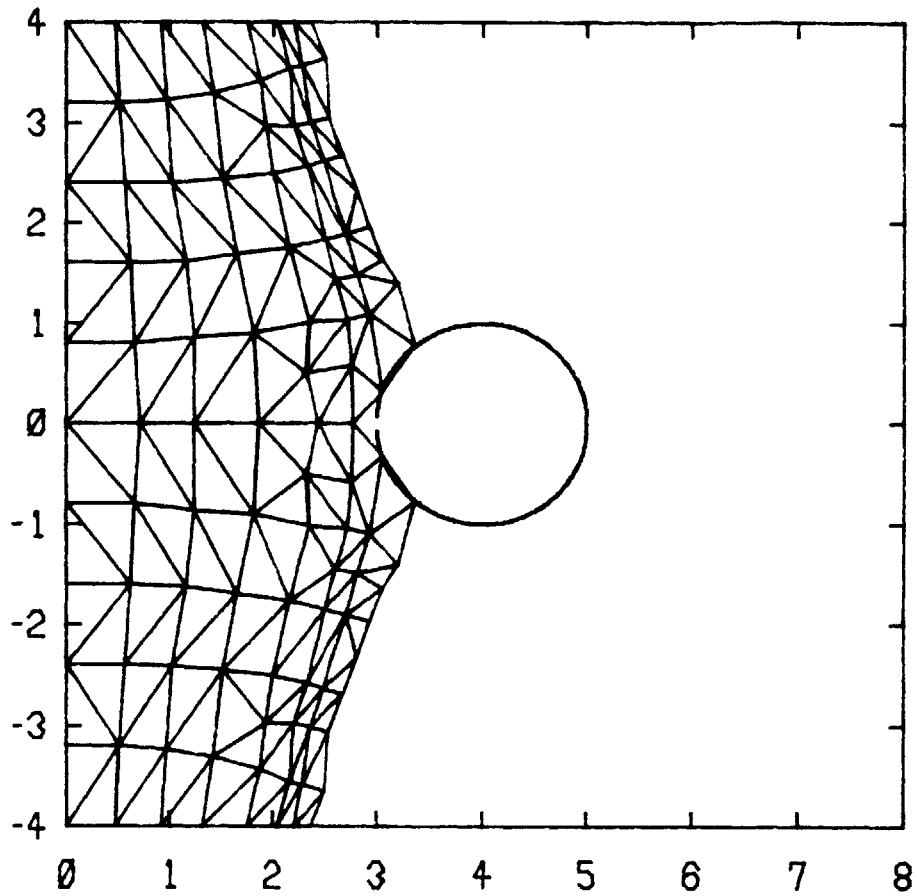
FILLING TIME : 0.253 SEC

Figure 6-5: Cavity Filling Simulation; Mesh Generated at 0.253 sec.
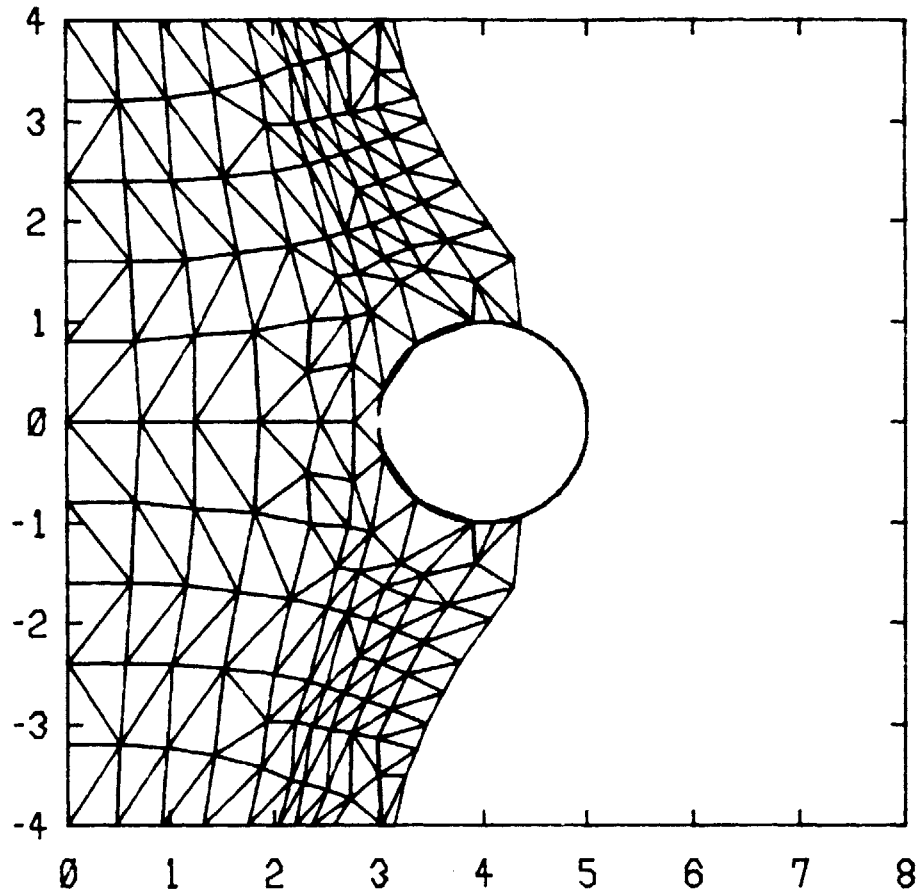
Figure 6-6: Cavity Filling Simulation; Mesh Generated at 0.322 sec.
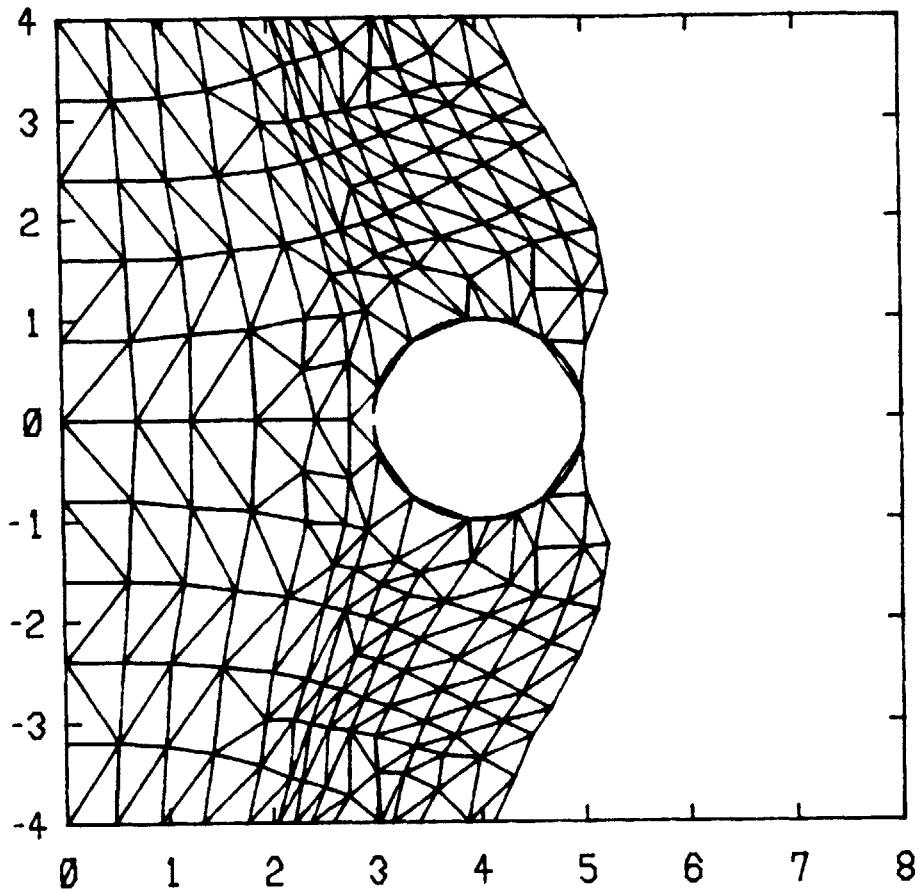
FILLING TIME : 0.402 SEC

Figure 6-7: Cavity Filling Simulation; Mesh Generated at 0.402 sec.

FILLING TIME : 0.46 SEC
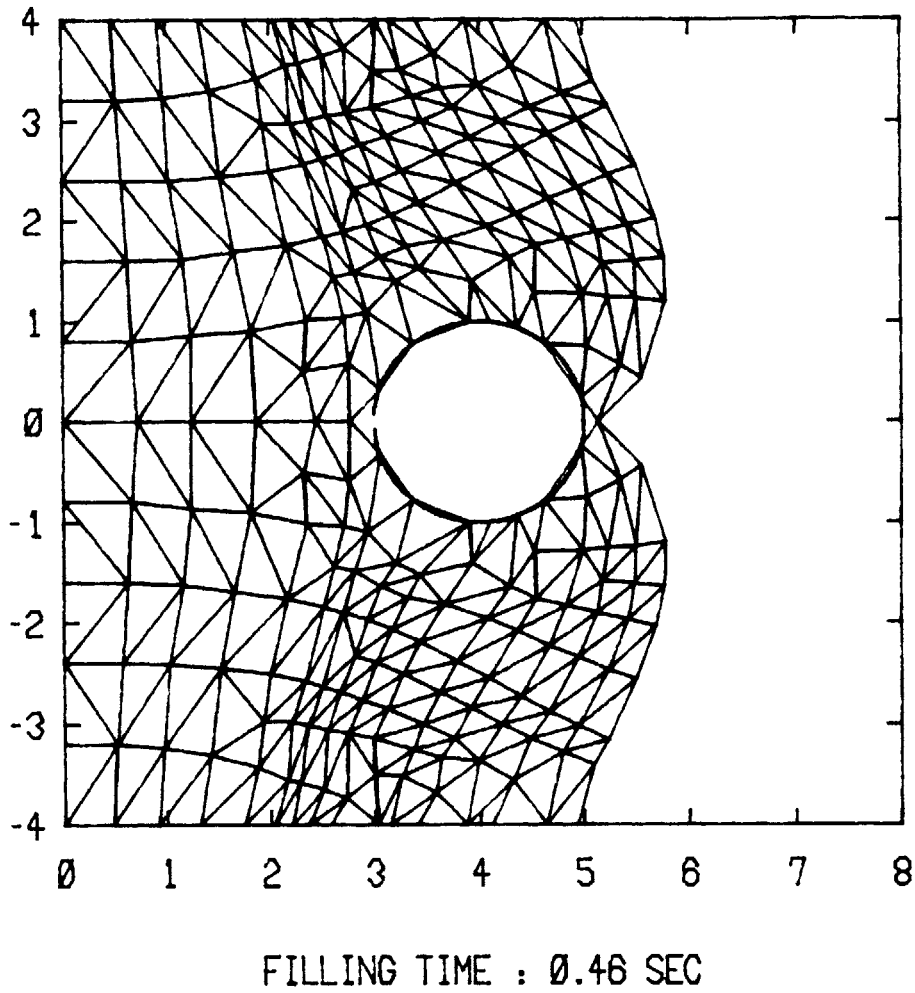
Figure 6-8: Cavity Filling Simulation; Mesh Generated at 0.46 sec
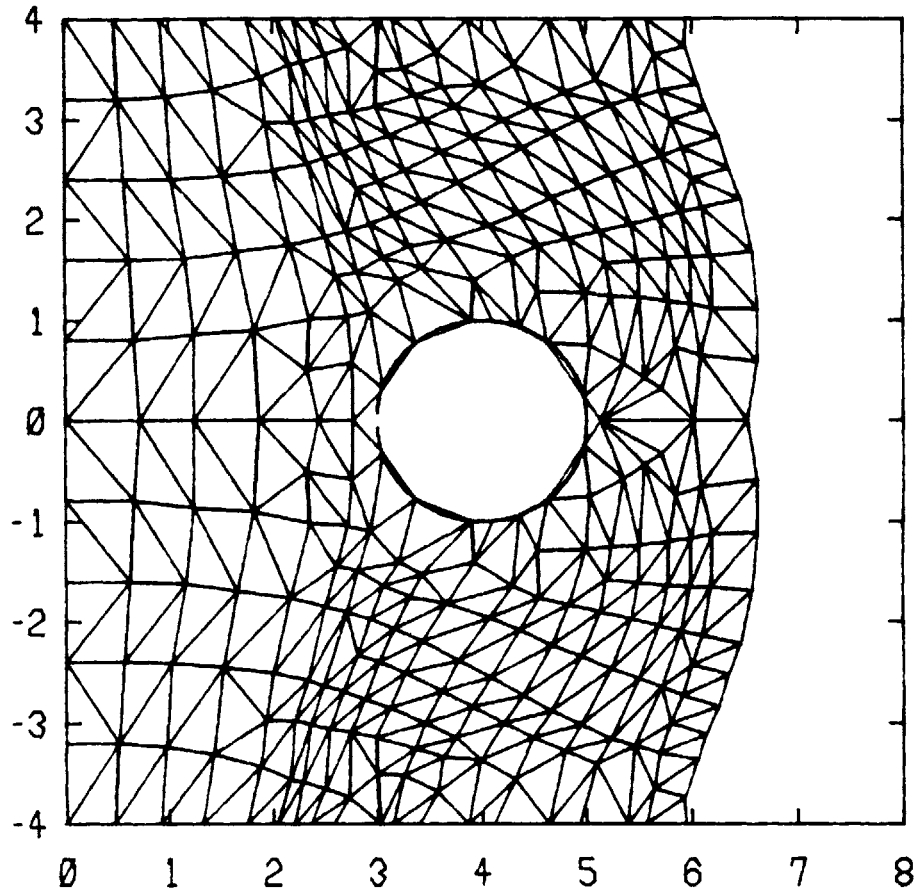
FILLING TIME : 0.548 SEC

Figure 6-9: Cavity Filling Simulation; Mesh Generated at 0.548 sec
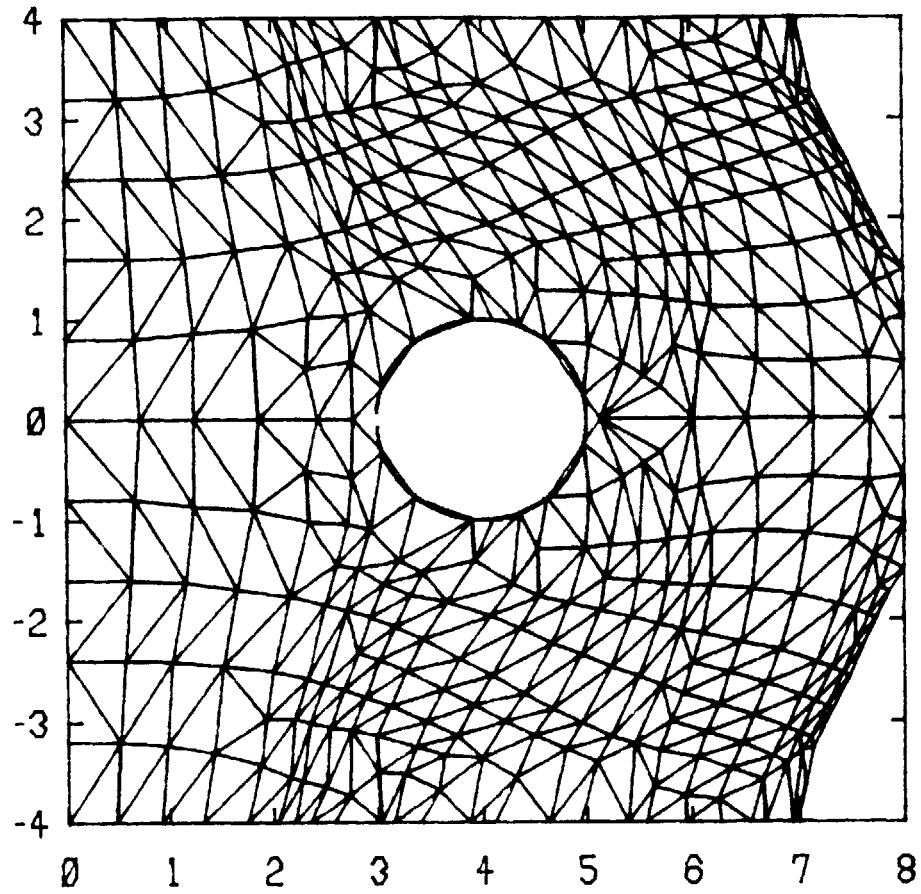
FILLING TIME : 0.663 SEC

Figure 6-10: Cavity Filling Simulation; Mesh Generated at 0.663 sec.
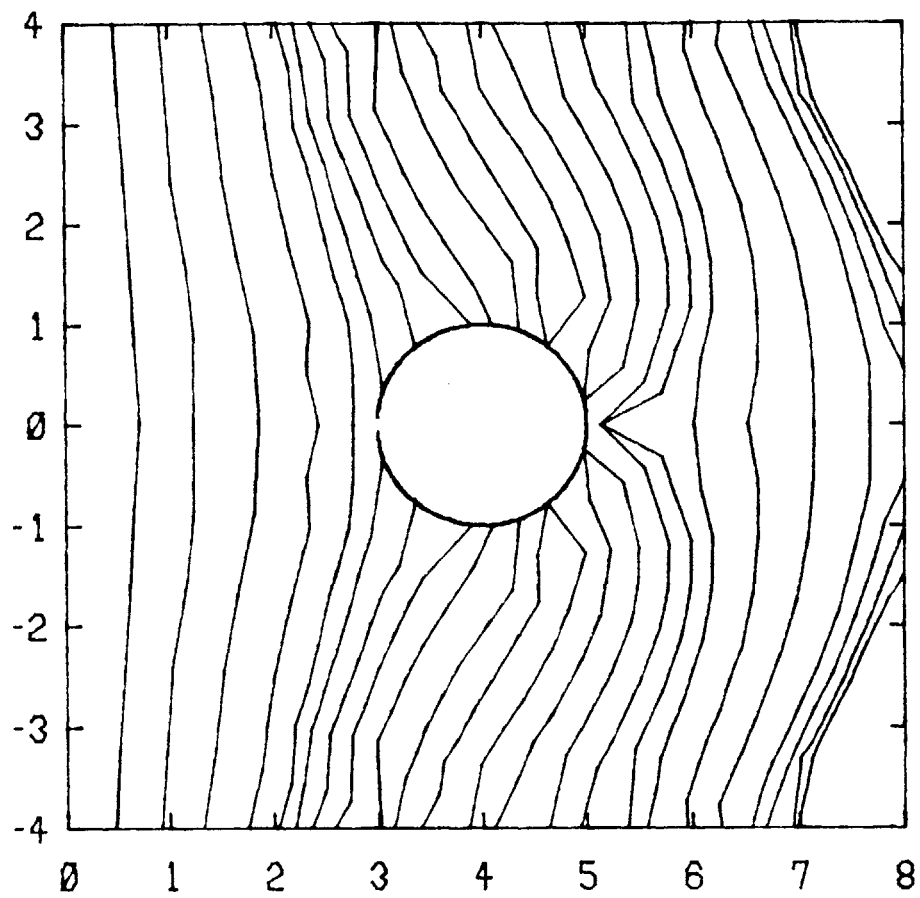
Figure 6-11: Predicted Melt Fronts; weld line is expected.

$Enter file name: INJJ

INJJ is the expert model for injection molding. For more details, see Appendix B.

Type ? for a summary of valid responses to any question asked by the program.

CASE TYPE: (1)Case Entry   (2)Visit Entry   (3)Case Review
             (4)Case Deletion   (5)Demo Entry   (6)Program Exit:
$* 1

$Enter Name or ID Number: CAVITY1

$Enter Date of Visit: 4/21/85

Enter Initial Findings (Press RETURN to begin questioning):
$* (RETURN)

    1. WHAT MATERIAL:
        1) POLYSTYRENE
        2) OTHERS
       Choose one:
$ * 1

    2. MELT TEMPERATURE[K]:
$ * 493

    3. MOLD TEMPERATURE[K]:
$ * 303

    4. INJECTION SPEED[cm**3/sec]
$ * 10

5. PUMP CAPACITY OF THE MACHINE[HP]
$ * 20

The necessary injection power predicted from the filling simulation will be compared

with the pump power of the machine with the specified injection rate.

      6. MICROSTRUCTURE IS NOT CHECKED YET
$ * Y

      7. SHORT SHOT:
            1) SHORT SHOT DOES NOT OCCUR
            2) SHORT SHOT OCCURS
            3) SHORT SHOT NOT KNOWN
         Choose one:
$ * 1

From the result of filling simulation, designer readily determines the short shot

possibility.

      8. WHAT KIND OF APPLICATION:
            1) GENERAL APPLICATION, e.g.toys
            2) HIGH STRESS APPLICATION, e.g.cars
         Choose one:
$ * 1

If the applied stress is large and determined, the expert system will ask the user to do

the stress analysis and to determine the location of the maximum stress.

      9. THERE IS A EDGE
$ * Y

      10. TYPICAL POINT ON THE EDGE1(X-COORD)
$ * 2.0

      11. TYPICAL POINT ON THE EDGE1(Y-COORD)
$ * 0.1

      12. ANGLE OF THE EDGE TO X-AXIS

$ * 0.0

13. THERE ARE MORE EDGES
$ * N

14. CHECK WELDLINE POSSIBILITY:
     1) WELDLINE IS NOT POSSIBLE
     2) THERE ARE INSERTS
     3) MULTIPLE GATING
     4) FLOW FRONTS MERGE SOMEWHERE
    Checklist:
$ * 2

15. X-POSITION AROUND INSERT FAR FROM GATE
$ * 5.5

16. Y-POSITION AROUND INSERT FAR FROM GATE
$ * 0.1

17. DIRECTION OF WELDLINE CAUSED BY INSERT(X-AXIS REF)
$ * 0.0

18. WELDLINE BY INSERT IS ALONG EDGES
$ * Y

19. OTHER POSSIBLE STRESS CONCENTRATED REGIONS(HOLES,etc)
$ * N

20. SUDDENLY ENLARGING DISCONTINUOUS GEOMETRY IN FLOW DIRECTION
$ * N

. . . .

At this point, the expert system summarizes the currently available information.

SUMMARY

Name: CAVITY1
Case: 4 Visit: 1   Date: 04/21/85

WHAT MATERIAL:
    POLYSTYRENE

MELT TEMPERATURE[K]: 493

MOLD TEMPERATURE[K]: 303

INJECTION SPEED[cm**3/sec] 10

CLAMPING FORCE OF THE MACHINE[TON] 200

MICROSTRUCTURE IS NOT CHECKED YET

SHORT SHOT:
    SHORT SHOT DOES NOT OCCUR

WHAT KIND OF APPLICATION:
    GENERAL APPLICATION,e.g.toys

THERE IS AN EDGE

TYPICAL POINT ON THE EDGE1(X-COORD) 2

TYPICAL POINT ON THE EDGE1(Y-COORD) 0.1

ANGLE OF THE EDGE TO X-AXIS 0

CHECK WELDLINE POSSIBILITY:
    THERE ARE INSERTS

X-POSITION AROUND INSERT FAR FROM GATE 5.5

Y-POSITION AROUND INSERT FAR FROM GATE 0.1

DIRECTION OF WELDLINE CAUSED BY INSERT(X-AXIS REF) 0

WELDLINE BY INSERT IS ALONG EDGES

INTERPRETIVE ANALYSIS

Diagnoses are considered in the categories:
definite, probable, possible.

Based on the information provided, the differential diagnosis is

MECHANICAL PERFORMANCE IS NOT KNOWN   -- Definite
WELDLINE EXISTS   -- Definite
BAD WELDLINE EXISTS   -- Definite

Diagnosis of MECHANICAL PERFORMANCE IS NOT KNOWN is supported by
the user findings:

     MICROSTRUCTURE IS NOT CHECKED YET

Diagnosis of WELDLINE EXISTS is supported by the user findings:
     THERE ARE INSERTS

Diagnosis of BAD WELDLINE EXISTS is supported by the user
findings:
     WELDLINE BY INSERT IS ALONG EDGES

RECOMMENDATIONS

Based on the information provided, the design recommendation
is:

RUN MICROSTRUCTURE PREDICTION PROGRAM IN FOLLOWING ASPECTS;
RUNNING FORMAT--RUN(STAN)
WELDLINE ANALYIS IS REQUIRED.
STRENGTH ELLIPSE IS REQUIRED.

End of diagnostic consultation: 21-APR-85

Command Mode: FIX x, WHY, DX, SUM, NEW, ASK, QUIT, etc,
              ? for HELP

Based on the expert system's request, user runs the microstructure prediction program

as follows.

```
$: RUN(STAN)

$(Running Program.
+....Done)
```

As soon as the analysis finishes, all the necessary analytical data is transferred to the

expert system automatically via a data communication file within the program.

```
$: DX
```

User requests the expert system design diagnosis and recommendations with the new

finding from the analysis program.

```
INTERPRETIVE ANALYSIS
----------------------


Diagnoses are considered in the categories:
definite, probable, possible.

Based on the information provided, the differential diagnosis is

WELDLINE EXISTS                              -- Definite
BAD WELDLINE EXISTS                          -- Definite

ACCEPTABLE MICROSTRUCTURE                    -- Probable
```

This is decided based on the shape and the major axis direction of predicted strength

ellipses. Fig. 6-12 shows typical shapes of strength ellipse at different locations.

```
Diagnosis of WELDLINE EXISTS is supported by the user findings:
     THERE ARE INSERTS ;

Diagnosis of BAD WELDLINE EXISTS is supported by the user
findings:
     WELDLINE BY INSERT IS ALONG EDGES

Diagnosis of ACCEPTABLE MICROSTRUCTURE is supported by the user
```

findings:
    THERE IS AN EDGE
    STRENGTH RATIO PERPENDICULAR TO THE ORIENTATION DIRECTION
    Between 0.8 and 1

RECOMMENDATIONS

Based on the information provided, the design recommendation
is:
    MOVE GATE POSITION

Diagnosis of MOVE GATE POSITION is supported by the user findings
    BAD WELDLINE EXISTS

Although the state of molecular orientation inside the molded part is acceptable in

general, the expert system points out that the weldline along the edge should be avoided

by changing the gate position.

$Would you like to SAVE this visit? *yes
 (CASE   4: VISIT   1 SAVED)
 (Done)
 End of diagnostic consultation: 21-APR-85
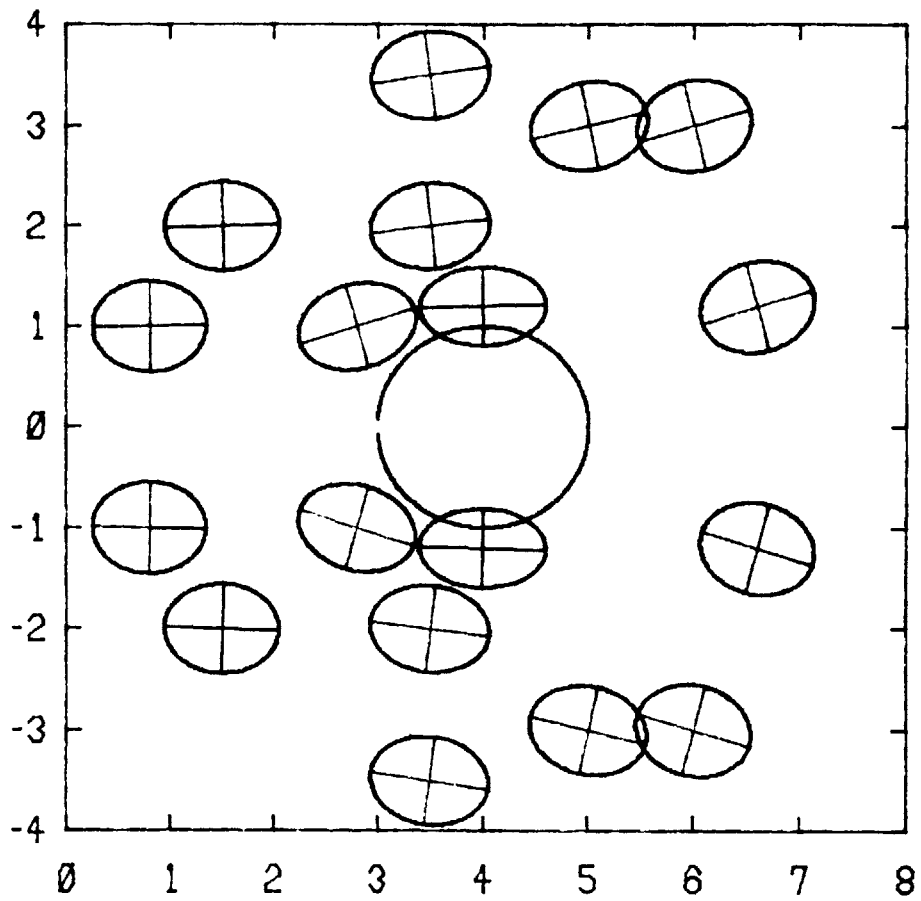
Figure 6-12: Predicted Strength Ellipses at Different Locations

Chapter 7
Conclusions and Recommendations

An interactive computer-based design system is developed to eliminate the need for costly iterations of protype tooling in injection molding. Toward this end, a knowledge-based synthesis system is constructed to apply the principle of a rational design strategy for injection molding by combining a rule-based expert system with process analysis programs. This system can evaluate a design based on the moldability of the design and the mechanical acceptabily of a molded part, which are scientifically testable by mathematical process models. This system can also generate optimal design alternatives heuristically based on the scientific evaluation.

An interactive mold filling simulation program is derived. The thermomechanical properties of a molded part are predicted *via* a user-transparent cavity filling simulation program. An automatic mesh generation program is uniquely developed to complete the cavity filling simulation in real time. Boundary-pressure-reflection scheme is established to solve the typical moving boundary problem of mold filling. Two cavity filling simulation have been carried out successfully by the automated simulation program developed in this thesis in short time.

In order to simulate the flow into an arbitrary shaped cavity, a sophiscated graphics system need to be integrated with the numerical schemes. By automating the input/output data processing for a complicated geometry, the layflat approximation and the automatic mesh generation can be used to simulate a real

injection molding process.

A theoretical model for weldline strength is presented to provide a comprehensive knowledge of the bonding process at the weldline interface. Based on the mathematical models for weldline and molecular orientation, the spatial variation of microstructural anisotropies within a molded part is predicted from the result of cavity filling simulation. The magnitude and the direction of a local anisotropy is represented by a simple strength ellipse, the shape of which can be used as a intuitional design index for determining the mechanical performance of a molded part.

A multi-level expert system is built which can communicate with the analysis programs within the control of the expert system. Heuristic knowledges for injection molding are formalized as production rules of the expert consultation system. The current knowledge base contains decision rules in the respect to moldability and mechanical acceptability of the design which have become scientifically testable in this thesis. More orderly formalized knowledge about the injection molding process will enhance the performance of the synthesis system to evaluate and modify the design in every aspect of the precess.

A prototype knowledge-based system integrates the heuristic knowledge and the process analysis, two domains of knowledge of injection molding, into a rational design strategy. The knowledge-based synthesis system interprets the analytical results from the process simulation, evaluates the design and generates recommendations for rational design alternatives before the physical entity is made.

References

[1]   Suh, N.P.
        Manufacturing and Productivity.
        In . key note paper at the Sagamore Conference, 1984.

[2]   Rinderle, J.R.
        Measures of Functional Coupling in Design.
        PhD thesis, Massachusetts Institute of Technology, 1982.

[3]   Suh, N.P., Bell, A.C. and Gossard, D.C.
        On An Axiomatic Approach to Manufacturing and Manufacturing Systems.
        J. of Eng. for Industry, Trans. ASME 100(2), May, 1978.

[4]   Winston, P.H.
        Artificial Intelligence.
        Addison Wesley, 1984.

[5]   Bakerdjian, Z. and Kamal, M.R.
        Distribution of Some Physical Properties in Injection Molded Thermoplastic
            Articles.
        Polym. Eng. Sci. 17(2), February, 1977.

[6]   Ballman, R.L. and Toor, H.L.

        Modern Plastics 38:113, October, 1960.

[7]   Bown, J.
        Injection Molding of Plastic Components.
        McGraw Hill, London, 1979.

[8]   Boyer, R.F.

        Journal of Polymer Science 14:267, 1966.

[9]   Broutman, L.J. and Mcgarry, F.J.

        Journal of Applied Polymer Science 9:609, 1965.

[10]   Buchanan, B. and Feigenbaum, E.
         Dendral and MetaDendral: Their Applications and Dimensions.
         Artificial Intelligence 11:5-24, 1978.

[11]   Bueche, F., Cashin, W.M. and Debye, P.
         The Measurement of Self-Diffusion in Solid Polymers.
         Journal of Chemical Physics 20:1956, 1952.

[12]   Bueche, F.
         Viscosity, Self-Diffusion and Allied Effects in Solid Polymers.
         Journal of Chemical Physics 20:1959, 1952.

[13]   Cogswell, F.N.
         Polymer Melt Rheology.
         John Wiley and Sons, London, 1981.

[14]   Curtis, J.W.
         The Effect of Pre-Orientation on the Fracture Properties of Glassy Polymers.
         Journal of Physics. D: Appl. Phys. 3:1413, 1970.

[15]   Davis, R. and King, J.
         An Overview of Production Systems.
         In Elcock, E.W. and Michie, D. (editor), *Medical Intelligence 8*, pages 300-332.
             Wiley, 1976.

[16]   Dietz, W. and White, J.L.

         Rheologica Acta 17:676, 1978.

[17]   Dietz, W.

         Polym. Eng. Sci. 18:1030, 1978.

[18]   Dietz, White and Clark.
         Orientation, Development and Relaxation in Injection Molding of Amorphous
             Polymers.
         Polym. Eng. Sci. 18(4):273, March, 1978.

[19]   Duda, R.O. Gaschnig, J.G. and Hart, P.E.
         Model Design in the Prospector Consultant System for Mineral Exploration.
         In Michie, D. (editor), *Expert System in the Microelecronic Age.* Edinburgh
             Univ. Press, 1979.

[20]   Duda, R.O. and Gaschnig, J.G.
         Knowledge-Based Ststem Come of Age.
         BYTE Megazine , September, 1981.

[21]   Flory, P.J.
         Principles of Polymer Chemistry.
         Cornell Univ. Press, Ithaca, N.Y., 1978.

[22]   Gutfinger, C., Broyer, E. and Tadmor, Z.
         Melt Solidification in Polymer Science.
         Polym. Eng. Sci. 15(7), July, 1975.

[23]   Hagerman,E.M.
         Weldline Fracture in Molded Parts.
         Plastics Eng. 29(10), 1973.

[24]   Han, C.D. and C.A. Villamizar.
         Measurement of Pressure and Stress Birefringence Patterns During the Mold
             Filling and Cooling Operations.
         In . SPE 35th ANTEC Tech. Papers, Montreal, May, 1977.

[25]   Hardenbrook, S.B. and Schnall, J.A.
         *Use of Tensile Test to Relate Melt Weldline Strength to Injection Molding
             Process Variables.*
         Technical Report MID-R-12-79, Eastman Kodak, 1979.

[26]   Harry, D.H. and Parrot, R,G.

         Polym. Eng. Sci. 10:209, 1970.

[27]   Hart, P.
         Directions for Artificial Intelligence in the Eighties.
         SIGNART Newsletter 79:11-16, 1982.

[28]   Hoare, Linda and Hull, D.
         The Effect of Orientation on the Mechanical Properties of Injection Molded
             Polystyrene.
         Polym. Eng. Sci. 17(3), March, 1977.

[29]   Hull, D.
         An Introduction to Composite Materials.
         Cambridge Univ. Press, 1981.

[30]   Isayev, A.I. and Hieber, C.A.

.

Rheol. Acta 19:168, 1980.

[31]   Jackson, G.B. and Ballman, R.L.
The Effect of Orientation on the Physical Properties of Injection Moldings.
SPE Journal :1147, October, 1960.

[32]   Janeschitz-Kriegl, H.
Injection Molding of Plastics: Some Idea about the Relationship between Mold
        Filling and Birefringence.
Rheol. Acta 16(4):23, 1977.

[33]   Jud, K. and Kaush, H.H.
Fracture Mechanical Studies of the Strength Resulting from Polymer
        Interdiffusion.
In Francois, D. (editor), *Fracture Research*. Pergamon Press, .

[34]   Kamal, M.R. and Kenig, S.
The Injection Molding of Thermoplastics Part 1: Theoretical Model.
Polym. Eng. Sci. 12(4), July, 1972.

[35]   Kamal, M.R. and Kenig, S.
The Injection Molding of Thermoplastics Part 2: Experimental Test of the
        Model.
Polym. Eng. Sci. 12(4), July, 1972.

[36]   Kamal, M.R. and Tan, V.
Orientation in Injection Molded Polystyrene.
Polym. Eng. Sci. 19(8), 1979.

[37]   Kamal, M.R. and Lafleur, P.G.
Computer Simulation of Injection Molding.
Polym. Eng. Sci. 22:1066, 1982.

·[38]   Kenig, S. and Kamal, M.R.
Cooling Molded Parts - A Rigorous Analysis.
SPE Journal 26, July, 1970.

[39]   Kenig, S. and Kamal, M.R.
Heat Transfer in the Cooling of Thermoplastic Melts under Pressure.
The Canadian J. of Chemical Eng. 49, April, 1971.

[40]   Kim, B.H.
       Low Thermal Inertia Injection Molding.
       PhD thesis, Massachusetts Institute of Technology, 1983.

[41]   Kim, Y.H. and Wool, R.P.
       A Theory of Healing at a Polymer-Polymer Interface.
       Macromolecules 16:1115, 1983.

[42]   Kim, S.G. and Suh, N.P.
       Performance Prediction of Weldline Strength in Amorphous Polymers.
       In . SPE 42th ANTEC Tech. Papers, New Orleans, May, 1984.

[43]   Koda, H.
       Effects of Molding Conditions on Properties of Injection Molded
           Polycarbonates.
       J. of Applied Polymer Science 12:2257, 1968.

[44]   Kuo, Y. and Kamal, M.R.
       Flows of Thermoplastics in the Filling and Packing Stages of Injection
           Molding.
       In *Proceedings of International Conference on Polymer Processing.* MIT,
           Cambridge, MA., August, 1977.

[45]   Laun, H.M., Wagner, M.H. and Janeschitz-kriegl, H.

       Rheol. Acta 18:615, 1979.

[46]   Malguarnera, S.C. and Manisali, A.
       The Effect of Processing Parameters on thr Tensile Properties of Weldlines in
           Injection Molded Thermoplastics.
       Polym. Eng. Sci. 21:586, 1981.

[47]   McDermott, J.
       R1: An Expert in the Computer System Domain.
       In *Proceedings of the First Annual National Conference on Artificial
           Intelligence,* pages 269-271. 1980.

[48]   Menges, G. and Wubken, G.
       Influence of Processing Conditions on Molecular Orientation in Injection
           Moldings.
       In . SPE 31st ANTEC, Montreal, May, 1973.

[49]   Menges, G., Thienel, P. and Wubken, G.
       A Method to Estimate the Relaxation of Molecular Orientation in Plastics.
       Kunstoffe 66:42-48, January, 1976.

[50]   Moldflow Australia Pty. Ltd.
       The Mold Flow Philosophy.
       .

[51]   Moses, J.
       Symbolic Integration.
       PhD thesis, M.I.T., 1967.

[52]   Newell, A. and Simon, H.A.
       GPS, A Program that Simulates Human Thought.
       In Feigenbaum, E.A. and Feldman, J.A. (editor), *Computers and Thought.*
           McGraw-Hill, N.Y., 1963.

[53]   Postans, J.H.
       Plastic Molding.
       Oxford Univ. Press, 1978.

[54]   Rheinfeld, D.
       Influencing Molding Quality during Injection Molding.
       In *Injection Molding Technology.* VDI-Verlag GmbH, 1981.

[55]   Richardson, S.
       .

       J. of Fluid Mechanics 56:609, 1972.

[56]   Saltuk, I., Siscovic, N. and Griskey, R.G.
       .

       Polym. Eng. Sci. 12:397, 1972.

[57]   Shortliffe, E.H.
       Computer Based Medical Consultation: MYCIN.
       Elsevier, N.Y., 1976.

[58]   Spencer, R.S. and Gilmore, G.D.
       Equation of State for Polystyrene.
       J. of Applied Physics 20:502, 1949.

[59]   Spencer, R.S. and Gilmore, G.D.
       Equation of State for High Polymers.
       J. of Applied Physics 21, June, 1950.

[60]   Spencer, R.S. and Gilmore, G.D.
       Some Flow Phenomena in the Injection Molding of Polystyrene.
       J. of Colloid Science 6:118, 1951.

[61] Spencer, R.S.
      Volume-Temperature-Time Relationships for Polystyrene.
      J. of Colloid Science 4:229, 1949.

[62] Stefik, M.J.
      Inferring DNA Structures from Segmentation Data.
      Artificial Intelligence 11:85-114, 1978.

[63] Tadmor, Z.
      Molecular Orientation in Injection Molding.
      J. of Applied Polymer Science 18:1753, 1974.

[64] Tadmor, Z. and Gogos, C.G.
      Principles of Polymer Processing.
      Wiley, 1977.

[65] Tan, V. and Kamal, M.R.
      The Effects of Processing Variables on the Distribution of Morphological
          Zones and Orientation in Injection Molded PE.
      In *Proceedings of International Conference on Polymer Processing.* MIT,
          Cambridge, MA., August, 1977.

[66] Tobolsky.
      Properties and Structures of Polymer.
      Wiley, N.Y., 1960.

[67] VanMelle, W.
      A Domain-independent Production Rule System for Consultation Programs.
      In *Proceedings of the Sixth International Conference on Artificial Intelligence,*
          pages 923-925. Tokyo, Japan, 1979.

[68] Voyutskii.
      Autohesion and Adhesion of High Polymers.
      Wiley Interscience, N.Y., 1963.

[69] Wales, L.L.S.
      The Application of Flow Birefringence to Rheological Studies to Polymer Melts.
      Delft Univ. Press, 1976.

[70] Wang, K.K., et al.
      Computer Aided Injection Molding System.
      Technical Report 2-10, Cornell Injection Molding Program, .

[71]   Weiss, S.M., Kulikowski, C.A. and Safir, A.
         Glaucoma Consultation by Computer.
         Computers in Biology and Medicine 8:25-40, 1978.

[72]   Weiss, S.M., Kulikowski, C.A., etal.
         Building Expert System for Controlling Complex Programs.
         In *Proceedings of the First Annual National Conference on Artificial
             Intelligence*, pages 322-326. Pittsburg, P.A., 1982.

[73]   Weiss, S.M. and Kulikowski, C.A.
         A Practical Guide to Designing Expert System.
         Rowman and Allanheld Publishers, N.J., 1984.

[74]   Weiss, S.M., Kern, K.B., etal.
         A Guide to the Expert Consultation System.
         Technical Report CBM-TR-94, Rutgers University, December, 1984.

[75]   White, J.
         Fluid Mechanical Analysis of Injection Mold Filling.
         Polym. Eng. Sci. 15(1), January, 1975.

[76]   White, J.L. and Dietz, W.
         Some Relationships betwwen Injection Molding Conditions and the
             Characteristics of Vitrified Molded Parts.
         Polym. Eng. Sci. 19(15):1081, 1979.

[77]   Williams, G. and Lord, H.A.
         Mold Filling Studies for the Injection Molding of Thermoplastic Materials
             Part 1: The Flow of Plastic Materials in Hot and Cold Walled Circular
             Channels.
         Polym. Eng. Sci. 15(8), August, 1975.

[78]   Wool, R.P. and O'Connor, K.M.

         Journal of Applied Physics 52:5953, 1981.

[79]   Wu, P.C., Huang, C.F. and Gogos, C.G.
         Simulation of the Mold Filling Process.
         Polym. Eng. Sci. 14(3), March, 1974.

Appendix A
Functional Flow Charts of the Analysis Programs

The following pages contain the functional flow charts of the cavity filling simulation and the microstructure prediction program developed in this thesis as parts of the knowledge-based synthesis program.

An interactive cavity filling simulation program is developed by modifying the basic FEM/FDM numerical scheme coded by Cornell Injection Molding Program. The boundary-pressure-reflection scheme is the key idea in deriving the automatic mesh generation procedure which enables the real time cavity filling simulation.

A spatial distribution of microstructural anisotropies of the quasi-three dimensional injection molded part is predicted by the performance prediction program. The prediction program determines the magnitude and the direction of the molecular orientation and its effect on the strength of the part, and the strength of the weldline structure. A communication program between the expert system and the performance prediction program is provided.

Detailed program listings are not presented in this thesis. A separate technical manual will be provided to the MIT-Industry Polymer Processing Program.

```
┌─────────────────────────────────────────┐
│           READ INPUT DATA               │
└─────────────────────────────────────────┘
                    │
┌─────────────────────────────────────────┐
│      SOLVE THE PRESSURE DISTRIBUTION     │
└─────────────────────────────────────────┘
                    │
┌─────────────────────────────────────────┐
│   ADVANCE BOUNDARY NODES AT THE          │
│   CURRENT MELT FRONT                     │
└─────────────────────────────────────────┘
                    │
┌─────────────────────────────────────────┐
│   DETECT POSSIBLE MELT-BOUNDARY          │
│   IMPINGEMENT                            │
└─────────────────────────────────────────┘
                    │
┌─────────────────────────────────────────┐
│   SOLVE PRESSURE REFLECTIONS AND         │
│   REDISTRIBUTE THE BOUNDARY NODAL        │
│   PRESSURES                              │
└─────────────────────────────────────────┘
                    │
┌─────────────────────────────────────────┐
│   CALCULATE NODAL VELOCITIES             │
└─────────────────────────────────────────┘
                    │
┌─────────────────────────────────────────┐
│   CALCULATE TEMPERATURE DISTRIBUTION     │
│   IN PLANAR COORDINATES AND THE GAP      │
│   DIRECTION                              │
└─────────────────────────────────────────┘
                    │
┌─────────────────────────────────────────┐
│   PREDICT NEW MELT FRONT                 │
└─────────────────────────────────────────┘
                    │
┌─────────────────────────────────────────┐
│   GENERATE FINITE ELEMENT MESHES         │
│   BASED ON THE NEW MELT FRONT            │
│   CONFIGURATION                          │
└─────────────────────────────────────────┘
                    │
┌─────────────────────────────────────────┐
│   EDIT MESHES TO MAINTAIN THE            │
│   NUMERICAL STABILITY OF THE ANALYSIS    │
└─────────────────────────────────────────┘
                    │
┌─────────────────────────────────────────┐
│   PREPARE THE INPUT DATA FILE FOR        │
│   FOLLOWING TIME STEP                    │
└─────────────────────────────────────────┘
                    │
┌─────────────────────────────────────────┐
│   WRITE THERMOMECHANICAL DATA BASE       │
└─────────────────────────────────────────┘
                    │
              (  STOP  )
```

Figure A-1: Flow Chart for the Cavity Filling Simulation Program

```
              ┌─────────────────────┐
              │        READ         │
              │  THERMOMECHANICAL   │
              │     DATA BASE       │
              └──────────┬──────────┘
                         │
              ┌──────────▼──────────┐
              │     CALCULATE       │
              │       NODAL         │
              │  THERMOMECHANICAL   │
              │     PROPERTIES      │
              └──────────┬──────────┘
                         │
              ┌──────────▼──────────┐
              │        GET          │
              │   A REQUEST FROM    │
              │  THE EXPERT SYSTEM  │
              └──────────┬──────────┘
                         │
        ┌────────────────▼──────────┐      ┌──────────────┐
        │        SEARCH             │      │  CALCULATE   │
        │  AN ELEMENT CONTAINING    │─────▶│  NECESSARY   │
        │   THE TEST POSITION       │      │  INJECTION   │
        └────────────────┬──────────┘      │    POWER     │
                         │                 └──────┬───────┘
        ┌────────────────▼──────────┐             │
        │     CALCULATE             │             │
        │  THE THERMOMECHANICAL     │             │
        │  PROPERTIES BY INTER-     │             │
        │  POLATING NODAL VALUES    │             │
        └────────────────┬──────────┘             │
```

DETERMINE MAXIMUM BIREFRINGENCE

DETERMINE SURFACE BIREFRINGENCE

DETERMINE WELDLINE STRENGTH IF EXIXSTS

DETERMINE STRENGTH ELLIPSE AT THE TEST POINT

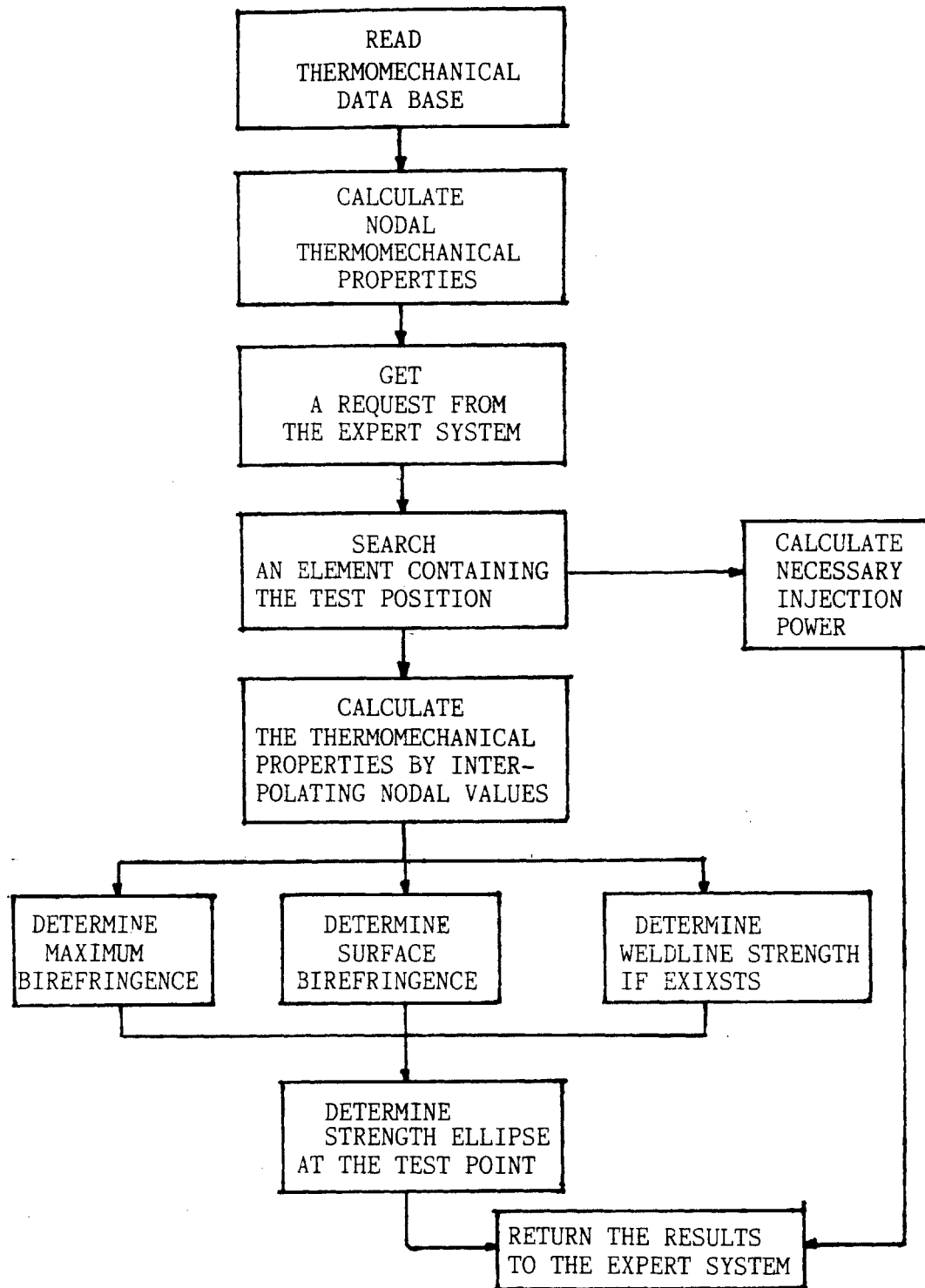RETURN THE RESULTS TO THE EXPERT SYSTEM

Figure A-2: Flow Chart for the Performance Prediction Program

Appendix B
Expert Model for Injection Molding

In the $EXPERT^{14}$ language format, three representational components for describing the heuristic knowledge are used to form an expert consultation model for injection molding. They are hypotheses, findings, and rules relating the findings and the hypotheses.

Hypotheses are the set of conclusions that may be inferred by the system. A measure of uncertainty can be associated with a hypothesis to control the priority of a decision. Within the *TAXONOMY* subsection, possible diagnostic conclusions are contained. The subsection, *TREATMENTS*, describes the types of advice that may be inferred by the expert system.

Findings list the observations either from the user or the analysis programs. They are responses to questions which can be reported in the form of logical, numerical and unknown results. There are four types of questions in this model;

1. multiple choice

2. checklist

3. numerical

4. yes/no

A checklist type question differs from a multiple choice question in that the choices

---

[14] expert system design package

are not mutually exclusive and more than one may be true.

Production rules are used to represent the reasoning procedure of the expert. The production rules in this system are categorized in terms of the three types of logical relationships between findings and hypotheses as follows.

- FF rules: finding to finding rules

- FH rules: finding to hypothesis rules

- HH rules: hypothesis to hypothesis rules

The following is the overall format of the model constructed in this thesis. Two asterisks indicate one of the three major sections. A single asterisk indicates a subsection.

**HYPOTHESES

*TAXONOMY
NADA   MATERIAL DATA IS NOT AVAILABLE
MCNC   IMPROPER MACHINE; REQUIRED INJECTION POWER IS NOT IN THE+
         RANGE OF MACHINE CAPACITY
UNMA   MOLDABILITY IS NOT PREDICTED.
MAST   NOT MOLDABLE. CHANGE PROCESSING CONDITIONS AND+
         RUN FLOW SIMULATION.
UNKM   MECHANICAL PERFORMANCE IS NOT KNOWN
WDLE   WELDLINE EXISTS
WEWD   WEAK WELDLINE
ADMS   BAD COMBINATION OF MICROSTRUCTURE AND GEOMETRY
JETY   JETTING IS POSSIBLE
ACMS   ACCEPTABLE MICROSTRUCTURE
ACGM   ACCEPTABLE GEOMETRY; NO NEED TO CHECK STRESS ANALYSIS

*INTERMEDIATE HYPOTHESES'
WELD   BAD WELDLINE EXISTS

*TREATMENTS
DAIN   INPUT NEW MATERIAL DATA
NOTR   DESIGN IS GENERALLY ACCEPTABLE
FSFR   CHANGE DESIGN FOLLOW TREATMENTS BELOW

```
FSIR    FLOW SIMULATION IS REQUIRED.RUN FLOW SIMULATION PROGRAM.+
        --RUN(CIMP)
RMIC    RUN MICROSTRUCTURE PREDICTION PROGRAM IN FOLLOWING
        ASPECTS; RUNNING FORMAT--RUN(STAN)
WDIR    WELDLINE ANALYIS IS REQUIRED.
SEIR    STRENGTH ELLIPSE IS REQUIRED.
CHMC    CHANGE MACHINE
TMIN    INCREASE MELT TEMPERATURE
TMDC    DECREASE MELT TEMPERATURE
TDIN    INCREASE MOLD TEMPERATURE
INJI    INCREASE INJECTION SPEED
INJD    DECREASE INJECTION SPEED
CGPO    MOVE GATE POSITION
CGSH    CHANGE GATE SHAPE
ADSG    ADD SECONDARY GEOMETRY
CHPG    CHANGE PRIMARY SHAPE


**FINDINGS


*BEGIN QUESTIONAIRE


*MULTIPLE CHOICE
WHAT MATERIAL:
PSTY    POLYSTYRENE
OTHR    OTHERS


*NUMERICAL/MIN=400/MAX=600
TMLT    MELT TEMPERATURE[K]:


*NUMERICAL/MIN=280/MAX=500
TMLD    MOLD TEMPERATURE[K]:


*NUMERICAL
INJS    INJECTION SPEED[cm**3/sec]


*NUMERICAL
CFML    INJECTION POWER OF THE MACHINE[HP]


*YES/NO
CKMC    MICROSTRUCTURE IS NOT CHECKED YET


*MULTIPLE CHOICE
SHORT SHOT:
SHNO    SHORT SHOT DOES NOT OCCUR
SHOC    SHORT SHOT OCCURS
```

SHUK   SHORT SHOT NOT KNOWN

*MULTIPLE CHOICE
WHAT KIND OF APPLICATION:
GNAP   GENERAL APPLICATION.e.g.toys
HSAP   HIGH STRESS APPLICATION.e.g.cars

*MULTIPLE CHOICE
IS LOAD DETERMINED:
SPLC   SPECIFIC LOADING CONDITION
NSLC   NON-SPECIFIC LOADING CONDITION

*NUMERICAL
SPXC   X-COORD OF MAX. STRESS POINT

*NUMERICAL
SPYC   Y-COORD OF MAX. STRESS POINT

*NUMERICAL
ULSX   MAX PRINCIPAL STRESS TO STRENGTH RATIO

*NUMERICAL
ULSY   MIN PRINCIPAL STRESS TO STRENGTH RATIO

*NUMERICAL
ORIO   ANGLE OF THE MAX PRINCIPAL STRESS AXIS TO X-AXIS

*YES-NO
EDG1   THERE IS A EDGE

*NUMERICAL
CHX1   TYPICAL POINT ON THE EDGE1(X-COORD)

*NUMERICAL
CHY1   TYPICAL POINT ON THE EDGE1(Y-COORD)

*NUMERICAL
ORI1   ANGLE OF THE EDGE TO X-AXIS

*YES-NO
EDG2   THERE ARE MORE EDGES

*NUMERICAL
CHX2   TYPICAL POINT ON THE EDGE2(X-COORD)

*NUMERICAL
CHY2   TYPICAL POINT ON THE EDGE2(Y-COORD)

*NUMERICAL
ORI2   ANGLE OF THE EDGE2 TO X-AXIS

*CHECK LIST
CHECK WELDLINE POSSIBILITY:
NOWD   WELDLINE IS NOT POSSIBLE
INSR   THERE ARE INSERTS
MULG   MULTIPLE GATING
MERG   FLOW FRONTS MERGE SOMEWHERE

*NUMERICAL
CHX3   X-POSITION AROUND INSERT FAR FROM GATE

*NUMERICAL
CHY3   Y-POSITION AROUND INSERT FAR FROM GATE

*NUMERICAL
ORI3   DIRECTION OF WELDLINE CAUSED BY INSERT(X-AXIS REF)

*YES-NO
ALE3   WELDLINE BY INSERT IS ALONG EDGES

*NUMERICAL
CHX4   X-POSITION OF WELDLINE CAUSED BY MULTIPLE GATES

*NUMERICAL
CHY4   Y-POSITION OF WELDLINE CAUSED BY MULTIPLE GATES

*NUMERICAL
ORI4   DIRECTION OF WELDLINE CAUSED BY MULTIPLE GATES

*YES-NO
ALE4   WELDLINE BY MULTIPLE GATES IS ON THE EDGE

*NUMERICAL
CHX5   X-POSITION OF WELDLINE BY MERGING FLOW FRONTS

*NUMERICAL
CHY5   Y-POSITION OF WELDLINE BY MERGING FLOW FRONTS

*NUMERICAL
ORI5   DIRECTION WELDLINE CAUSED BY MERGING FRONTS

*YES-NO
ALE5   WELDLINE DUE TO MERGING MELT FRONTS IS ON THE EDGE

*YES-NO
STCN   OTHER POSSIBLE STRESS CONCENTRATED REGIONS(HOLES,etc)

*NUMERICAL
CHX6   X-POSITION OF STRESS CONCENTRATOR

*NUMERICAL
CHY6   Y-POSITION OF STRESS CONCENTRATOR

*NUMERICAL
ORI6   DIRECTION OF MAX. STRESS OF CONCENTRATION

*YES-NO
SUDN   SUDDENLY ENLARGING DISCONTINUOUS GEOMETRY IN FLOW
         DIRECTION

*NUMERICAL
CHX7   X-POSITION OF THE DISCONTINUITY

*NUMERICAL
CHY7   Y-POSITION OF THE DISCONTINUITY

*YES-NO
CFOK   REQUIRED CLAMPING FORCE IS IN THE RANGE OF MACHINE
         CAPACITY

*YES-NO
UXOK   X-DIRECTIONAL STRENGTH IS GOOD ENOUGH

*YES-NO
UYOK   Y-DIRECTIONAL STRENGTH IS GOOD ENOUGH

*NUMERICAL
ORD1   ANGLE DIFFERENCE BETWEEN EDGE AXIS AND MAJOR ORIENTATION

*NUMERICAL
STM1   STRENGTH RATIO PERPENDICULAR TO THE ORIENTATION
         DIRECTION

*NUMERICAL
ORD2   ANGLE DIFFERENCE BETWEEN EDGE2 AXIS AND MAJOR ORIENTATION

*NUMERICAL
STM2   STRENGTH RATIO ON MINOR ORIENTATION DIRECTION

*NUMERICAL
STM3   STRENGTH RATIO ON WELDLINE1 DIRECTION

*NUMERICAL
STM4   STRENGTH RATIO ON WELDLINE2 DIRECTION

*NUMERICAL
STM5   STRENGTH RATIO ON WELDLINE3 DIRECTION

*NUMERICAL
ORD6   ANGLE DIFFERENCE BETWEEN MAX. STRESS DIR. AND MAJOR
        ORIENTATION

*NUMERICAL
STM6   STRENGTH RATIO IN MAX STRESS DIRECTION

*END QUESTIONAIRE

*PRINT CONTROL/CATEGORIES=(0.5,0.7,0.9)
NADA/C
UNMA/C
        F(SHUK,T)
MAST/C
        F(SHOC,T)
UNKM/C
        F(CKMC,T)
WDLE/C
        F(INSR,T),F(MULG,T),F(MERG,T),
/   F(CHX3,*:*),F(CHY3,*:*)
/   F(CHX4,*:*),F(CHY4,*:*)
/   F(CHX5,*:*),F(CHY5,*:*)
JETY/C
        F(SUDN,T)
/   F(CHX7,*:*),F(CHY7,*:*)
ACGM/C
ADMS/C
        F(SPLC,T),F(EDG1,T),F(EDG2,T),F(STCN,T)
        F(UXOK,F),F(UYOK,F)
        F(STM1,0.8:1.0),F(STM2,0.8:1.0),F(STM6,0.7:1.0)
/   F(SPXC,*:*),F(SPYC,*:*),F(ORIO,*:*)
/   F(CHX1,*:*),F(CHY1,*:*)
/   F(CHX2,*:*),F(CHY2,*:*)

```
WELD/C
        F(ALE3,T),F(ALE4,T),F(ALE5,T)
/       F(CHX3,*:*),F(CHY3,*:*)
/       F(CHX4,*:*),F(CHY4,*:*)
/       F(CHX5,*:*),F(CHY5,*:*)
MCNC/C
ACMS/C
        F(SPLC,T),F(EDG1,T),F(EDG2,T),F(STCN,T)
        F(UXOK,T),F(UYOK,T)
        F(STM1,0.8:1.0),F(STM2,0.8:1.0),F(STM6,0.7:1.0)
RMIC/C
DAIN/C
NOTR/C
        H(ACGM,0.8:1.0)
FSIR/C
        H(UNMA,1.0:*),H(MAST,1.0:*)
WDIR/C
SEIR/C
CHMC/C
        H(MCNC,0.8:1.0)
TMIN/C
        F(SHOC,T),H(WEWD,0.8:1.0)
TMDC/C
TDIN/C
        F(SHOC,T),H(WEWD,0.8:1.0)
INJI/C
        F(SHOC,T)
INJD/C
CGPO/C
        H(WELD,0.7:1.0),H(WEWD,0.8:1.0)
CGSH/C
        H(WELD,0.7:1.0),H(WEWD,0.8:1.0)
ADSG/C
        H(ADMS,0.7:1.0),H(WELD,0.7:1.0),H(WEWD,0.8:1.0)
CHPG/C

**RULES
*FF RULES
F(OTHR,T)->F(TMLT:STM6,U)
F(SHOC,T)->F(GNAP:STM6,U)
F(SHUK,T)->F(GNAP:STM6,U)
F(SHNO,T)->F(CFOK:STM6,U)
F(GNAP,T)->F(SPLC:ORIO,U)
F(NSLC,T)->F(SPXC:ORIO,U)
F(EDG1,F)->F(CHX1:ORI2,U)
```

```
F(EDG2,F)->F(CHX2:ORI2,U)
F(NOWD,T)->F(CHX3:ALE5,U)
F(INSR,F)->F(CHX3:ALE3,U)
F(MULG,F)->F(CHX4:ALE4,U)
F(MERG,F)->F(CHX5:ALE5,U)
F(STCN,F)->F(CHX6:ORI6,U)
F(SUDN,F)->F(CHX7:CHY7,U)


*FH RULES
F(OTHR,T)->H(NADA,1.0)
F(SHUK,T)->H(UNMA,1.0)
F(SHOC,T)->H(MAST,1.0)
F(SHNO,T)&F(CKMC,T)->H(UNKM,1.0)
[1:F(INSR,T),F(MULG,T),F(MERG,T)]&F(NOWD,F)->H(WDLE,1.0)
F(SUDN,T)->H(JETY,0.7)
F(SHNO,T)&F(EDG1,F)&F(INSR,F)&F(MULG,F)&F(MERG,F)&F(STCN,F)&+
F(SUDN,F)&F(GNAP,T)->H(ACGM,0.8)
F(SPLC,T)&F(CKMC,F)&[1:F(UXOK,F),F(UYOK,F)]->H(ADMS,1.0)
F(CKMC,F)&F(EDG1,T)&[2:F(ORD1,0:30),F(STM1,0.0:0.8)]->H(ADMS,0.8)
F(CKMC,F)&F(EDG1,T)&[1:F(ORD1,50:90),F(STM1,0.8:1.0)]->H(ACMS,0.8
F(CKMC,F)&F(EDG2,T)&[2:F(ORD2,0:30),F(STM2,0.0:0.8)]->H(ADMS,0.8)
F(CKMC,F)&F(EDG2,T)&[1:F(ORD2,50:90),F(STM2,0.8:1.0)]->H(ACMS,0.8
F(CKMC,F)&F(INSR,T)&F(STM3,0.0:0.7)->H(WEWD,0.7)
F(CKMC,F)&F(MULG,T)&F(STM4,0.0:0.7)->H(WEWD,0.7)
F(CKMC,F)&F(MERG,T)&F(STM5,0.0:0.7)->H(WEWD,0.7)
F(CKMC,F)&F(STCN,T)&[1:F(ORD6,70:90),F(STM6,0.0:0.7)]->H(ADMS,0.9
[1:F(ALE3,T),F(ALE4,T),F(ALE5,T)]->H(WELD,1.0)
F(CFOK,F)->H(MCNC,0.8)


*HH RULES
*IF
F(OTHR,T)
*THEN
H(NADA,1.0:*)->H(DAIN,1.0)
*END
*IF
F(CKMC,T)
*THEN
H(UNMA,1.0:*)->H(FSIR,1.0)
H(MAST,1.0:*)->H(FSFR,1.0)
F(SHOC,T)&H(FSFR,0.9:1.0)->H(TMIN,0.9)
F(SHOC,T)&H(FSFR,0.9:1.0)->H(INJI,0.8)
F(SHOC,T)&H(FSFR,0.9:1.0)->H(TDIN,0.7)
H(MCNC,0.8:1.0)&F(SHOC,F)->H(TMIN,0.9)
H(MCNC,0.8:1.0)&H(TMIN,0.8:1.0)&F(SHOC,T)->H(TDIN,0.8)
```

```
*END
*IF
F(CKMC,T)
*THEN
H(ACGM,0.7:1.0)->H(NOTR,0.8)
H(UNKM,0.9:1.0)&H(ACGM,-1.0:0.6)->H(RMIC,1.0)
H(WDLE,0.9:1.0)&H(ACGM,-1.0:0.6)->H(WDIR,1.0)
H(UNKM,0.9:1.0)&H(ACGM,-1.0:0.6)->H(SEIR,1.0)
*END
*IF
F(CKMC,F)
*THEN
H(MCNC,0.7:1.0)->H(CHMC,0.9)
H(WEWD,0.8:1.0)->H(TMIN,0.8)
H(WEWD,0.8:1.0)->H(TDIN,0.9)
H(WEWD,0.7:1.0)&H(WELD,0.8:1.0)->H(CGPO,1.0)
H(WEWD,0.7:1.0)&H(WELD,0.8:1.0)->H(ADSG,0.8)
[1:H(ADMS,0.7:*),H(WELD,0.7:1.0)]->H(CGPO,1.0)
[1:H(ADMS,0.7:*),H(WELD,0.7:1.0)]->H(ADSG,0.8)
[1:H(ADMS,0.7:*),H(WELD,0.7:1.0)]->H(CGSH,0.7)
H(JETY,0.6:1.0)->H(ADSG,0.9)
*END
```